

Verification of Performance and Design Criteria for High Performance Steel Bridges

James A Swanson, Ph.D.
Daniel G Linzell, P.E., Ph.D.
Caroline R Bennett, Ph.D.
Min Lin



for the
Ohio Department of Transportation
Office of Research and Development

Report Number *FHWA/OH-2006/2*
State Job Number *14789(0)*

January 2006

UNIVERSITY OF 
Cincinnati



1. Report No. FHWA/OH-2006/2	2. Government Accession No.	3. Recipient's Catalog No.	
4. Title and subtitle Verification of Performance and Design Criteria for High Performance Steel Bridge Girders		5. Report Date January 2006	
		6. Performing Organization Code	
7. Author(s) James A. Swanson Daniel G. Linzell Caroline R. Bennett Min Lin		8. Performing Organization Report No.	
		10. Work Unit No. (TRAIS)	
9. Performing Organization Name and Address University of Cincinnati Department of Civil & Environmental Engineering PO Box 210071 Cincinnati, OH 45221-0071		11. Contract or Grant No. 147890(1)	
		13. Type of Report and Period Covered	
12. Sponsoring Agency Name and Address Ohio Department of Transportation 1980 West Broad Street Columbus, Ohio 43223		14. Sponsoring Agency Code	
		15. Supplementary Notes	
16. Abstract <p>High Performance Steel (HPS) has quickly gained popularity in United States bridge applications due to its high yield strength and better weldability, toughness, ductility, and weathering characteristics. However, a great deal of information is missing from the body of knowledge on HPS performance and design criteria, especially concerning HPS-70W (485W) produced by thermo-mechanical controlled processing (TMCP). This research examines material characteristics and fatigue performance of HPS-70W (485W) TMCP, as well the performance of Ohio's first HPS bridge in service.</p> <p>Data from 96 tensile tests show that yield and ultimate strengths of HPS-70W (485W) TMCP is dependent upon plate thickness and orientation. 75 Charpy V-Notch (CVN) specimens were tested, and all met the ASTM A709 requirement for minimum toughness. Twenty-nine specimens were tested to investigate the fatigue resistance of continuous plates with punched, drilled, and reamed holes. Results from this investigation suggest that current restrictions mandated by some state DOTs concerning punching holes are not overly restrictive when HPS-485W (70W) is utilized. Performance of drilled and sub-punched and reamed specimens met or exceeded AASHTO (2004) requirements for Category B details. Performance of Submerged Arc Weld (SAW) and Narrow Gap Improved Electroslag Weld (NGI-ESW) welded butt-splices utilizing HPS-70W (485W) were examined. All specimens performed considerably better than predicted by the AASHTO fatigue life equation.</p>			
17. Key Words Steel, High Performance Steel, HPS, TMCP, Bridge, Roundhousing, Toughness, Fatigue, Punched, Drilled, Reamed, Weld, Electroslag, Screed, Skewed, Distribution Factor		18. Distribution Statement No restrictions. This document is available to the public through the National Technical Information Service, Springfield, Virginia 22161	
19. Security Classif. (of this report) Unclassified	20. Security Classif. (of this page) Unclassified	21. No. of Pages 144	22. Price

Verification of Performance and Design Criteria for High Performance Steel Bridges

James A Swanson, Ph.D.

Associate Professor, Cincinnati Infrastructure Institute, Dept. of Civil &
Environmental Engineering, University of Cincinnati, Cincinnati, OH 45221-0071

Daniel G Linzell, P.E., Ph.D.

Associate Professor, Department of Civil and Environmental Engineering,
Pennsylvania State University, State College, PA 16802

Caroline R Bennett, Ph.D.

Assistant Professor, Dept. of Civil, Environmental, & Architectural Engineering,
University of Kansas, Lawrence, Kansas 66045-7609

Min Lin

Structural Engineer, Biggs Cardosa Associates, Inc.
San Jose, CA, 95117

Report #FHWA/OH-2006/2
Cincinnati Infrastructure Institute
College of Engineering
Cincinnati, OH 45221-0071

January 2006

A Report to Sponsors:
U.S. Department of Transportation
Federal Highway Administration
and
Ohio Department of Transportation
State Job No. 14789(0)
Contract No. 11009

Prepared in cooperation with the Ohio Department of Transportation and the
U.S. Department of Transportation, Federal Highway Administration

The contents of this report reflect the views of the author(s) who is(are) responsible for the facts and the accuracy of the data presented herein. The contents do not necessarily reflect the official views or policies of the Ohio Department of Transportation or the Federal Highway Administration.
This report does not constitute a standard, specification or regulation.

Acknowledgements

The authors would like to acknowledge the Ohio Department of Transportation (ODOT) and the Innovative Bridge Research and Construction (IBRC) program sponsored by the Federal Highway Administration (FHWA) for their ongoing cooperation and funding of this project. The authors would also like to thank Arcmatic for welding the plates joined by NGI-ESW during a demonstration project, the Stupp Bridge Company and Peddinghouse Corporation for their cooperation and support in fabricating the specimens. The assistance provided by Thomas Hansley with field testing coordination is also gratefully acknowledged. Finally, the authors would like to acknowledge the assistance of Eric Dues, Sarita Kesler, and John Hattin in the material characterization phase of the project.

Table of Contents

ACKNOWLEDGEMENTS.....	I
TABLE OF CONTENTS.....	III
LIST OF FIGURES	V
LIST OF TABLES	IX
FOREWORD.....	XI
EXECUTIVE SUMMARY	XIII
CHAPTER 1 - CHARACTERIZATION OF MATERIAL PROPERTIES.....	1
1.1 INTRODUCTION	1
1.2 BACKGROUND.....	2
1.3 OBJECTIVES	3
1.4 EXPERIMENTAL SETUP.....	4
1.5 RESULTS AND DISCUSSION.....	7
1.6 CONCLUSIONS.....	17
CHAPTER 2 - FATIGUE BEHAVIOR OF BOLTED SPLICES IN HPS-70W.....	19
2.1 INTRODUCTION	19
2.2 BACKGROUND.....	20
2.3 OBJECTIVES	21
2.4 EXPERIMENTAL SETUP.....	21
2.5 RESULTS AND DISCUSSION.....	25
2.6 CONCLUSIONS.....	31
CHAPTER 3 - FATIGUE BEHAVIOR OF WELDED SPLICES IN HPS-70W	33
3.1 INTRODUCTION	33
3.2 BACKGROUND.....	35
3.3 OBJECTIVES	36
3.4 EXPERIMENTAL SETUP.....	37
3.5 RESULTS AND DISCUSSION.....	41
3.6 CONCLUSIONS.....	43
CHAPTER 4 - AUTOMATED ULTRASONIC INSPECTION OF WELDED JOINTS	45

CHAPTER 5 - ERECTION STUDY OF A SKEWED HPS-70W BRIDGE	47
5.1 INTRODUCTION	47
5.2 OBJECTIVES	49
5.3 STRUCTURE DESCRIPTION.....	50
5.4 FIELD MONITORING	52
5.5 NUMERICAL PROGRAM	53
5.6 MODEL CALIBRATION.....	54
5.7 POUR SEQUENCE STUDY	66
5.8 CONCLUSION.....	70
CHAPTER 6 - FIELD TESTING OF IN-SERVICE HPS-70W BRIDGE.....	73
6.1 INTRODUCTION	73
6.2 BACKGROUND.....	74
6.3 OBJECTIVES AND SCOPE.....	78
6.4 FIELD TESTING PROCEDURES.....	80
6.5 POST-PROCESSING OF FIELD EXPERIMENT DATA.....	100
6.6 DISTRIBUTION FACTOR EVALUATION	103
6.7 SUMMARY AND CONCLUSIONS.....	114
CHAPTER 7 - SUMMARY OF CONCLUSIONS AND RECOMMENDATIONS	115
7.1 INTRODUCTION	115
7.2 CLOSURE.....	118
REFERENCES.....	119

List of Figures

FIGURE 1-1: SAMPLE LOCATIONS OF SPECIMENS FROM $\frac{7}{8}$ " (22 MM) AND 2" (51 MM) PLATES (NOT TO SCALE).....	4
FIGURE 1-2: ASTM-E8 SHEET-TYPE COUPON SPECIMEN, DIMENSIONS TYPICAL FOR ALL TENSILE TESTS	5
FIGURE 1-3: TYPICAL STRESS-STRAIN CURVE FOR TMCP 70W COUPON FROM 2" (51 MM) PLATE.....	10
FIGURE 1-4: TYPICAL STRESS-STRAIN CURVE FOR TMCP 70W COUPON FROM $\frac{7}{8}$ " (22 MM) PLATE	10
FIGURE 1-5: COUPON STRENGTH AVERAGES FOR ORIENTATION PARALLEL AND TRANSVERSE TO THE DIRECTION OF ROLLING	12
FIGURE 1-6: TENSILE STRESS DISTRIBUTION OVER CROSS-SECTIONS OF $\frac{7}{8}$ " (22 MM) THICK PLATE.....	13
FIGURE 1-7: TENSILE STRESS DISTRIBUTION OVER CROSS-SECTIONS OF 2" (51 MM) THICK PLATE.....	14
FIGURE 1-8: TOUGHNESS DISTRIBUTION OVER CROSS-SECTIONS OF $\frac{7}{8}$ " (22 MM) PLATE	15
FIGURE 1-9: TOUGHNESS DISTRIBUTION OVER CROSS-SECTIONS OF 2" (51 MM) PLATE	16
FIGURE 2-1: DIMENSIONS OF BOLTED SPLICE FATIGUE SPECIMENS, IN (MM).....	22
FIGURE 2-2: TEST SET-UP	25
FIGURE 2-3: S-N DIAGRAM FOR 29 BOLTED SPLICE FATIGUE SPECIMENS	27
FIGURE 2-4: AASHTO (2004) CONSTANT A VS. DIAMETER TO THICKNESS RATIO	29
FIGURE 2-5: AASHTO (2004) CONSTANT A VS. HOLE DIAMETER	29
FIGURE 2-6: AASHTO (2004) CONSTANT A VS. PLATE THICKNESS	30
FIGURE 2-7: DIFFERENT HOLE TYPES.....	30
FIGURE 3-1: TWO HPS-485W (70W) PLATES WELDED TOGETHER USING NGI-ESW	38
FIGURE 3-2: TYPICAL SAW AND NGI-ESW WELDED FATIGUE SPECIMENS	39
FIGURE 3-3: WELDED SPECIMEN FATIGUE TEST SETUP	40
FIGURE 4-1: TEST SET UPS FROM AUTOMATED ULTRASONIC TESTING COMPANIES	46
FIGURE 5-1: DECK POURING METHODS.....	50
FIGURE 5-2: FRAMING PLAN AND TYPICAL CROSS SECTION	51
FIGURE 5-3: DECK-POUR ORIENTATION – PERPENDICULAR TO BRIDGE CENTERLINE.....	52
FIGURE 5-4: LOCATION OF STRAIN GAGES	53
FIGURE 5-5: THREE-DIMENSIONAL FE MODEL WITH FINAL CALIBRATION BOUNDARY CONDITIONS.....	54
FIGURE 5-6: COMPARING GIRDER STRESSES, PINNED AND ROLLER ABUTMENT SUPPORTS	57
FIGURE 5-7: EXPERIMENTAL AND NUMERICAL BOTTOM FLANGE STRESS VARIATIONS, G1 AND G5.....	59
FIGURE 5-8: MEASURED TEMPERATURE VARIATION DURING DECK POUR	60
FIGURE 5-9: EXPERIMENTAL AND NUMERICAL BOTTOM FLANGE STRESS VARIATIONS, G1 AND G5, INCLUDING TEMPERATURE.....	61
FIGURE 5-10: INCORPORATION OF TIME-DEPENDANT MODULUS INTO NUMERICAL MODELS.....	62
FIGURE 5-11: EXPERIMENTAL AND NUMERICAL BOTTOM FLANGE STRESS VARIATIONS, G1 AND G5, INCLUDING TIME-DEPENDANT MODULUS	64

FIGURE 5-12: EXPERIMENTAL AND NUMERICAL BOTTOM FLANGE STRESS VARIATIONS, G1 AND G5, INCLUDING TEMPERATURE AND TIME-DEPENDANT MODULUS	65
FIGURE 5-13: DECK PLACEMENT SEQUENCE: (A) PERPENDICULAR TO GIRDER; (B) PARALLEL TO SKEW	66
FIGURE 5-14: NUMERICAL MODEL BOTTOM FLANGE STRESS VARIATIONS	68
FIGURE 5-15: NUMERICAL MODEL GIRDER VERTICAL DISPLACEMENTS	69
FIGURE 6-1: FAI-33-1309 BRIDGE CONFIGURATION.....	79
FIGURE 6-2: FAI-33-1309 TRANSVERSE CROSS SECTION	79
FIGURE 6-3: FAI-33-1309 GIRDER DETAILS	80
FIGURE 6-4: STRAIN TRANSDUCERS USED FOR FIELD TESTING	81
FIGURE 6-5: FIELD TEST #1 INSTRUMENTATION PLAN - PLAN VIEW	83
FIGURE 6-6: FIELD TEST #1 INSTRUMENTATION PLAN - SECTION VIEW.....	84
FIGURE 6-7: FIELD TEST #2 INSTRUMENTATION PLAN - PLAN VIEW	85
FIGURE 6-8: FIELD TEST #3 INSTRUMENTATION PLAN - PLAN VIEW	86
FIGURE 6-9: LOADED DUMP TRUCKS USED FOR TRUCK-LOAD TESTING	87
FIGURE 6-10: DATA FOR TRUCKS USED IN FIELD EXPERIMENT #1	88
FIGURE 6-11: DATA FOR TRUCKS USED IN FIELD EXPERIMENT #2	89
FIGURE 6-12: DATA FOR TRUCKS USED IN FIELD EXPERIMENT #3	90
FIGURE 6-13: MOVING LOAD TYPE #1	92
FIGURE 6-14: MOVING LOAD TYPE #2	92
FIGURE 6-15: MOVING LOAD TYPE #3	92
FIGURE 6-16: MOVING LOAD TYPE #4	92
FIGURE 6-17: MOVING LOAD TYPE #5	92
FIGURE 6-18: FIELD EXPERIMENT #1, STATIC POSITION 1	93
FIGURE 6-19: FIELD EXPERIMENT #1, STATIC POSITION 2.....	94
FIGURE 6-20: FIELD EXPERIMENT #1, STATIC POSITION 3.....	94
FIGURE 6-21: FIELD EXPERIMENT #1, STATIC POSITION 4.....	94
FIGURE 6-22: FIELD EXPERIMENT #1, STATIC POSITION 5.....	95
FIGURE 6-23: FIELD EXPERIMENT #1, STATIC POSITION 6.....	95
FIGURE 6-24: FIELD EXPERIMENT #1, STATIC POSITION 7.....	95
FIGURE 6-25: FIELD EXPERIMENT #1, STATIC POSITION 8.....	96
FIGURE 6-26: FIELD EXPERIMENT #1, STATIC POSITION 9.....	96
FIGURE 6-27: FIELD EXPERIMENT #1, STATIC POSITION 10.....	96
FIGURE 6-28: FIELD EXPERIMENT #1, STATIC POSITION 11	97
FIGURE 6-29: FIELD EXPERIMENT #1, STATIC POSITION 12.....	97
FIGURE 6-30: FIELD EXPERIMENT #1, STATIC POSITION 13.....	97
FIGURE 6-31: FIELD EXPERIMENT #1, STATIC POSITION 14.....	98
FIGURE 6-32: FIELD EXPERIMENT #2, STATIC POSITION 1.....	98

FIGURE 6-33: FIELD EXPERIMENT #2, STATIC POSITION #2.....	98
FIGURE 6-34: FIELD EXPERIMENT #2, STATIC POSITION #3.....	99
FIGURE 6-35: FIELD EXPERIMENT #2, STATIC POSITION #4.....	99
FIGURE 6-36: FIELD EXPERIMENT #2, STATIC POSITION #5.....	99
FIGURE 6-37: FIELD EXPERIMENT #3, STATIC POSITION #1.....	100
FIGURE 6-38: FIELD EXPERIMENT #3, STATIC POSITION #2.....	100
FIGURE 6-39: FIELD EXPERIMENT #3, STATIC POSITION #3.....	100
FIGURE 6-40: COMPARISON BETWEEN RAW FIELD DATA AND FILTERED TRUCK-LOAD RESPONSE	102
FIGURE 6-41: FIELD EXPERIMENT #1, MOVING LOAD TESTS	107
FIGURE 6-42: FIELD EXPERIMENT #1, STATIC TESTS, ONE LANE LOADED.....	108
FIGURE 6-43: FIELD EXPERIMENT #1, STATIC TESTS, TWO LANES LOADED	108
FIGURE 6-44: FIELD EXPERIMENT #2, MOVING LOAD TESTS	109
FIGURE 6-45: FIELD EXPERIMENT #2, MOVING LOAD TESTS	110
FIGURE 6-46: FIELD EXPERIMENT #2, STATIC TESTS, ONE LANE LOADED.....	110
FIGURE 6-47: FIELD EXPERIMENT #2, STATIC TESTS, TWO LANES LOADED	111
FIGURE 6-48: FIELD EXPERIMENT #3, MOVING LOAD TESTS	112
FIGURE 6-49: FIELD EXPERIMENT #3, MOVING LOAD TESTS	112
FIGURE 6-50: FIELD EXPERIMENT #3, STATIC TESTS, ONE LANE LOADED.....	113
FIGURE 6-51: FIELD EXPERIMENT #3, STATIC TESTS, TWO LANES LOADED	113

List of Tables

TABLE 1-1: AVERAGE TENSILE TESTING RESULTS.....	8
TABLE 1-2: MILL CERTIFICATES FOR $\frac{7}{8}$ " (22 MM) HPS-70W PLATE.....	9
TABLE 1-3: MILL CERTIFICATE FOR 2" (51MM) HPS-70W PLATE.....	9
TABLE 2-1: BOLTED SPLICE FATIGUE SPECIMEN DESCRIPTIONS.....	23
TABLE 2-2: BOLTED SPLICE FATIGUE SPECIMEN RESULTS.....	26
TABLE 3-1: WELDED BUTT-SPLICE FATIGUE SPECIMEN DESCRIPTIONS.....	38
TABLE 3-2: WELDED SPLICE FATIGUE SPECIMEN RESULTS.....	42
TABLE 5-1: COMPARISON BETWEEN NUMERICAL AND FIELD FLANGE STRESSES, PINNED AND ROLLER SUPPORTS.....	56
TABLE 6-1: MOVING LOAD TESTS OF THE FAI-33-1309 BRIDGE.....	93

Foreword

This document is the final report for an extensive research project that was conducted at the University of Cincinnati focusing on a new grade of High Performance Steel (HPS). The project was funded by the Ohio Department of Transportation and the Federal Highway Administration through the Innovative Bridge Research and Construction Program. As part of the dissemination effort associated with this project, many of the findings have been or will be published as articles in peer reviewed journals. As a result, many of the chapters in this report consist of slightly modified versions of those journal articles. A description of the material characterization portion of the research is provided in Chapter 1 while research into the fatigue characteristics of bolted and welded splices in HPS girders are discussed in Chapter 2 and Chapter 3, respectively. Chapter 4 consists of a summary the automated ultrasonic inspection study that was conducted and the field studies are summarized next with Chapter 5 focusing on an investigation of the erection procedures and Chapter 6 focusing on the in-service performance of Ohio's first HPS Bridge. Finally, Chapter 7 provides a summary and conclusion for the report.



The Ohio Department of Transportation Office of Research & Development Executive Summary Report

Verification of Performance and Design Criteria for Higher Performance Steel Bridges

Start Date: Aug 1, 2001
Duration: 52 Months
Completion Date: Dec 31, 2005
Report Date: Dec 31, 2005
State Job Number: 14789(0)
Report Number: FHWA/OH-2006/2
Funding: \$178,160
Principle Investigator:

*James A Swanson, Ph.D.
University of Cincinnati
513-556-3774*

ODOT Contacts:

*Technical:
John Randall
Engineer, Bridge Maintenance
614-387-6210*

*Administrative:
Monique R. Evans, P.E.
Administrator, R&D
614-728-6048*

*For copies of this final report go to
<http://www.dot.state.oh.us/divplan/research>
or call 614-644-8173.*

*Ohio Department of Transportation
Office of Research & Development
1980 West Broad Street
Columbus, OH 43223*

Problem

A new grade of high performance steel has recently been developed that can help reduce costs associated with construction and maintenance of highway bridges. This new grade of steel, designated as HPS-70W, was developed through a cooperative research agreement between the FHWA, the United States Navy, and the American Iron and Steel Institute. The steel has a higher yield strength, improved weathering characteristics, and is much tougher than existing grades of steel. One of the most promising applications for the new steel is in the fabrication of bridge girders. The improved material properties enable engineers to span greater distances, eliminate intermediate piers, alleviate clearance problems, and provide increased resistance to fatigue and corrosion. Currently, HPS is available as plate material produced using a Q&T process. Using this process, the length of plate is limited to approximately 50 feet - a length that is significantly shorter than most bridge girders. A new thermo-mechanical-controlled-process (TMCP) has been developed that allows plates to be rolled in much longer lengths. The focus of this study is to determine if design and fabrication procedures used for HPS-70W Q&T steel are appropriate for HPS-70W TMCP.

Objectives

Before HPS-70W TMCP steel can be widely used, fabrication and design guidelines need to be verified and/or modified. The objectives of the proposed research are to:

1. Verify the mechanical properties of HPS-70W TMCP steel by performing coupon testing of plate material
2. Evaluate the performance of punched and drilled bolt holes in thicker HPS-70W steel plates
3. Examine erection stresses on a bridge constructed of HPS-70W TMCP while the concrete deck is cast to provide data for investigating alternative erection schemes.
4. Verify existing performance criteria by performing load testing of a bridge constructed from HPS-70W TMCP steel.

Description

The project consisted of tensile coupon testing and Charpy V-notch toughness testing of numerous specimens fabricated from 7/8" thick and 2" thick HPS-70W TMCP plates, fatigue testing of dog-bone samples with punched, drilled, and sub-punched and reamed holes to investigate the fatigue resistance of HPS-70W TMCP steel for these details, fatigue testing of samples welded by conventional submerged arc welding (SAW) processes and by newer narrow gap improved electro slag welding (NGI-ESW) processes, field monitoring of girder stresses during concrete deck installation, and periodic field monitoring of service stresses due to truck loads.

Conclusions & Recommendations

During the study, the material properties of HPS-70W were found to be adequate, though some of the samples exhibited a roundhousing phenomenon that resulted in a poorly defined yield point and a 0.2% offset yield stress below ASTM minimums. Some questions remain concerning the influence of plate thickness on toughness. The fatigue performance of samples with punched, drilled, and sub-punched and reamed holes was comparable with what would be expected from conventional HSLA steels. Fatigue resistance of samples welded with SAW and NGI-ESW processes was found to be more than adequate. Finally, field test data showed that current design criteria are appropriate for HPS-70W TMCP but that some gains could be made by considering different screed alignments during deck casting.

Implementation Potential

Based on the results of this study, the authors can conclude that HPS-70W TMCP is ready for broad use in bridges within the state of Ohio and across the nation. Other studies have demonstrated that economic gains can be realized by using this product. The current investigation has shown that current design criteria results in adequate performance based on all measures.

Chapter 1 - Characterization of the Material

Properties of HPS-70W TMCP

1.1 INTRODUCTION

Since first efforts were made towards developing High Performance Steel (HPS) in 1992 through a joint collaboration of the American Iron and Steel Institute (AISI), the Federal Highway Administration (FHWA), and the U.S. Navy, HPS has become increasingly common for bridge girder applications. Because of the higher yield strength associated with ASTM A709 Grade HPS-70W (485W), as well as its increased ductility, toughness, weldability, and improved weathering ability, this newly developed grade of steel is highly attractive for applications in bridges. As a result of its increased strength when compared to conventional 50^{ksi} steel, HPS-70W enables lighter sections to be used, leading to sizeable cost savings in overall construction. Lighter bridge girders often equate to shallower sections, which provide greater clearances for the roads underneath. The reduction of carbon within the chemistry of the steel has produced better toughness and weldability characteristics, which translate to better fatigue details and cost savings. The enhanced weathering capability of HPS-70W is also an attractive feature as reduced corrosion damage translates to lessened life-cycle costs. These benefits have prompted the use of HPS bridge girders to grow considerably - currently there are more than 200 HPS bridges under design or construction in 39 states (AISI 2004).

Length of HPS plate is currently limited by choice of production process, of which there are two available: Quenching and Tempering (Q&T) and a Thermo-Mechanical Controlled Process (TMCP). The Q&T procedure allows plates up to 4" (102 mm) thick to be created in lengths limited to 50' (15 m), which can cause a great deal of undesirable splices in longer girders. HPS-70W can be produced in sheets up to 125' (38 m) in length and 2" (51 mm) thick by using TMCP (ISG 2003). Given the increased plate lengths, this manufacturing process could potentially be a great improvement over Q&T due to the exclusion of splices over a greater

length of material. Because of its recent introduction, there is very little available data concerning the material properties of HPS-70W TMCP. Relatively little is known concerning the effect of this new production method upon the intra-plate variability of both tensile strength and toughness.

As a part of the FHWA's initiative to use innovative materials in bridge design and construction, the Ohio Department of Transportation (ODOT) has constructed a HPS-70W TMCP four-span, five-girder, highway bridge in Lancaster, Ohio. Research concerning that bridge has been ongoing, part of which has been to adequately characterize the HPS-70W TMCP steel used in its construction. Because of the promise that HPS-70W TMCP appears to demonstrate with respect to bridge girder applications, it is important that the behavior of the material, as well as the entire bridge as a structural system, is well understood. This chapter focuses on material aspects of the HPS-70W TMCP bridge girders.

1.2 BACKGROUND

A great deal of attention has been devoted to HPS since its development in 1992, but only a limited amount of research has been directed towards its material properties, most of which has focused on the Q&T-produced grade. Research which has been directed towards HPS-70W TMCP has been primarily investigative in nature; Manganello (1995), Krouse (1999), Focht and Manganello (1996), Bodnar (1995), and Chilton and Manganello (1996) all discussed the efforts to develop a non-Q&T HPS, but none of those early candidates were ever made available to the bridge-building industry. HPS-70W TMCP is currently being used in bridge construction across the United States. Unfortunately, very little literature has been published on the version of HPS-70W TMCP that is currently in production and use.

Early development of a non-Q&T, TMCP, version of HPS-70W failed primarily due to difficulty obtaining the required 70^{ksi} (485 MPa) yield strength. "Roundhousing" problems were encountered, wherein the tensile tests exhibited continuous yielding behavior, and no well-defined yield point was present. When the 0.2% offset method was used to find the apparent yield stress, those values obtained were lower than 70^{ksi} (485 MPa). Bodnar (1995) explained the continuous yield behavior as being caused by the presence of large volume fractions of

bainite. It was suggested by many authors that more work be done to develop a more successful HPS-70W TMCP candidate (Krouse, 1999; Chilton and Manganello, 1996; Focht and Manganello, 1996; Wilson, 1999).

Chen et. al. (2003) performed a study in which tensile strength and toughness of HPS-70W TMCP were examined. Properties for both 1/4" (6.4 mm) and 2" (51 mm) plates were studied. The investigation into the tensile strength of the two plate sizes revealed that the static yield strengths for both plate thicknesses were somewhat below ASTM A709 (2001) specified bounds. The average strength for the 1/4" (6.4 mm) plate was 64.7^{ksi} (446 MPa) with coupons oriented transverse to the direction of rolling and was 63.5^{ksi} (438 MPa) with coupons oriented parallel to the direction of rolling. The average yield strength for the 2" (51 mm) plate coupons (all of which were oriented parallel to the direction of rolling) was found to be 65.7^{ksi} (453 MPa). The average ultimate strength for the 1/4" (6.4 mm) plate was greater than specified minimums; 93.0^{ksi} (641 MPa) transverse to the direction of rolling and 94.7^{ksi} (653 MPa) parallel to the direction of rolling. However, the average ultimate strength for the 2" (51mm) plate was found to be 75.1^{ksi} (518 MPa), which is lower than specified minimums found in ASTM A709 (2001). The investigation also revealed that the 1/4" (6.4 mm) plate was considerably less tough than the 2" (51 mm) plate.

1.3 OBJECTIVES

The objective of this study is to characterize material properties of HPS-70W TMCP. This includes performing tensile and toughness tests, and comparing results to existing ASTM A709 requirements for HPS-70W Q&T.

Tensile and toughness testing are necessary to investigate whether or not this material performs to the same standard as it is held to in design. It is also important to investigate the presence of any notable intraplate variability for either tensile or toughness strength, which could conceivably be an issue due to possible uneven cooling present in TMCP production as opposed to the more uniform cooling found in Q&T.

1.4 EXPERIMENTAL SETUP

Two large HPS-70W TMCP plates were obtained from Bethlehem Steel, one $\frac{7}{8}$ " (22 mm) thick and the other 2" (51 mm) thick, for the purpose of fabricating the flanges of the Lancaster bridge girders, as well as supplying enough steel with which to perform adequate material testing. Gross dimensions of the plates were 6'-0" x 66'-11" x $\frac{7}{8}$ " (1.8 m x 20.4 m x 22 mm) and 5'-11" x 104'-6" x 2" (1.8 m x 31.9 m x 51 mm). The two large HPS plates were cut into multiple smaller plates, from which the bridge girder flanges were cut. Tensile and Charpy V-Notch (CVN) specimens were machined. Dimensions of the plates, as well as the location of the CVN and tensile specimens are shown in Figure 1-1. The CVN and tensile specimens were taken in groups from each location with three CVN samples being cut from each location, and the number of tensile specimens varying between three and four.

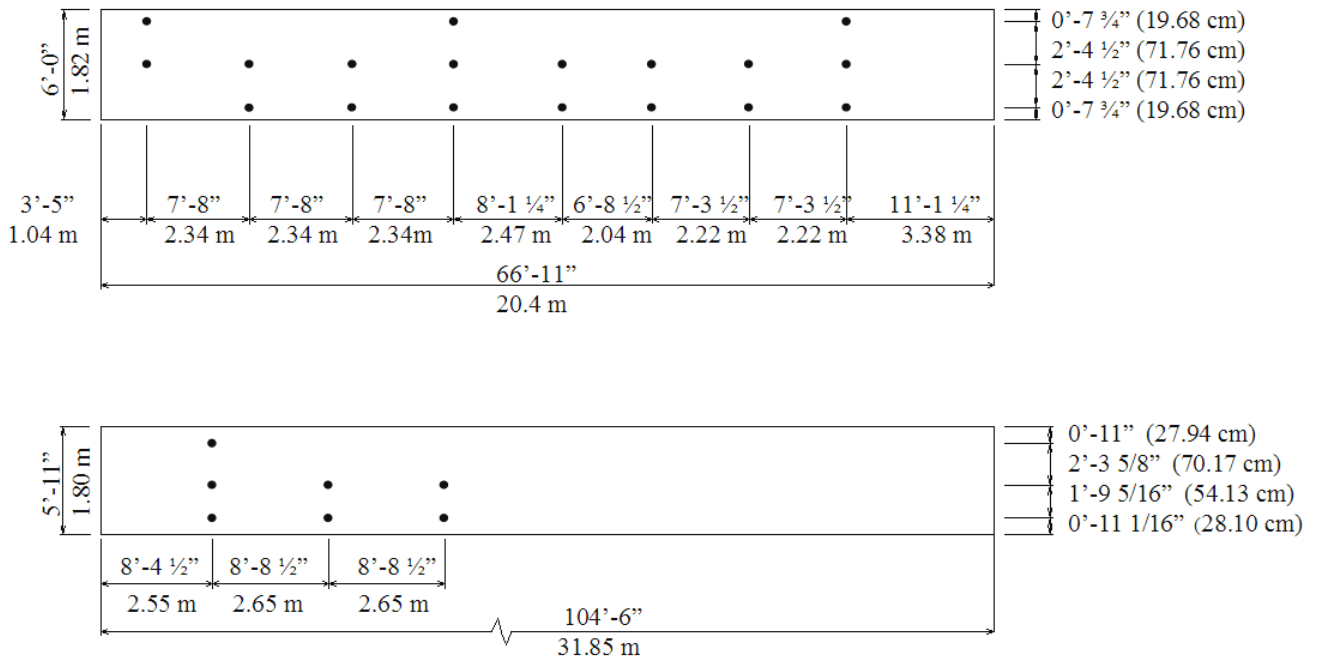


Figure 1-1: Sample Locations of Specimens from $\frac{7}{8}$ " (22 mm) and 2" (51 mm) Plates (not to scale)

A total of 96 tensile tests were completed to investigate characteristics of the material's stress-strain curves and to examine differences in strength due to thickness, plate orientation, and location. 75 CVN tests were performed to determine if HPS-70W TMCP meets the toughness

requirements set forth by ASTM A709, and to investigate any variation in toughness within the two plates.

1.4.1 Tensile Testing

To examine the effect of plate thickness on tensile strength and variability, 70 of the 96 tensile coupons were machined from $\frac{7}{8}$ " (22 mm) thick plate, while the remaining 26 specimens originated from 2" (51 mm) thick plate. 35 of the $\frac{7}{8}$ " (22 mm) thick coupons were oriented such that their longitudinal axis was transverse to the direction of rolling, with the other 38 specimens oriented parallel to the direction of rolling. The 2" (51 mm) thick coupons were divided such that 12 were oriented transverse to rolling, and 14 oriented parallel to the direction of rolling. The governing specification for tensile testing was ASTM E8 (2001). A sheet-type coupon was chosen for the shape of all tensile tests, as is shown in Figure 1-2.

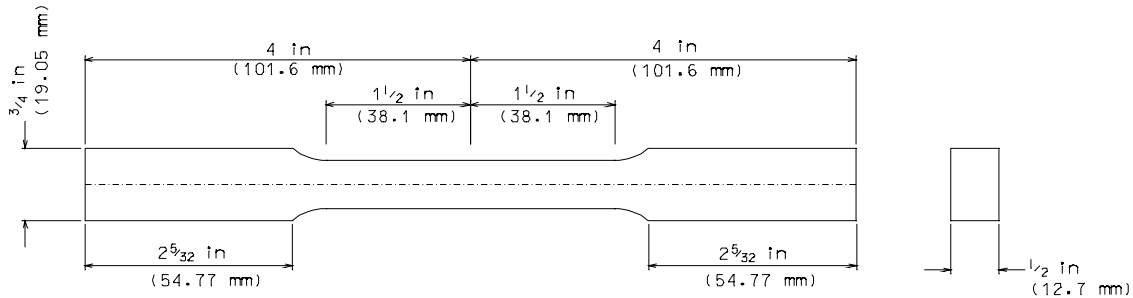


Figure 1-2: ASTM-E8 Sheet-Type Coupon Specimen, Dimensions Typical for All Tensile Tests

Tensile specimens were tested in a MTS 312 load frame, with a maximum load capacity of 55^{kip} (245 kN) and a 50^{kip} (220 kN) capacity load cell. A strain-extensometer with a range of +/-500,000 $\mu\epsilon$ was used to measure strain in the specimens. The coupons were tested axially under stroke control, loaded at a rate of 0.015" (0.38 mm) per minute (corresponding to an elastic rate of 50^{ksi} (345 MPa) per minute), up to 0.10" (2.54 mm) of stroke displacement, upon which the loading rate was increased to 0.13" (3.30 mm) per minute until fracture (Dues et al. 2002).

The load rate of 0.015ⁱⁿ/_{min} (0.38^{mm}/_{min}) up to and through the onset of yield is in accordance with ASTM E8 (2001) and ASTM A370 (2002), which require a stress rate between 10^{ksi}/_{min} (68.9^{MPa}/_{min}) and 100^{ksi}/_{min} (689^{MPa}/_{min}), the former of which states that "The speed of the

testing machine shall not be increased in order to maintain a stressing rate when the specimen begins to yield. In practice, it is simpler to use either a strain rate, a rate of separation of the heads, or a free-running crosshead speed which approximates the desired stressing rate” (ASTM E8 2001). After yielding was reached, the strain rate was increased to $0.13^{\text{in}}/\text{min}$ ($3.30^{\text{mm}}/\text{min}$), which is less than the ASTM E8 suggested rate of $0.05 - 0.5^{\text{in}}/\text{in}$ ($1.27 - 12.7^{\text{mm}}/\text{mm}$) of the reduced section per minute, corresponding to a rate $0.15 - 1.5^{\text{in}}/\text{min}$ ($3.81 - 38.1^{\text{mm}}/\text{min}$) for the 3” (76.2 mm) reduced section being examined. While this discrepancy should be recognized, it must also be noted that the slightly slower test rate used affects only the ultimate strength results, and will always provide more conservative results than if a faster test rate was used. This point will be discussed further in the results section, and it will be shown that the experiment’s validity did not suffer as a result of this incongruity.

A stress-strain diagram was plotted for each tensile coupon, and from these plots, the coupons’ moduli of elasticity, dynamic yield stresses, static yield stresses, dynamic ultimate strengths, static ultimate strengths, and percent elongations were determined. The modulus of elasticity, E , was determined by fitting a straight line to the data points composing the elastic portion of the stress-strain diagram, up to the data point corresponding with approximately 50% of the mill-certified yield strength. This limitation helped to ensure that the modulus of elasticity was indeed being calculated within the elastic region of the curve. The 0.2% offset method was used to determine the dynamic yield stress, F_{yd} . The static yield stress, F_{ys} was found for each specimen to provide a more normalized comparison between these tensile tests and those performed by others. Strain was held constant for 30 seconds twice during the testing to establish the difference between dynamic and static stresses. These two differences were then averaged, finding $(\sigma_d - \sigma_s)$ for each coupon. The static yield stress was then calculated by subtracting this difference, $(\sigma_d - \sigma_s)$, from the dynamic yield stress, F_{yd} , as shown in Equation 1-1.

$$F_{ys} = F_{yd} - (\sigma_d - \sigma_s) \quad (1-1)$$

The dynamic ultimate strength, F_{ud} , of each coupon was taken as the maximum stress resisted by that coupon during loading. The same methodology used to find the static yield stress was used to determine static ultimate strength, F_{us} . Here the quantity $(\sigma_d - \sigma_s)$ was subtracted from F_{ud} , as shown in Equation 2-1.

$$F_{us} = F_{ud} - (\sigma_d - \sigma_s) \quad (1-2)$$

Finally, percent elongation was measured for each specimen, using two sets of center-punched gage marks for each sample (Dues et al. 2002). The distance between the gage marks for both pairs was measured before and after testing; two sets of marks were used in case fracture were to occur at one of the marks.

1.4.2 Toughness Testing

To examine plate toughness, 75 CVN specimens from the HPS-70W TMCP plates were tested in accordance with ASTM E23 (2001) and ASTM A-370 (2001). 54 of the toughness specimens were cut from the $\frac{7}{8}$ " (22 mm) plate, while the remaining 21 were taken from the 2" (51 mm) plate; all were oriented parallel to direction of rolling. The 75 CVN specimens were tested at -10°F (-23°C) to facilitate an easy comparison to the AASHTO-LRFD Zone III requirement for 35 ft-lbs (48 J) of impact resistance at -10°F (-23°C) (AASHTO 1998). The specimens were taken in groups of three from various locations along the length and width of the two large plates, as shown in Figure 1-1, which closely corresponded to locations for the tensile specimens from those same plates. It was hoped that, as for the tensile specimens, by cutting the toughness specimens from varying locations along the HPS-70W plate, a general trend could be established for variation of toughness across or along a plate.

1.5 RESULTS AND DISCUSSION

1.5.1 Tensile Testing

Averaged tensile test results for each of the measured parameters are shown in Table 1-1. They show that the average static and dynamic yield stresses are both below the 70^{ksi} (485 MPa) minimum set forth by ASTM A709 (2001) for HPS-70W. The low yield stresses can partially be explained by a relatively low (yet ASTM E-8 acceptable) stroke test rate through the yield region. Low testing rates provide conservative values for strengths. Unfortunately, ASTM A709 (2001) provides both upper and lower bounds for the rate of crosshead separation within which tensile tests are deemed acceptable. This creates a problematic situation when comparing results to other work, for test rates are rarely published along with the tensile results. Therefore, although these yield stresses appear to be low, it is difficult to accurately compare them to

previous work, or even to mill certificates that describe tensile properties of the original plates, as are shown in Table 1-2 and Table 1-3. Static yield stresses can be calculated if the specimens are held in strain control to provide consistent information for the sake of comparison, but static yield values are also often not published in previous work; the values required by ASTM are for dynamic testing only. For these reasons, the rate of crosshead separation used here is a poor explanation for the low yield stresses. For the results to be ASTM acceptable, they must pass at any test rate within the aforementioned limits, including the more conservative values near the lower bound that were used herein.

Table 1-1: Average Tensile Testing Results

	E ksi (Gpa)	F_{yd} ksi (Mpa)	F_{ys} ksi (Mpa)	F_{ud} ksi (Mpa)	F_{us} ksi (Mpa)	% Elongation
Average Experimental Values	30,958 (214)	68.2 (470)	65.0 (448)	95.1 (656)	91.9 (634)	27.4
ASTM A709 Required Values for HPS-70W	--	70.0 (485)	--	85.0 - 110 (585-760)	--	19.0
Standard Deviation	874 (6.0)	5.3 (37.0)	5.4 (37.0)	3.0 (21.0)	3.0 (21.0)	3.5
Coefficient of Variation	2.80%	7.90%	8.30%	3.20%	3.30%	12.80%

A more reasonable explanation for the low yield stresses become apparent when tensile results are examined in relation to the thickness of the plates from which they originated. The average yield strength for the 7/8" (22 mm) plate was found to be 71.1^{ksi} (490 MPa) and the average yield strength for the 2" (51 mm) plate was 60.2^{ksi} (415 MPa). The difference between the results from the 7/8" (22 mm) plate and the 2" (51 mm) plate is quite significant - 10.9^{ksi} (75.1 MPa), or a 15.3% difference. Upon examination of the 2" (51 mm) plate coupons, it can be seen that almost all of the specimens exhibited roundhousing, or continuous yielding behavior, as is shown in Figure 1-3. Very few of the 7/8" (22 mm) coupons exhibited the same phenomena, with a typical stress-strain diagram for those coupons shown in Figure 1-4. Comparison of these data shows that there may be some inherent difficulties in the TMCP method when producing plates of greater thickness.

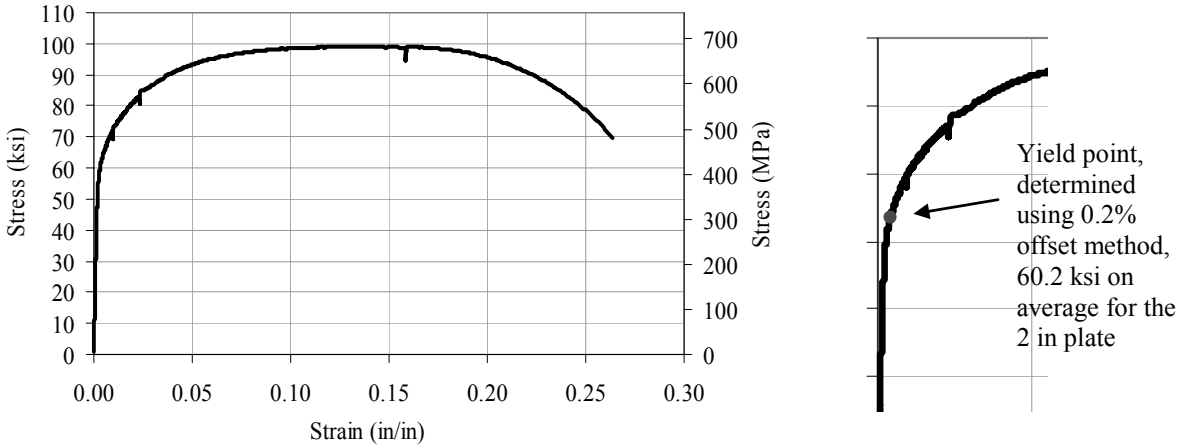


Figure 1-3: Typical Stress-Strain Curve for TMCP 70W Coupon from 2" (51 mm) Plate

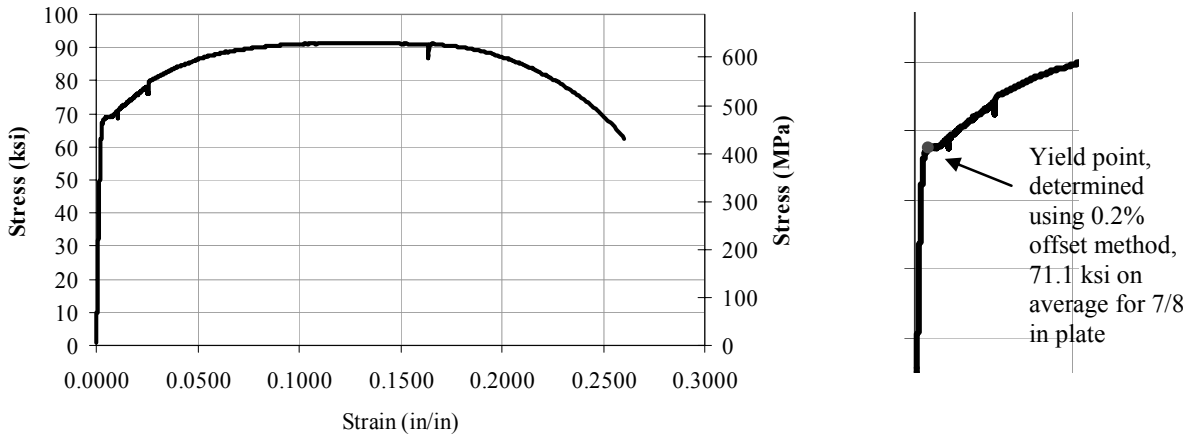


Figure 1-4: Typical Stress-Strain Curve for TMCP 70W Coupon from 7/8" (22 mm) Plate

The ultimate strengths for both plate thicknesses, however, fell within reasonable limits. ASTM A709 (2001) imposed limits are 85-110^{ksi} (585-760 MPa), and measured averages for dynamic and static ultimate strengths were found to be 95.1^{ksi} (656 MPa) and 91.9^{ksi} (634 MPa), respectively. It is doubtful that a higher rate of crosshead separation would cause the average ultimate strength to exceed the 110^{ksi} (760 MPa) limit, but testing should be conducted at the high end of the ASTM E8 test rate range to verify this hypothesis. Thus, even with the conservative test rate used for the post-yield regions, ultimate strengths lie within an acceptable range according to ASTM A709 (2001). Other independent research performed by Chen et. al. (2003) also discovered low yield strength for HPS-70W TMCP.

Mill certificates (Table 1-2 and Table 1-3) reported higher values for yield and ultimate strengths of both plates than were found in this study, providing an average yield strength of 81.8^{ksi} (564 MPa) for the 7/8" (22 mm) plate, which is 13.1% higher than the experimental results of the current study, and 80.9^{ksi} (558 MPa) for the 2" (51 mm) plate, which is 25.6% higher than the results determined in this study. It should be noted that plate producers are generally perceived to test at the upper end of the ASTM test rate range, which may explain this discrepancy.

Remaining tensile properties measured for this investigation also fell within acceptable limits. The coupons exhibited excellent ductility characteristics; percent elongation was experimentally found to be 27.4%, which is 44% larger than the ASTM A709 (2001) required 19% elongation. The modulus of elasticity was also found to be reasonable, at 30,958^{ksi} (213 GPa).

An interesting phenomenon occurs when coupon strengths are examined in relation to the orientation of those coupons. Orientation of the coupon has a discernible effect upon the strength of the specimen, and is more notable for yield strength than ultimate strength, as is shown in Figure 1-5. For almost all cases, coupons cut transverse to the direction of rolling exhibited higher strengths than those cut parallel. One possible explanation for this occurrence might be that the microstructure tends to align itself perpendicular to the direction of rolling during the cooling process (Dues et al. 2002). There is a larger disparity in yield strength between the two orientations than there is for ultimate strength; a 4.2% difference in yield strength exists between transverse and parallel coupons, while there is a 1.5% difference in ultimate strengths of those same coupons.

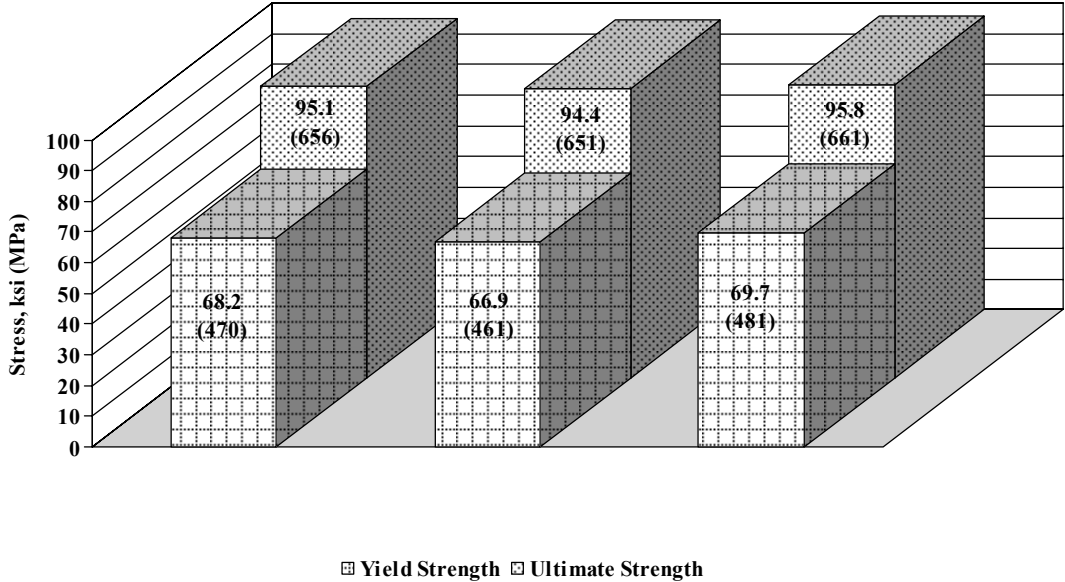


Figure 1-5: Coupon Strength Averages for Orientation Parallel and Transverse to the Direction of Rolling

It has been questioned whether the cooling process inherent in TMCP causes any intraplate variation across the plates' dimensions. Upon examination, the data does show noticeable intraplate variation in yield and ultimate strengths for both the 7/8" (22 mm) and the 2" (51 mm) plates, shown in Figure 1-6 and Figure 1-7. For both thicknesses, the HPS-70W TMCP plates exhibit higher yield and ultimate strengths towards the plate edges than they do along their central longitudinal axis. For a majority of the cases, minimum strengths were found to lie along the centerline of the plates' longitudinal axes, while higher tensile strengths were observed to lie nearer the plates' width boundaries, leading to a "cupped" shape for the tensile stress distribution across the plates' widths. This trend is manifested most clearly by ultimate strengths of coupons taken from plates of both thicknesses, but is also valid for the yield strengths. Also, while the "cupped" tensile stress distributions are more apparent for the 7/8" (22 mm) plate than for the 2" (51 mm) plate because of the larger number of samples, a similar trend can be identified for the 2" (51 mm) plate tensile stress distributions, where, except for a single data point, the centerline tensile strengths are lower than those along the edge.

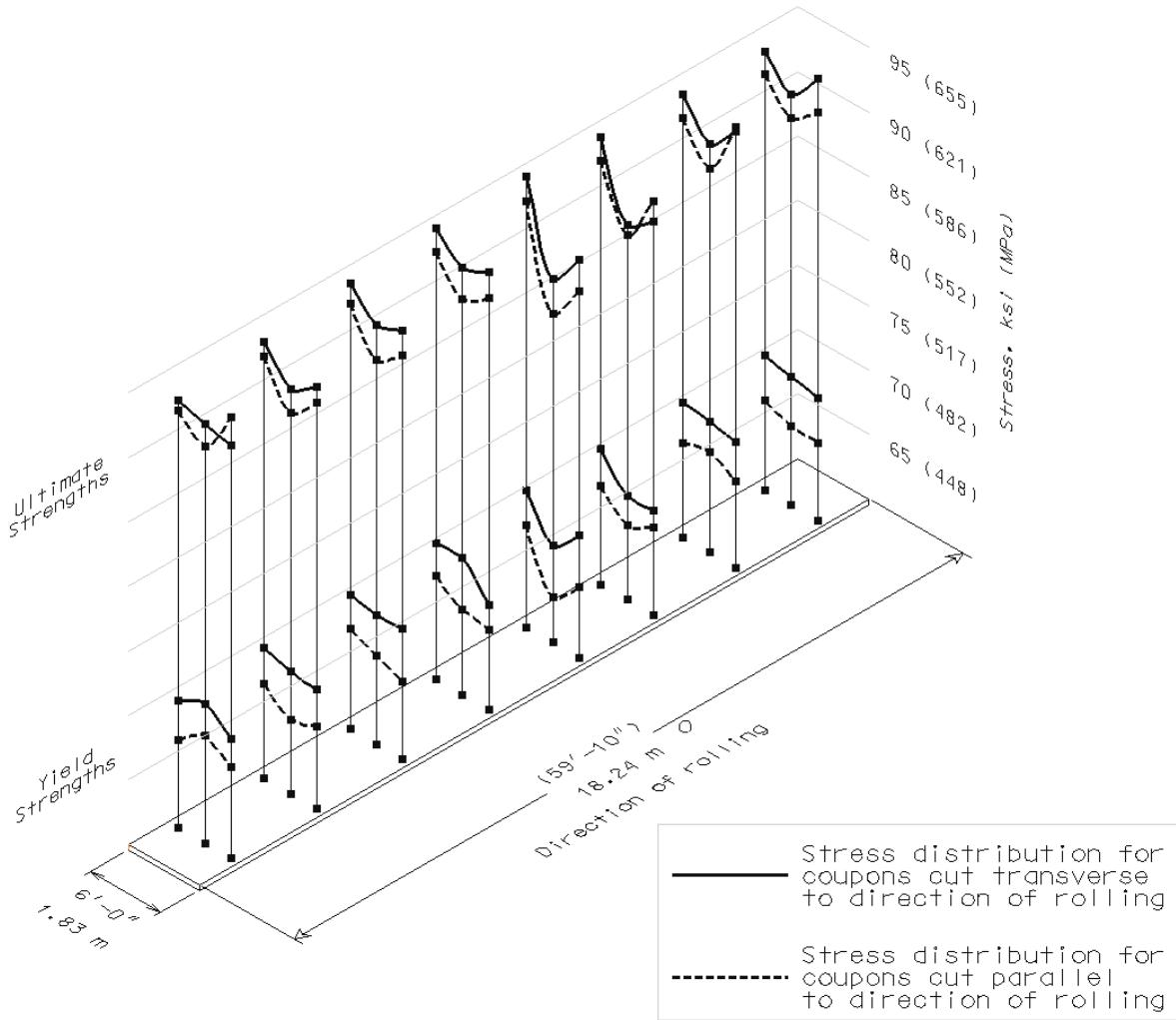


Figure 1-6: Tensile Stress Distribution over Cross-Sections of $\frac{7}{8}$ " (22 mm) Thick Plate

It should be noted that five of the data points on the far edge of the $\frac{7}{8}$ " (22 mm) plate, shown in Figure 1-6, were not directly measured from experimental data, but were interpolated from three other data points lying in the same rear line of sampling locations. The inclusion of the interpolated points enabled examination of a greater number of complete stress distributions for the $\frac{7}{8}$ " (22 mm) plate. Only one data point was available in the rear line of samples for the 2" (51 mm) plate so interpolation was not possible. Therefore, Figure 1-7 shows one three-point stress distribution and two two-point distributions.

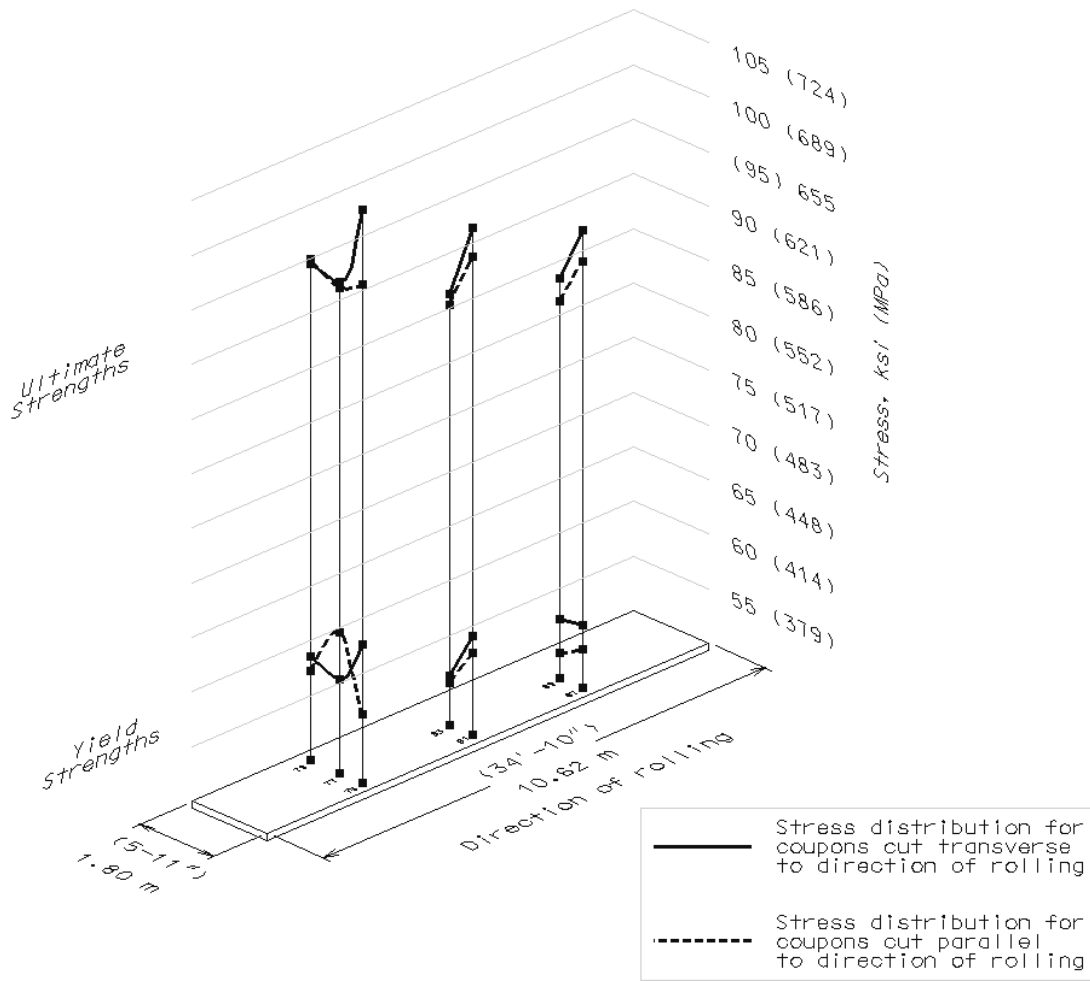


Figure 1-7: Tensile Stress Distribution over Cross-Sections of 2" (51 mm) Thick Plate

1.5.2 Toughness Testing

Three CVN samples were machined from each small plate cut from the two large, rolled plates (Figure 1-1). The three results at each particular location were averaged to plot the results along the plate dimensions, as is shown in Figure 1-8 for the $\frac{7}{8}$ " (22 mm) plate and in Figure 1-9 for the 2" (51 mm) plate. The average toughness for the $\frac{7}{8}$ " (22 mm) plate was found to be 139 ft-lbs (188 J) with a standard deviation of 31.4 ft-lbs (42.6 J), and the average toughness for the 2" (51 mm) plate was seen to be 85.1 ft-lbs (115 J) with a standard deviation of 27.4 ft-lbs (37.1 J). 68% of all the CVN specimens fell within one standard deviation of the mean, and 96% of the total test sample fell within two standard deviations of the mean.

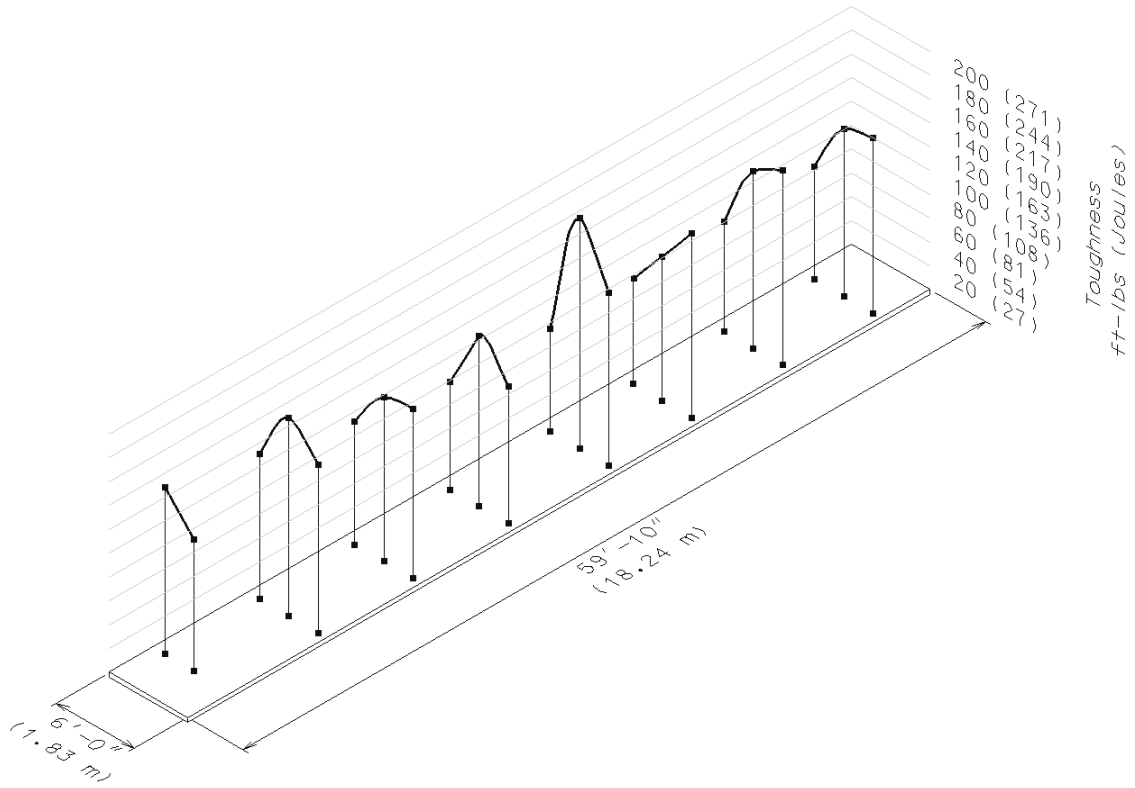


Figure 1-8: Toughness Distribution over Cross-Sections of $\frac{7}{8}$ " (22 mm) Plate

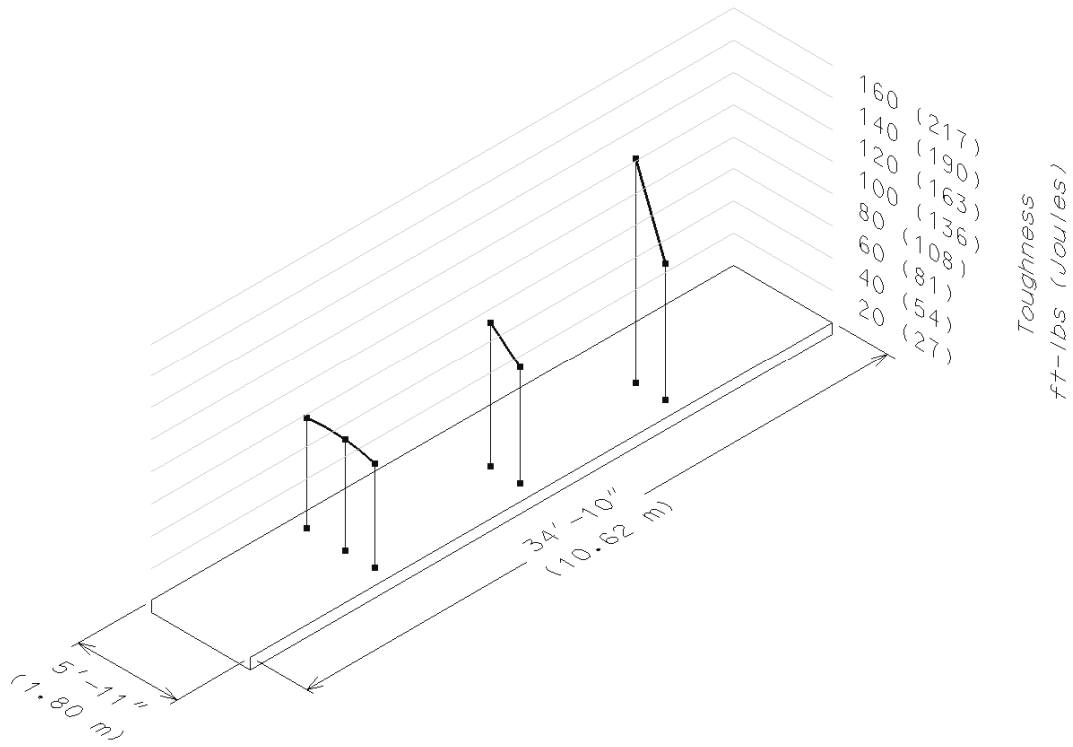


Figure 1-9: Toughness Distribution over Cross-Sections of 2” (51 mm) Plate

While both of these averages well exceed the AASHTO-LRFD (1998) required value of 35.0 ft-lbs (48.0 J) at -10°F (-23°C), it shows a potential limitation of TMCP, as well as why plate thickness created by this process is currently constrained to 2” (51 mm). If the current results are linearly extrapolated to obtain a fictional toughness strength for a 3” (76mm) thick plate, a toughness of 37.5 ft-lbs (50.8 J) is obtained; if extrapolated further to explore a potential 4” thick plate, a negative value for the toughness is obtained. The latter case is obviously under strength with respect to the AASHTO requirements, but even the fictional 3” (76 mm) plate with its apparent “passing” toughness of 37.5 ft-lbs (50.8 J) is close enough to the limiting envelope to potentially be unreasonable without further refinement to the TMCP process.

As there were more samples taken from the 7/8” (22 mm) plate than for the 2” (51 mm) plate (Figure 1-1), a more complete distribution was obtained for the former, but again, a similar trend can be noted for both cases, as is shown in Figure 1-8 and Figure 1-9. As was the case for the tensile data, four data points lying in the rear line of sampling locations in Figure 1-8 were interpolated from the other three data points lying within that same section in order to obtain a

more complete plot. Distributions for both plate thicknesses suggest a concave down shape across the cross-section of the plates, where the maximum toughness strength is found along the centerline of the plates' longitudinal axes, and the minimum toughness strengths exist on the edges.

The shape of the toughness distribution is worthy of note, because it is exactly opposite from that for tensile strength distribution. This suggests that there is an inverse relationship between tensile and toughness strengths for these specimens; as tensile strength increases, toughness decreases, with the opposite holding true as well. Bodnar (1995) attributed a similar inverse relationship to the presence of bainite in his progress report on as-rolled Nb-V weathering steel for bridge applications. This seems to be a reasonable conclusion for the cause of the inverse relationship seen in the present study as well. Bodnar also attributed low yield strengths seen in that investigation to the presence of large fractions of bainite; the same issue has occurred in this research, as well. Although the 2" (51 mm) plate coupons exhibited low yield stresses, they also exhibited the highest ultimate strengths and the lowest toughness strengths. Further study should be performed on current HPS-70W TMCP to determine whether bainite is the root cause of low yield strength and toughness in the thicker plates.

1.6 CONCLUSIONS

HPS-70W TMCP is a promising grade of bridge steel, but its usefulness seems to be limited by plate thickness. Experimentally, it meets or exceeds many of the required properties for the Q&T grade described in ASTM A709, regardless of plate thickness. It certainly meets the requisites for toughness and ultimate strength, and the intra-plate variability of tensile strength and toughness for the thicknesses tested does not seem to be a great concern. However, HPS-70W TMCP does not meet the same yield strength criterion as is posed for the HPS-70W Q&T when examining the 2" plate. The experimentally found average dynamic yield strength of 68.2^{ksi} (470 MPa) is below the required 70^{ksi} (485 MPa), and this should be recognized by designers and dealt with in the steel-making industry. Further research should be conducted to determine the cause of the roundhousing phenomena in thicker plates.

Chapter 2 - Fatigue Behavior of Bolted Splices in HPS-70W

2.1 INTRODUCTION

High performance steel (HPS) is increasingly being used for new bridge construction because of its improved properties over conventional structural steel. In particular, ASTM A709 Grade HPS-70W (485W) has found a niche amongst designers wishing to capitalize on its high yield strength, increased ductility, toughness, weldability, and improved weathering characteristics. Possessing a higher yield strength than conventional 50^{ksi} (345 MPa) structural steel, HPS-70W has allowed shallower girders to be constructed, leading to both weight savings and increased clearances. A decrease in the carbon content within the chemical makeup of HPS-70W has led to increases in toughness and better weldability characteristics. The corrosion resistance of HPS is also an appealing feature, due to reduced life-cycle costs. Currently, over 200 HPS bridges have been designed or constructed in 39 different states (AISI 2004).

While HPS-70W is marketed as being more resistant to fatigue than conventional bridge steel, it is currently still held to the same fatigue design standards in AASHTO (2004). It is possible that these standards may be more restrictive than necessary with respect to HPS-70W, impairing designers' abilities to fully capitalize upon its increased strength. For this reason, it is important that testing be conducted to quantify the fatigue resistance of HPS-70W. In addition to this, many state Departments of Transportation (DOTs) currently do not allow punching of holes in any structural steel primary member greater than 0.625" (15.875 mm) thick, instead requiring that the holes be drilled or sub-punched and reamed (ODOT 2002; INDOT 1999; MDOT 2003; ILDOT 2002). It is necessary to examine different methods for creating holes to evaluate the current DOT restrictions in lieu of the increased fatigue resistance of HPS-70W.

As a part of the FHWA's initiative to use innovative materials in bridge design and construction, the Ohio Department of Transportation (ODOT) has constructed a four-span, five-girder, highway bridge in Lancaster, Ohio, made of HPS-70W TMCP. Research concerning that

bridge has been ongoing, part of which has focused on adequately characterizing the fatigue properties of HPS-70W used in its construction. Because HPS-70W appears to demonstrate promise with respect to bridge girder applications, it is important that the behavior of the material, as well as the entire bridge as a structural system, is well understood. This paper focuses on fatigue characteristics of HPS-70W bolted splice connections.

2.2 BACKGROUND

A great deal of attention has been devoted to HPS since its development in 1992, but comparatively little work has been done to quantify its performance under fatigue. There is a copious amount of published work mentioning that HPS-70W exhibits better fatigue resistance properties than conventional bridge steel does (Wassef et al. 1996; Kulicki 2000; Yakel et al. 1999; Barsom 1997), but little independent experimental work has been performed to support these claims.

A study was performed by Wright (2002), in which fracture tests were performed on full-scale HPS-70W I-girders. The girders were cyclically loaded until fatigue cracks formed, upon which they were cooled to -29.2°F (-34°C), and then finally were subjected to a typical design overload. The HPS-70W test girders were able to carry the overload until approximately 50% of the tension flange was lost, corresponding to net section stress levels exceeding yield before failure. This result compared favorably to similar test girders fabricated of Grade 50 (345) steel, which exhibited lower crack-size tolerance and fracture at stress levels at approximately 60% of yield on the net section.

Chen et al. (2003) recently performed a study which concluded that “The HPS-70W steel tested provides a significantly higher fatigue limit than conventional structural steels.” However, that study did not consider specific connection details, examining only flat sheet-type fatigue specimens. The study compared cyclic and monotonic properties of high performance steel against that of lower strength structural steel (Grade A7). The specimens examined in this study were machined from $\frac{1}{4}$ ” (6.4 mm) and 2” (51 mm) HPS plates. Specimens were fatigued under strain amplitudes varying from 0.1% to 0.625%, and failure was considered as having occurred

when the tensile load decreased by 50%. Tests were also conducted on 0.25" (6.4 mm) ASTM A7 plate as a basis for comparison.

2.3 OBJECTIVES

One goal of this ongoing research is to quantify the fatigue resistance of HPS-70W in a bolted splice connection, which is a detail commonly used in steel bridge construction. To adequately characterize the fatigue characteristics of this connection configuration it is important that geometric properties of the specimens are considered, including hole diameter, thickness, and surface roughness.

Many state departments of transportation (DOTs) currently require that material thicker than $\frac{5}{8}$ " (15.9 mm) be drilled or sub-punched and reamed rather than simply being punched to create the holes. This mandate may increase fabrication time if the processes are not entirely automated, and it is reasonable to hypothesize that with the increased toughness of HPS and the improved efficiency of punching machines that this requirement may be more conservative than necessary. One goal of this research is to determine if the maximum thickness of $\frac{5}{8}$ " (15.9 mm) for punching is an appropriate upper limit for HPS-70W.

2.4 EXPERIMENTAL SETUP

Two large HPS-70W TMCP plates were obtained from Bethlehem Steel, one $\frac{7}{8}$ " (22 mm) thick and the other 2" (51mm) thick, for the purpose of fabricating the flanges of the Lancaster bridge girders, and to supply steel for adequate material testing. Gross dimensions of the plates were 6'-0" x 66'-11" x $\frac{7}{8}$ " (1.8 m x 20.4 m x 22 mm) and 5'-11" x 104'-6" x 2" (1.8 m x 31.9 m x 51 mm). The two large HPS plates were cut into multiple smaller plates, from which the bridge girder flanges were cut. 29 bolted splice fatigue specimens were machined from the remaining steel.

The fatigue specimens all had similar edge dimensions, which are shown in Figure 1-1. These specimens were created to examine a bolted splice connection, which is considered to be a Category B detail by AASHTO (2004). However, plate thickness, hole diameter, and method of

hole creation were varied to examine the effects of differences in geometry and hole creation processes on the fatigue strength of the bolted splices. Details for each specimen are shown in Table 2-1. Each specimen had three holes along the length of the reduced section, with each of the holes produced by one of three hole creation processes: punching, drilling, or sub-punching and reaming. The plates were machined from their initial thickness to their final thickness before the holes were made.

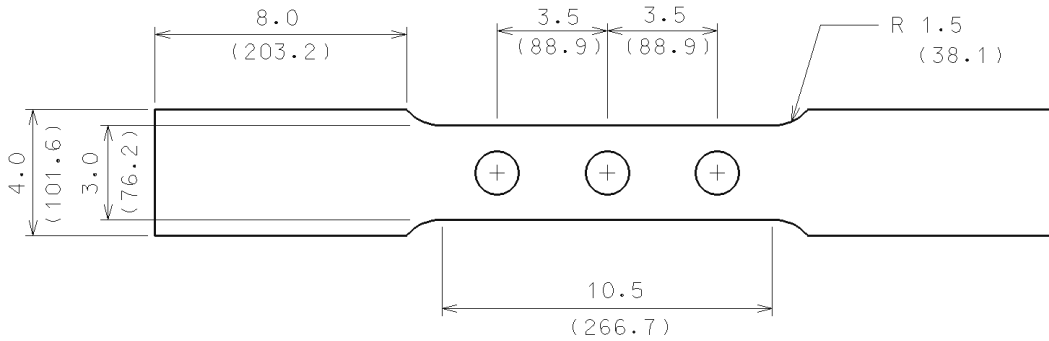


Figure 2-1: Dimensions of Bolted Splice Fatigue Specimens, in (mm)

Each fatigue specimen was tested at a stress range of either 16.0^{ksi} (110 MPa) or 22.9^{ksi} (158 MPa). The first stress range of 16.0^{ksi} (110 MPa) was chosen as it is the constant-amplitude fatigue threshold (infinite life stress range) for a Category B detail. Six of the 29 specimens were tested at this stress range, all having punched holes. The second stress range of 22.9^{ksi} (158 MPa) was chosen as it corresponds to a 1,000,000 cycle fatigue life for a category B detail, and was calculated using the AASHTO (2004) equation:

$$\Delta F_n = \left(\frac{A}{N} \right)^{\frac{1}{3}} \geq \frac{1}{2} (\Delta F)_{TH} \quad (2-1)$$

where: ΔF_n is the stress range, A is a constant for a given detail defined by AASHTO (2004), N is the number of fatigue cycles to failure, and $(\Delta F)_{TH}$ is the constant-amplitude fatigue threshold. For a Category B detail, A is $1.2 \times 10^{10} \text{ ksi}^3$ ($39.3 \times 10^{11} \text{ MPa}^3$). The equation is an approximation of logarithmic behavior, with a coefficient of $\frac{1}{3}$ defining the slope constant for the S-N curves. The presence of the one-half factor on the right hand side of Equation 2-1 ensures that when the design stress range is less than one-half of the constant-amplitude fatigue

threshold, the detail will theoretically provide infinite life (AASHTO 2004). 22 of the specimens were tested at the 22.9^{ksi} (158 MPa) stress range, with one specimen (Specimen 1) inadvertently tested at a stress range of 23.9^{ksi} (164.8 MPa).

Table 2-1: Bolted splice fatigue specimen descriptions

Test ID	Hole Diameter in (mm)	Thickness in (mm)	Hole	Target Stress MPa (ksi)
1	0.9375 (23.8)	0.625 (15.9)	Punched	23.9 (164.8)
2	0.9375 (23.8)	0.750 (19.1)	Punched	22.9 (157.9)
3	0.9375 (23.8)	0.875 (22.2)	Punched	22.9 (157.9)
4	1.0625 (27.0)	0.625 (15.9)	Punched	22.9 (157.9)
5	1.0625 (27.0)	0.750 (19.1)	Punched	22.9 (157.9)
6	1.0625 (27.0)	0.875 (22.2)	Punched	22.9 (157.9)
7	1.1875 (30.2)	0.875 (22.2)	Punched	16.0 (110.3)
8	1.0625 (27.0)	1.000 (25.4)	Punched	22.9 (157.9)
9	1.0625 (27.0)	1.000 (25.4)	Drilled	22.9 (157.9)
10	1.0625 (27.0)	1.000 (25.4)	Punched	16.0 (110.3)
11	1.1875 (30.2)	0.625 (15.9)	Punched	22.9 (157.9)
12	1.1875 (30.2)	0.625 (15.9)	Reamed	22.9 (157.9)
13	1.1875 (30.2)	0.750 (19.1)	Punched	22.9 (157.9)
14	1.1875 (30.2)	0.750 (19.1)	Reamed	22.9 (157.9)
15	1.1875 (30.2)	0.750 (19.1)	Punched	16.0 (110.3)
16	1.1875 (30.2)	0.875 (22.2)	Punched	22.9 (157.9)
17	1.1875 (30.2)	0.875 (22.2)	Reamed	22.9 (157.9)
18	1.1875 (30.2)	0.875 (22.2)	Drilled	22.9 (157.9)
19	1.1875 (30.2)	1.000 (25.4)	Punched	22.9 (157.9)
20	1.1875 (30.2)	1.000 (25.4)	Reamed	22.9 (157.9)
21	1.1875 (30.2)	1.000 (25.4)	Drilled	22.9 (157.9)
22	1.1875 (30.2)	1.000 (25.4)	Punched	16.0 (110.3)
23	1.2500 (31.8)	0.625 (15.9)	Punched	22.9 (157.9)
24	1.1875 (30.2)	0.625 (15.9)	Punched	16.0 (110.3)
25	1.2500 (31.8)	0.750 (19.1)	Punched	22.9 (157.9)
26	1.2500 (31.8)	0.875 (22.2)	Punched	22.9 (157.9)
27	1.2500 (31.8)	1.000 (25.4)	Punched	22.9 (157.9)
28	1.2500 (31.8)	1.000 (25.4)	Drilled	22.9 (157.9)
29	1.2500 (31.8)	1.000 (25.4)	Punched	16.0 (110.3)

There are two primary approaches to performing fatigue testing. The first approach is to test a number of identical specimens at different stress ranges, allowing the data points to define a curve on an S-N diagram. This procedure is suitable when identical specimens are being examined for fatigue strength. The second method, the technique employed in the current study, is to test several different types of specimens at the same stress range. This method is more appropriate for the current investigation because it lends itself to easy comparisons between the

different types of specimens. The results for various types of specimens are more likely to stand apart, resulting in more meaningful data presentation.

Each specimen was tested in a MTS 312 universal testing frame having a maximum load capacity of 55^{kip} (245 kN) and containing a 50^{kip} (220 kN) capacity load cell. The fatigue specimens were tested in load control under tension force only, and were preloaded to a lower load (LL) of 0.50^{kip} (2.22 kN) to ensure that they remained in tension. The upper load (UL) for the tensile range was calculated as:

$$UL = LL + \Delta F_n \times A_{net} \quad (2-2)$$

where: ΔF_n was either 16.0^{ksi} (110 MPa), 22.9^{ksi} (158 MPa), or 23.9^{ksi} (164.8 MPa) and A_{net} was taken as the average net area at the three holes, not including the extra $\frac{1}{16}$ " (1.59 mm) that is traditionally added to account for damaged material around the hole. The test setup is shown in Figure 2-2. Specimens were loaded sinusoidally at a rate of 2 Hz until either failure or infinite fatigue life was achieved. Crack detection settings were defined in the software controlling the MTS machines to recognize failure, and were kept as precise as possible in order to detect cracks in early stages of formation. The intent of this approach was to cause the machine to cease cycling upon formation of a crack, detected by a stroke limit setting. Infinite fatigue life was taken as approximately 2.3 million cycles, which is approximately the point at which the AASHTO (2004) fatigue design curve for a Category B becomes a straight line. Specimens that reached infinite life were subsequently removed from the test setup.

Bolts were not placed in the three holes due to multiple considerations. First, there was concern that by installing tensioned bolts, localized compression might be introduced into the area surrounding the holes, lessening the effect of fatigue which was being applied in tension. Omitting the bolts from the test setup was conservative. Secondly, there has recently been some interest in the fatigue performance of holes in bridge members without bolts. It is not uncommon for bolts that are used for fit-up purposes during construction to be removed before the bridge is placed into service, leaving behind empty holes. Fatigue properties for such regions are not well understood.



Figure 2-2: Test Set-Up

2.5 RESULTS AND DISCUSSION

Summary results for the 29 bolted splice fatigue specimens are shown in Table 2-2. Data has also been plotted on a standard AASHTO (2004) S-N diagram in Figure 2-3. Each data point was assigned the appropriate fatigue category (A, B, B', C, D, E, or E') by calculating the AASHTO (2004) constant A for each specimen. The calculated constant for each specimen was then compared against the constant assigned to each fatigue category. The AASHTO (2004) category with the A value closest below the calculated value was assigned to the specimen. It should be reiterated that the bolted splice detail under investigation, regardless of hole creation method, is considered by AASHTO (2004) to be a Category B detail. However, many state DOTs do not permit holes to be punched in thicker plates [thickness greater than $\frac{5}{8}$ " (15.9 mm)].

Table 2-2: Bolted Splice Fatigue Specimen Results

Test ID	Hole	Target Stress Ksi (MPa)	Average Net Section Area mm ² (in ²)	N, Number of Cycles to Failure	AASHTO Category
1	Punched	23.9 (164.8)	--	356,823	C
2	Punched	22.9 (157.9)	1.58 (1020.5)	371,914	C
3	Punched	22.9 (157.9)	1.94 (1248.8)	518,587	B'
4	Punched	22.9 (157.9)	1.19 (766.9)	479,952	B'
5	Punched	22.9 (157.9)	1.43 (923.4)	377,387	C
6	Punched	22.9 (157.9)	1.69 (1091.4)	240,681	D
7	Punched	16.0 (110.3)	1.68 (1082.2)	953,106	D
8	Punched	22.9 (157.9)	1.97 (1273.1)	361,684	D
9	Drilled	22.9 (157.9)	1.92 (1237.0)	(2,353,874)	INF. LIFE
10	Punched	16.0 (110.3)	1.93 (1247.5)	(2,186,290)	INF. LIFE
11	Punched	22.9 (157.9)	1.13 (731.6)	454,891	B'
12	Reamed	22.9 (157.9)	1.12 (720.4)	(2,712,479)	INF. LIFE
13	Punched	22.9 (157.9)	1.36 (879.0)	392,249	C
14	Reamed	22.9 (157.9)	1.33 (858.5)	(2,396,323)	INF. LIFE
15	Punched	16.0 (110.3)	1.39 (896.2)	1,165,808	C
16	Punched	22.9 (157.9)	1.71 (1099.8)	253,772	D
17	Reamed	22.9 (157.9)	1.62 (1047.5)	(2,364,854)	INF. LIFE
18	Drilled	22.9 (157.9)	1.58 (1017.6)	(2,000,000)	INF. LIFE
19	Punched	22.9 (157.9)	1.86 (1197.5)	326,747	D
20	Reamed	22.9 (157.9)	1.79 (1153.3)	(2,232,370)	INF. LIFE
21	Drilled	22.9 (157.9)	1.83 (1177.2)	(2,709,305)	INF. LIFE
22	Punched	16.0 (110.3)	1.86 (1202.6)	59,400	C
23	Punched	22.9 (157.9)	1.10 (707.2)	489,884	C
24	Punched	16.0 (110.3)	1.12 (722.3)	1,285,563	C
25	Punched	22.9 (157.9)	1.32 (848.5)	408,255	C
26	Punched	22.9 (157.9)	1.63 (1052.1)	228,086	D
27	Punched	22.9 (157.9)	1.79 (1156.9)	296,015	D
28	Drilled	22.9 (157.9)	1.75 (1125.93)	(2,410,651) +/- 21,750	INF. LIFE
29	Punched	16.0 (110.3)	1.79 (1156.6)	780,143	D

Table 2-2 and Figure 2-3 indicate that the four drilled and the four sub-punched and reamed specimens rated as AASHTO (2004) Category B details. These eight specimens were tested at a 22.9^{ksi} (158 MPa) stress range, corresponding to a predicted failure at 1,000,000 cycles; all of the specimens reached infinite life and exceeded the calculated prediction. This may imply that there is some notable fatigue performance improvement in a bolted splice connection when HPS-70W is utilized. However, it is important to note that they still performed as Category B details. Testing should be performed at a higher stress range to examine if the detail performs at a Category A level when HPS-70W is utilized with drilled or sub-punched and reamed holes.

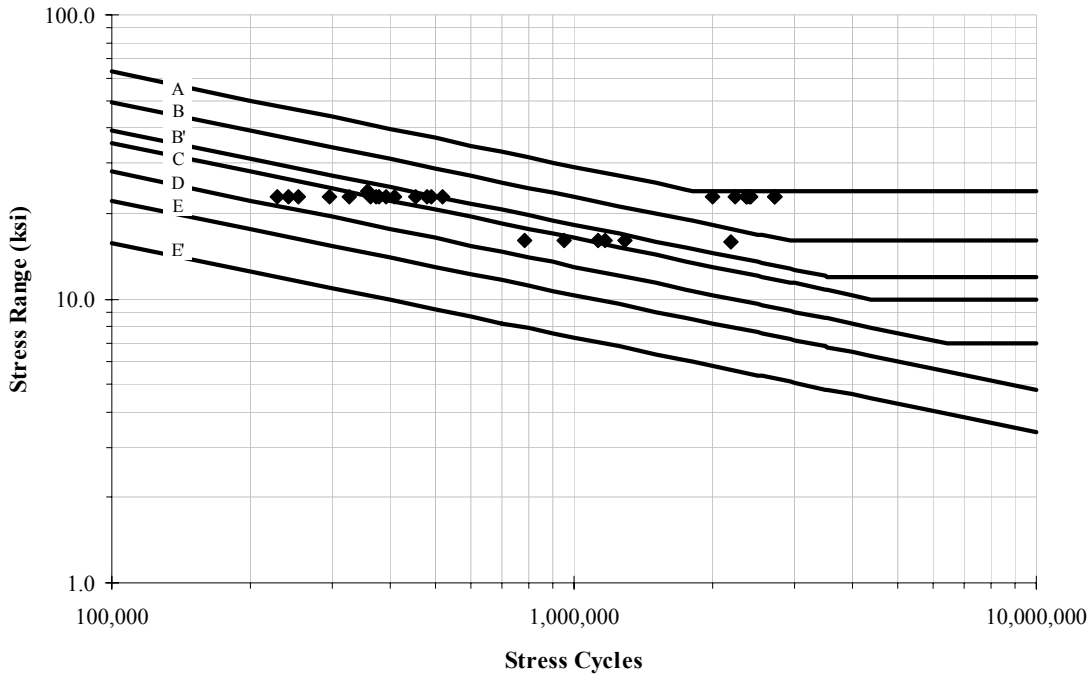


Figure 2-3: S-N Diagram for 29 Bolted Splice Fatigue Specimens

The 21 specimens having punched holes rated considerably below an AASHTO (2004) Category B detail. One of the punched specimens (5% of the specimen sample set) reached infinite life, three (14.3% of the sample set) rated as Category B', nine (43%) as Category C, and eight (38%) as Category D. Five of the six punched specimens tested at 16.0^{ksi} (110 MPa) failed to reach infinite life, while only one was considered to have achieved infinite life. None of the 15 punched specimens tested at or near 22.9^{ksi} (158 MPa) reached 1,000,000 cycles. The average result for the 21 punched specimens revealed a rating between AASHTO (2004) Category C and D. The results for the punched specimens suggest that any improvement in the fatigue performance of HPS-70W over that of conventional structural steel does not warrant lifting current DOT restrictions on punching holes in thicker plate. These restrictions are in place to ensure a certain level of quality in hole finish, necessary because of some practical considerations.

There are some practical limitations to punching holes in thicker plate. As plate thickness increases it becomes more difficult for holes to effectively be punched to size. The quality of the hole diminishes with thicker plate and the likelihood of the part becoming bent also

increases. Tool parts become dull more quickly, adding to overall machine expense and maintenance, and also detracting from the quality of the finished part. Every defect in a hole becomes a location for a potential crack to begin forming under fatigue. Two primary geometric variables which may effect the quality of a punched hole are hole diameter and plate thickness.

It is of interest to examine the data with respect to the geometric properties of the specimens. As mentioned earlier, the hole thickness and hole diameter were varied between specimens to investigate the possibility of presence of a relationship between the two parameters. To examine the effect of hole diameter and plate thickness on the fatigue strength of a HPS-70W bolted splice, the diameter to thickness ratio (d/t) was calculated for each specimen. The constant A , found in the AASHTO fatigue life equation (Equation 2-1) and linked directly to fatigue life, was calculated for each specimen using Equation 2-1. The ensuing data was plotted against the D/t ratios to gain a sense of the impact of the ratio on fatigue life for this connection type. The resulting graph is shown in Figure 2-4 and the plot suggests that this connection performs better under fatigue with an increasing d/t ratio. To examine whether the hole diameter or the plate thickness had a greater effect upon the fatigue performance, each of these values were separately plotted against A . It was found that there was very little correlation between hole diameter and A (Figure 2-5). However, there was a more notable correlation between plate thickness and A (Figure 2-6). This suggests that the better fatigue performance seen in specimens with higher d/t ratios was primarily due to utilization of thinner plate and was nearly independent of hole diameter.

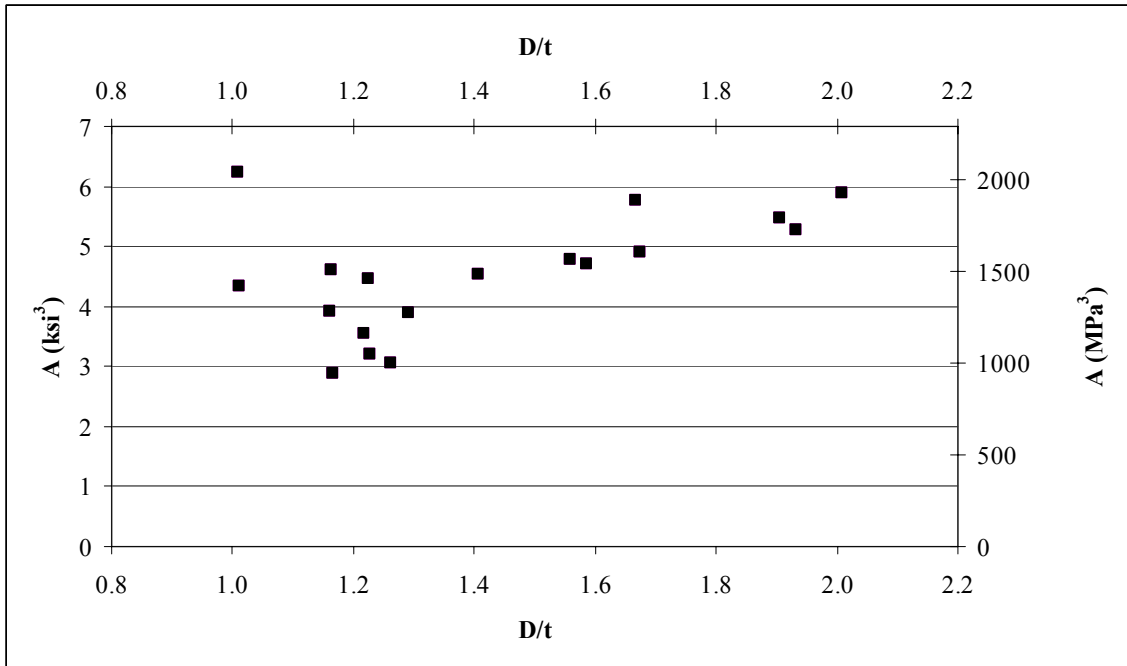


Figure 2-4: AASHTO (2004) Constant A vs. Diameter to Thickness Ratio

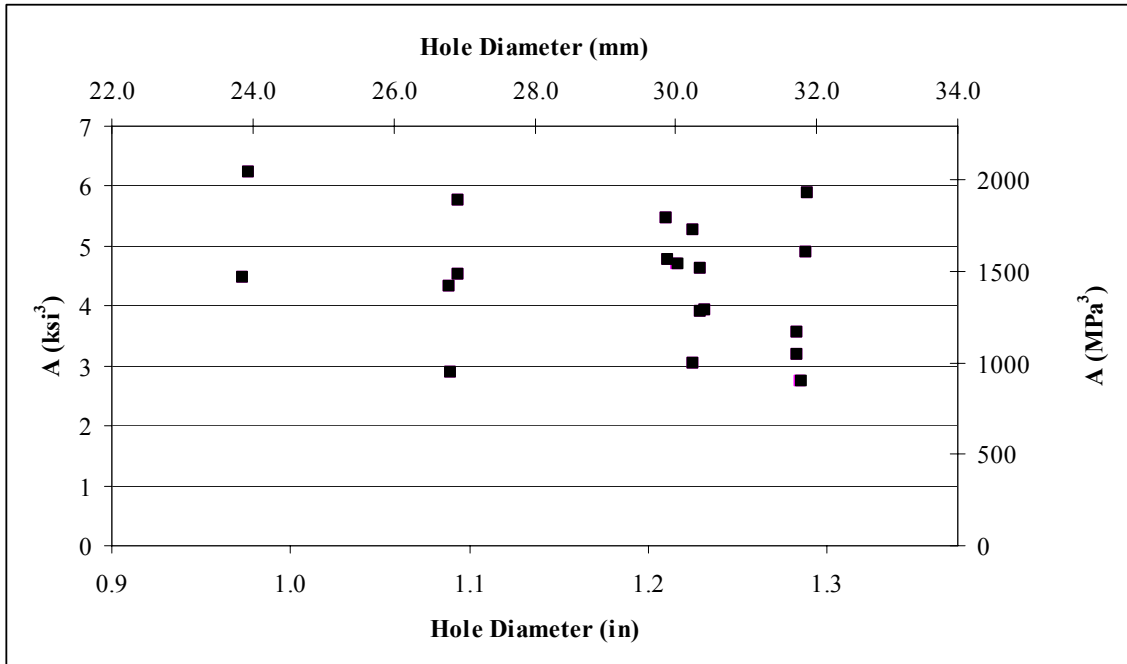


Figure 2-5: AASHTO (2004) Constant A vs. Hole Diameter

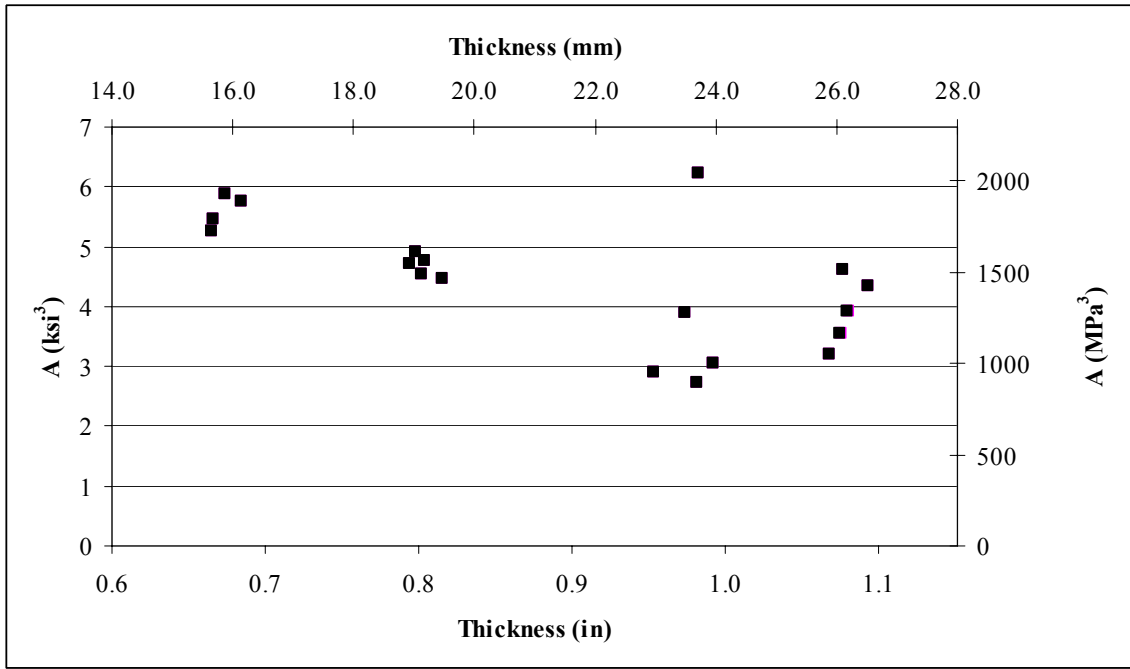


Figure 2-6: AASHTO (2004) Constant A vs. Plate Thickness

Another variable affecting fatigue life considered was surface roughness of the holes. Each hole in the specimens was visually and tactilely inspected and then classified using a comparator surface finish scale. The results were examined with respect to the fatigue life of each specimen, but no correlation was found to exist. It is possible that with the use of a more sensitive instrument a relationship between surface roughness and fatigue life could be identified. Pictures shown in Figure 2-7 show the difference in hole quality between the punched, drilled, and sub-punched and reamed hole types.

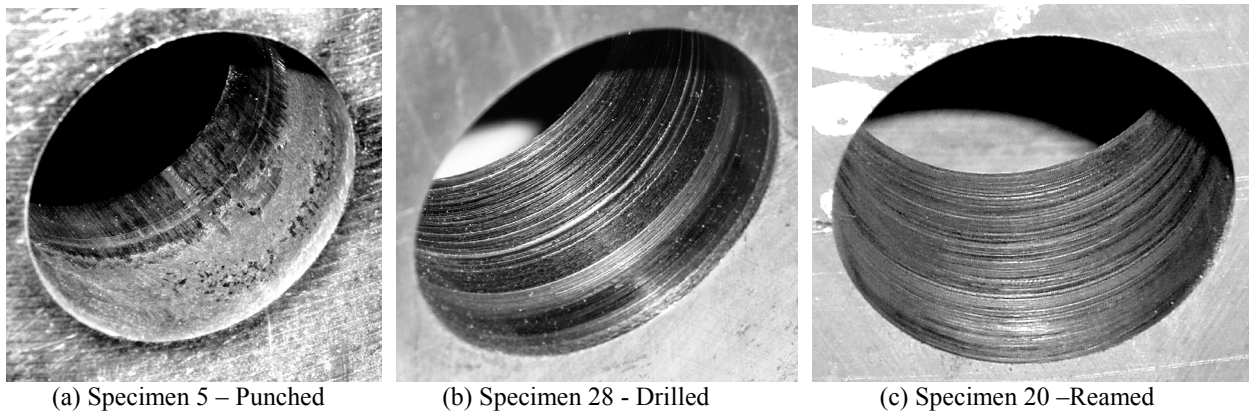


Figure 2-7: Different Hole Types

2.6 CONCLUSIONS

The HPS-70W drilled and sub-punched and reamed specimens rated at or above AASHTO (2004) Category B details, while the punched specimens rated between a Category C and D. This leads to conclusions that:

- Current provisions mandated by many state DOTs restricting punching holes in thicker plate are justified.
- The fatigue strength of the specimens having punched holes seems to be more dependent upon plate thickness than hole diameter.
- Current AASHTO (2004) fatigue design specifications appear to be applicable to HPS-70W bolted splice connections.

Overall, the HPS-70W bolted splices with drilled and sub-punched and reamed holes exhibited fatigue resistance at least as good as is required by AASHTO (2004), and in many cases, slightly better. This finding reinforces the applicability of HPS-70W to bridge girder applications.

Chapter 3 - Fatigue Behavior of Welded Splices in HPS-70W

3.1 INTRODUCTION

High performance steel (HPS) is increasingly being used for new bridge construction because of its improved properties over conventional structural steel. In particular, ASTM A709 Grade HPS-70W (485W) has found a niche amongst designers wishing to capitalize on its high yield strength, increased ductility, toughness, weldability, and improved weathering characteristics. Possessing a higher yield strength than conventional 50^{ksi} (345 MPa) structural steel, HPS-70W has allowed shallower girders to be constructed, leading to both weight savings and increased clearances. The corrosion resistance of HPS is also an appealing feature because of reduced life-cycle costs associated with it. A decrease in carbon content within the chemical makeup of HPS-70W has led to increases in toughness and better weldability characteristics. Currently, over 200 HPS bridges have been designed or constructed in 39 different states (AISI 2004).

While HPS-70W is marketed as being more resistant to fatigue than conventional bridge steel, it is currently still held to the same fatigue design standards in AASHTO (2004). It is possible that these standards may be more restrictive than necessary with respect to HPS-70W, impairing designers' abilities to fully capitalize upon its increased strength. For this reason, it is important that testing be conducted to quantify the fatigue resistance of HPS-70W.

In addition to the base metal having increased resistance to fatigue and fracture, HPS-70W is also being hailed as having improved welding characteristics. Because of reduced carbon content within its chemistry, HPS is less susceptible to hydrogen cracking and hardening in the heat affected zone (HAZ) after welding (Yost 2002; Miller 2000; Adonyi 2000). HPS-70W also requires a lower preheat temperature than conventional steel necessitates, saving both money and time (Yost 2002; Miller 2000; Adonyi 2000).

Enabling even further capitalization upon the gains made in the material performance of HPS-70W, improved welding techniques have been introduced, including Narrow Gap Improved Electroslag Welding (NGI-ESW). Currently, the most widely-accepted method of creating welded butt-splice connections is Submerged Arc Welding (SAW). Unfortunately, this process can be time consuming and may require multiple weld passes in order to create a finished weld. An alternative to this method is NGI-ESW, which has benefits of time savings, reduced manpower, and fewer welding consumables (Wood and Devletian 1987). The NGI-ESW procedure allows welds of great thickness to be placed in a single pass, with minimum joint preparation and high welding speed (Ostwald and Munoz 1997). Electroslag welding is considered to be the most productive method of joining thick metals due to virtually unlimited deposition rates (Malin 2005).

Electroslag welding (ESW) procedures have been used in bridge construction in the past, but were prohibited following the discovery in 1977 of a 10 ft crack in a western Pennsylvanian bridge on I-79, attributed to the use of electroslag welding (Jata 2003). The electroslag welding procedures used in the 1970s consistently resulted in welds with defects and lacking adequate toughness (Densmore 2000). Since then, the ESW process has been improved; a narrower gap and consumable plate guide have been utilized in combination with reduced voltages and higher welding currents to define the NGI-ESW process (Wood and Devletian 1987). Major improvements made in the ESW process include consistent defect-free welds, superior fatigue performance, and better impact resistance in the weld and heat-affected zones (Densmore 2000). NGI-ESW has resulted in very high welding speeds, improved fracture toughness in the welds and heat affected zones, and fewer weld flaws such as fusion weld defects and cracking (Verma 2000). The moratorium put in place by the Federal Highway Administration (FHWA) in 1977 was rescinded on March 20, 2000 (Verma 2000), allowing NGI-ESW to be used for joining steel bridge members.

The combination of high fracture resistance in the base metal, better weldability characteristics, and new availability of improved welding techniques makes welded HPS-70W connections an excellent candidate for study. Because of these three new variables, it becomes important to quantify the level (and verify the existence) of potential improvement over similar welded connections which utilize conventional welding methods and 50^{ksi} structural steel. In

addition, NGI-ESW was developed primarily for joining 36^{ksi} (250 MPa) and 50^{ksi} (345 MPa) grades of steel. AWS D1.5 allows joining with NGI-ESW for ASTM A709 grades 36 (250), 50 (345), and 345W (50W), but not HPS-70W (FHWA 2003). It is necessary to evaluate the performance of HPS-70W joined using the NGI-ESW method to assess the appropriateness of including this combination in AWS D1.5 in the future.

As a part of the FHWA's initiative to use innovative materials in bridge design and construction, the Ohio Department of Transportation (ODOT) has constructed a four-span, five-girder, highway bridge in Lancaster, Ohio, made of HPS-70W TMCP. Because HPS-70W has demonstrated promise in bridge girder applications, it is important that the behavior of the material, as well as the entire bridge as a structural system, is well understood. This chapter focuses on fatigue characteristics of HPS-70W TMCP welded butt splice connections.

3.2 BACKGROUND

A great deal of attention has been devoted to HPS since its development in 1992, but comparatively little work has been done to quantify its performance under fatigue. There is a copious amount of published work mentioning that HPS-70W exhibits better fatigue resistance than conventional bridge steel (Wassef et al. 1996; Kulicki 2000; Yakel et al. 1999; Barsom 1997), but little independent experimental work has been performed to support these claims. While the improved toughness characteristics of HPS-70W have been well-documented, it has not been made clear whether improved toughness necessarily translates into improved fatigue resistance.

A study was performed by Wright (2002), in which fracture tests were performed on full-scale HPS-70W I-girders. The girders were cyclically loaded until fatigue cracks formed, upon which they were cooled to -34.0° C (-29.2° F), and then finally were subjected to a design overload. The HPS-70W test girders were able to carry the overload until approximately 50% of the tension flange was lost, corresponding to net section stress levels exceeding yield before failure. This result compared favorably to similar test girders fabricated of Grade 50 (345) steel, which exhibited lower crack-size tolerance and fracture stress levels at approximately 60% of yield on the net section.

Chen et al. (2003) recently performed a study which concluded that “The HPS-70W steel tested provides a significantly higher fatigue limit than conventional structural steels.” However, that study did not consider specific connection details, examining only flat sheet-type fatigue specimens. The study compared cyclic and monotonic properties of high performance steel against that of lower strength structural steel (Grade A7). The specimens examined in the study were machined from $\frac{1}{4}$ ” (6.40 mm) and 2” (51.0 mm) HPS plates. Specimens were fatigued under strain amplitudes varying from 0.100% to 0.625%, and failure was considered as having occurred when the tensile load decreased by 50%. Tests were also conducted on $\frac{1}{4}$ ” (6.40 mm) ASTM A7 plate as a basis for comparison.

A major study was performed by Wood and Devletian (1987) at the Oregon Graduate Center to investigate electroslag welding and to develop an improved ESW method, which ultimately resulted in the introduction of the NGI-ESW process. The goal of that project was to increase the reliability, integrity, and mechanical behavior of electroslag welds in A36 and A588 structural steel. Through use of a narrow gap ($\frac{3}{4}$ ” (19.0 mm) as compared to the $1\frac{1}{4}$ ” (32.0 mm) previously used in ESW) and a consumable guide tube in conjunction with reduced voltages and increased currents, the researchers were able to reduce heat input, increase welding speed, and improve overall weld quality. None of the 12 electroslag welds studied under fatigue conditions developed cracks, suggesting that sound ESW welds satisfy AASHTO fatigue requirements for Category B weldments.

3.3 OBJECTIVES

The primary goal of this research was to quantify the fatigue resistance of HPS-70W welded butt-splice connections, examining both the Submerged Arc Welding (SAW) and the Narrow Gap Improved Electroslag Welding (NGI-ESW) processes. Because of improved fracture resistance of the base metal, enhanced welding characteristics of the base metal, and the introduction of NGI-ESW, it is reasonable to hypothesize that a connection as described above might behave differently than a similar connection utilizing conventional structural steel and submerged arc welding procedures.

It is also the intention of this investigation to determine whether it is appropriate to include NGI-ESW procedures in conjunction with HPS-70W in the “Guide Specification for Highway Bridge Fabrication with HPS-70W (HPS-485W) Steel” (AASHTO 2003), an addendum to the AWS D1.5 specification.

3.4 EXPERIMENTAL SETUP

Two large HPS-70W TMCP plates were obtained from Bethlehem Steel, one $\frac{7}{8}$ ” (22.0 mm) thick and the other 2” (51.0 mm) thick, for the purpose of fabricating the flanges of the Lancaster bridge girders, and to supply steel for adequate material testing. Gross dimensions of the plates were 6’-0” x 66’-11” x $\frac{7}{8}$ ” (1.80 m x 20.4 m x 22.0 mm) and 5’-11” x 104’-6” x 2” (1.80 m x 31.9 m x 51.0 mm). The two large HPS plates were cut into multiple smaller plates, from which the bridge girder flanges were cut. Sections from the remaining plate steel were butt-welded by either SAW or NGI-ESW.

The Stupp Bridge Co. performed the welding for the SAW specimens; the plates were joined in a single-V-groove weld (butt joint) using a $\frac{3}{32}$ ” (2.40 mm) diameter, LA85 electrode. The recorded travel speed was 15 inches per minute. A current of 500 Amps and a voltage of 30V were utilized in the process. The Arcmatic Integrated Systems Co. performed a demonstration of the NGI-ESW process using their proprietary VertaSlag system at Stupp Bridge’s headquarters, producing the plates joined by NGI-ESW used in this investigation. A gap size of $\frac{3}{4}$ ” (19.1 mm) was used along with a shoe speed of $1\frac{1}{4}$ ” (38.1 mm) per minute. The welding wire used was a proprietary Arcmatic wire, VMC-105, similar to what was used in the Oregon Graduate Institute described in Wood and Devletian (1987). A picture of two plates joined by the NGI-ESW method is shown in Figure 3-1.

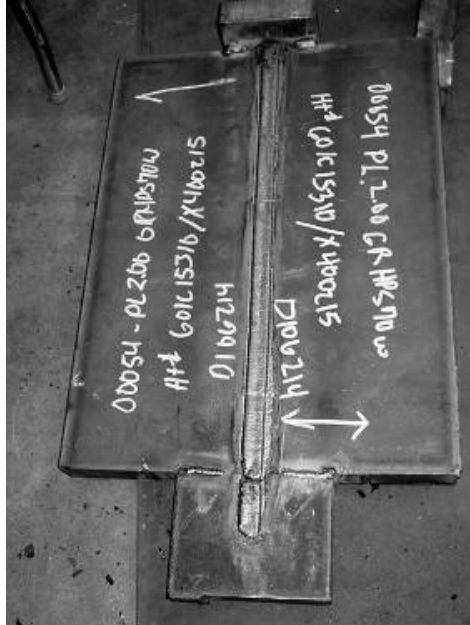


Figure 3-1: Two HPS-485W (70W) plates welded together using NGI-ESW

Ten specimens were machined from the welded plates, five originating from plates joined by SAW and five specimens from plates joined by NGI-ESW. The locations of any existing flaws were known from radiographic inspection of the welds, and the specimens were fabricated so as to avoid any such flaws. The dimensions of the machined specimens and the respective stress ranges at which they were tested are shown in Table 3-1. Each specimen was machined such that the butt-weld was located at the mid-length of the specimen. A diagram depicting typical specimens is shown in Figure 3-2.

Table 3-1: Welded Butt-Splice Fatigue Specimen Descriptions

Test ID	Average Width	Average Thickness	Average Cross Sectional Area	Target Stress
	in (mm)	in (mm)	in ² (mm ²)	ksi (MPa)
SAW-1	0.89 (22.61)	2.03 (51.56)	1.80 (1161)	22.3 (153.4)
SAW-2	0.88 (22.35)	2.03 (51.56)	1.79 (1155)	23.5 (162.0)
SAW-3	0.90 (22.86)	1.52 (38.61)	1.36 (877.4)	29.2 (201.3)
SAW-4	0.90 (22.86)	1.50 (38.10)	1.34 (864.5)	29.2 (201.3)
SAW-5	0.91 (23.11)	1.39 (35.31)	1.26 (812.9)	29.2 (201.3)
NGI-ESW-1	0.70 (17.78)	2.02 (51.31)	1.41 (909.7)	29.2 (201.3)
NGI-ESW-2	0.70 (17.78)	2.02 (51.31)	1.40 (903.2)	29.2 (201.3)
NGI-ESW-3	0.70 (17.78)	2.01 (51.05)	1.40 (903.2)	29.2 (201.3)
NGI-ESW-4	0.70 (17.78)	2.01 (51.05)	1.41 (909.7)	29.2 (201.3)
NGI-ESW-5	0.67 (17.02)	2.01 (51.05)	1.34 (864.5)	29.2 (201.3)

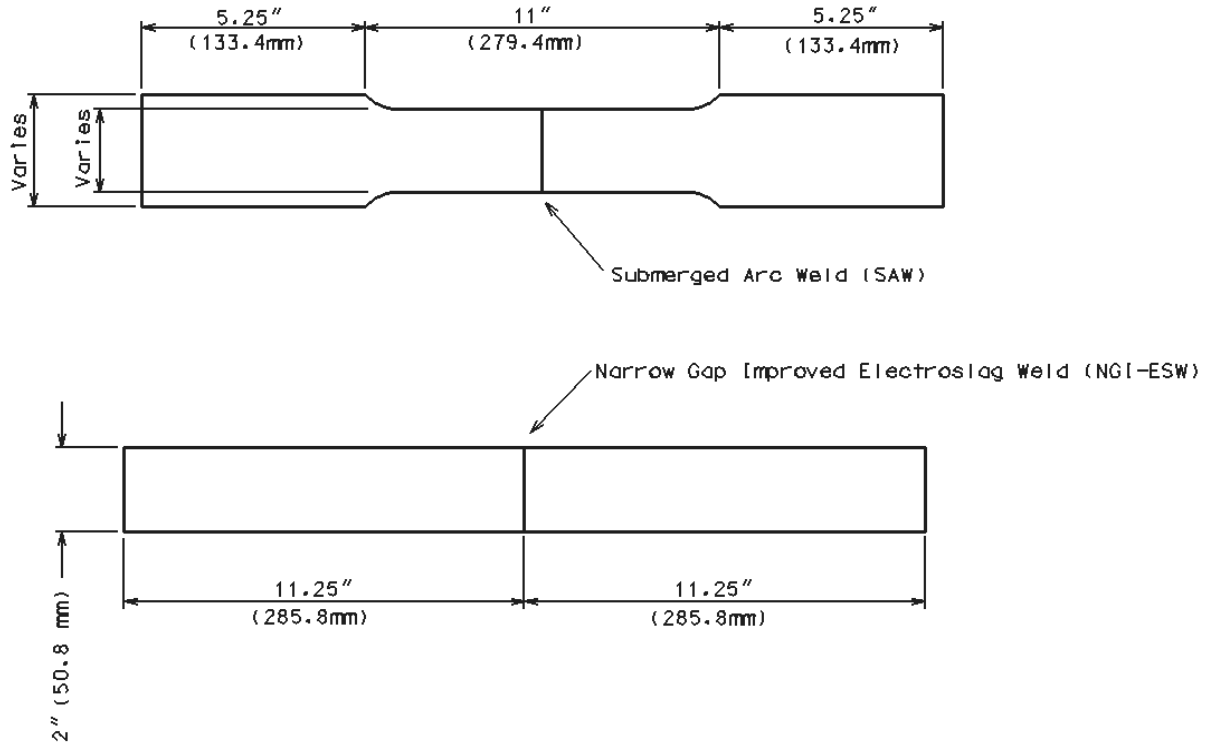


Figure 3-2: Typical SAW and NGI-ESW Welded Fatigue Specimens

Each specimen was tested in a MTS 312 universal testing frame having a maximum load capacity of 55^{kip} (245 kN) and containing a 50^{kip} (220 kN) capacity load cell. The welded fatigue specimens were tested in load control under tension force only, and were preloaded to a lower load (LL) of 0.50^{kip} (2.22 kN) to ensure that they remained in tension. The upper load (UL) for the tensile range was calculated as:

$$UL = 0.50 \text{ kips (or 2.22 kN)} + (\Delta F_n \times A_{net}) \quad (3-1)$$

where ΔF_n was either 22.3^{ksi} (153 MPa), 23.5^{ksi} (162 MPa), or 29.2^{ksi} (201 MPa) and A_{net} was taken as the average net area at three marked locations. The test setup is shown in Figure 3-3. Specimens were loaded sinusoidally at a rate of 5 Hz until either failure or infinite fatigue life was achieved. Crack detection settings were defined in the software controlling the MTS machine to recognize failure, and were kept as precise as feasible in order to detect cracks as early as possible. The intent of this approach was to cause the machine to cease cycling during

propagation of a crack, detected by a stroke limit setting. Infinite fatigue life was taken as 2.3 million cycles for a Category B detail; specimens that reached this point without formation of a crack were subsequently removed from the test setup.



Figure 3-3: Welded Specimen Fatigue Test Setup

There are two primary approaches to performing fatigue testing. The first approach involves testing a number of identical specimens at different stress ranges, allowing the data points to define a curve on an S-N diagram. This procedure is suitable when identical specimens are being examined for fatigue strength, and was the method originally chosen for this study. However, due to problems achieving the high loads required for failure a second approach was taken, involving testing several different types of specimens at the same stress range. This method may be more appropriate because it lends itself to easy comparisons between different types of specimens. The results for various types of specimens are more likely to stand apart, resulting in meaningful data presentation.

The five SAW butt-welded specimens were tested first. The reduced cross-sections of the first two specimens (SAW-1 and SAW-2) were $\frac{7}{8}$ " x 2" (22.2 mm x 50.8 mm). These two specimens were tested at stress ranges of 22.3^{ksi} (154 MPa) and 23.5^{ksi} (162 MPa) respectively, and both reached infinite life (approximately 2.3 million cycles). It was not possible to further

increase the applied load to cause failure due to test frame constraints, so it became necessary to reduce the specimens' cross-sections for the purpose of increasing the stress range. Therefore, the remaining three SAW specimens had reduced cross-section dimensions of approximately $\frac{7}{8}$ " x $1\frac{1}{2}$ " (22.2 mm x 38.1 mm). All of these specimens were tested at 29.2^{ksi} (201 MPa), corresponding to a theoretical failure at one million cycles for a Category A detail, as calculated by the AASHTO fatigue life equation, in an effort to cause failure in some of the remaining specimens. Infinite life was taken as two million cycles for the remaining specimens being tested at the Category A stress level. The five NGI-ESW specimens all had approximate cross-section dimensions of $1\frac{1}{16}$ " x 2" (17.5 mm x 50.8 mm), and were tested at 29.2^{ksi} (201 MPa).

After all ten specimens had been tested to infinite life, the investigators chose to continue testing two NGI-ESW specimens (NGI-ESW-4 and NGI-ESW-5) and two SAW specimens (SAW-4 and SAW-5) to investigate whether they would fail under fatigue in an extended test. Those four specimens were subjected to a second sequence of fatigue testing and were allowed to cycle for an additional three million cycles beyond the initial two million cycles, or until failure. Each of these specimens was cycled at a stress range of 29.2^{ksi} (201 MPa) during the extended testing, the same stress range they had been subjected to during initial testing.

3.5 RESULTS AND DISCUSSION

Summary results for the ten welded butt-splice fatigue specimens are shown in Table 2. All of the welded butt-splice specimens, both SAW and NGI-ESW, reached infinite life. The majority of these were tested at 201 MPa (29.2 ksi), which corresponds to a theoretical failure at one million cycles for a Category A detail. The fact that those Category B specimens reached more than one million cycles beyond the point of predicted failure for a Category A detail does indicate some notable improved fatigue performance over welded butt-splice details utilizing conventional structural steel, when using the AASHTO fatigue life equation as the basis for comparison.

Table 3-2: Welded Splice Fatigue Specimen Results

Test ID	Average Cross Sectional Area in² (mm²)	Target Stress ksi (MPa)	N, Number of Cycles (Initial Testing)	N_c, Cumulative Number of Cycles Including Extended Testing	AASHTO Category
SAW-1	1.80 (1161)	22.3 (153.4)	2,337,324	N/A	INF. LIFE
SAW-2	1.79 (1155)	23.5 (162.0)	2,389,594	N/A	INF. LIFE
SAW-3	1.36 (877.4)	29.2 (201.3)	3,024,304	N/A	INF. LIFE
SAW-4	1.34 (864.5)	29.2 (201.3)	3,203,331	6,089,462	INF. LIFE
SAW-5	1.26 (812.9)	29.2 (201.3)	2,042,607	3,290,522	INF. LIFE
NGI-ESW-1	1.41 (909.7)	29.2 (201.3)	2,467,568	N/A	INF. LIFE
NGI-ESW-2	1.40 (903.2)	29.2 (201.3)	2,247,517	N/A	INF. LIFE
NGI-ESW-3	1.40 (903.2)	29.2 (201.3)	2,252,530	N/A	INF. LIFE
NGI-ESW-4	1.41 (909.7)	29.2 (201.3)	2,082,447	5,189,557	INF. LIFE
NGI-ESW-5	1.34 (864.5)	29.2 (201.3)	2,013,353	5,407,444	INF. LIFE

The two NGI-ESW specimens which were subjected to extended testing both achieved an additional 3 million cycles without failure, resulting in approximately 5 million cumulative cycles without failure. One of the two SAW specimens under the extended test conditions, SAW-4, reached an additional 3 million cycles (approximately 5 million cumulative cycles without failure), whereas the other, SAW-5, failed at an additional 1.25 million cycles (approximately 3.3 million cumulative cycles without failure). The SAW specimen that failed under extended cycling (SAW-5) failed in the base metal at the fillet transition from the reduced section to the wider grip section. Failure likely occurred here due to stress concentrations at the fillet and a high likelihood of machining inconsistencies in this region. Although this specimen failed to achieve 5 million cycles, the result is not especially illuminating since the failure did not occur at the weld.

Each of the splices created using the NGI-ESW process performed at least as well as those created using SAW. Although the sample size is relatively small, this level of agreement suggests that, with good weld inspection and control, NGI-ESW is applicable for joining HPS-70W members in a butt-splice configuration. It seems reasonable to include HPS-70W welded butt-splices created using NGI-ESW in AWS D1.5 when judged on the basis of results from this study.

The fact that the NGI-ESW splices performed as well as the SAW splices supports the reintroduction of ESW to bridge girder applications and suggests that, when used in conjunction

with HPS, NGI-ESW can lead to sizeable gains in welding economy. Because the use of HPS has already led to significant cost savings in bridge construction, the use of NGI-ESW for joining members instead of the more costly SAW could result in considerably greater cost savings.

3.6 CONCLUSIONS

The results of this study suggest that:

- HPS-70W welded butt-splices created with NGI-ESW performed at least as well as similar connections created using SAW
- NGI-ESW and SAW HPS-70W welded butt-splices exhibited improved performance over the predicted fatigue life calculated using the AAHTO fatigue life equation
- NGI-ESW seems to be an appropriate method for joining HPS-70W in welded butt-splice connections
- It is reasonable to include HPS-70W welded butt-splices created using NGI-ESW in AWS D1.5
- Significant economic gains may be realized by utilizing NGI-ESW in welded butt-splices instead of SAW

Chapter 4 - Automated Ultrasonic Inspection of Welded Joints

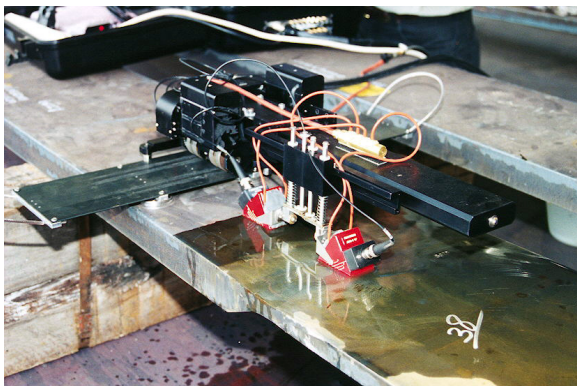
The viability of using computerized ultrasonic testing as an inspection method for welded joints in bridge girders was also examined. To study the accuracy of using computerized ultrasonic measurement techniques to detect weld flaws, results from UT scans of select welds were compared to radiographic test results.

Ultrasonic testing is a well established procedure for finding discontinuities in welds. Testing is accomplished by directing a beam of ultrasonic energy into the object to be tested. This beam travels through the object with insignificant energy loss, except when it is intercepted and reflected by a discontinuity. When the ultrasonic waves pulse strikes a discontinuity in the test piece, it is reflected back to its point of origin. The detection, location, and evaluation of discontinuities become possible because the velocity of sound through a material is nearly constant, making distance measurement possible, and the relative amplitude of a reflected pulse is more or less proportional to the size of the reflector (Anderson, 2002).

Currently, radiographic testing is required for all butt welds in flange material of plate girders or rolled beams. Ultrasonic testing offers economic advantages over radiography because radiography requires isolation of the part being examined to avoid exposing workers to radiation. Ultrasonic testing can be conducted without moving the part from welding station. Until recently, however, ultrasonic testing did not provide a permanent record of the examination. The introduction of computerized ultrasonic testing, though, eliminates this limitation.

Comparisons focused on attempting to detect flaws in bridge-girder flange welds that were placed using submerged arc welding (SAW) techniques. All specimens were produced by Stupp Bridge. Approximately 20 welds were inspected using both radiographic and automated ultrasonic techniques at the Stupp Bridge fabrication facility in Bowling Green, KY. Radiography was performed by Stupp Bridge.

Initially, three firms were scheduled to complete the automated ultrasonic testing: Automated Inspection Systems, Inc. (AIS); Force Institute; and RD Tech. However, only AIS and Force Institute were able to complete the testing. Figure 4-1 shows setup procedures for the AIS and Force Institute automated ultrasonic testing systems. Note that each setup required no movement of the part from its location within the fabrication shop or isolation of the system. Testing of each weld using the automated ultrasonic equipment took approximately 15 minutes. Results from the testing using both the radiographic and automated ultrasonic techniques indicated that the flange welds showed no flaws.



(A) AIS P-Scan Set Up



(B) Force Institute Set Up

Figure 4-1: Test Set Ups from Automated Ultrasonic Testing Companies

During the coordination of the automated ultrasonic inspection demonstration, RD Tech had agreed to provide a calibration plate with known flaws so that the capabilities of each system could be observed. Since RD Tech was not able to participate in the demonstration and therefore did not provide the calibration plate, no quantitative conclusions can be made from the demonstration. The UC research team repeatedly attempted to contact members of the FHWA Research Laboratories in McClean, VA, but had very limited success.

Chapter 5 - Erection Study of a Skewed HPS-70W Bridge

5.1 INTRODUCTION

There is a growing demand for skewed steel bridges as the needs for complex intersections and the problems with space constraint in urban areas arise. Skewed bridges are useful when roadway alignment changes are not feasible or economical due to the topography of the site and also at particular areas where environmental impact is an issue. The effects of skew on the response of completed structures have been well documented, with effects being shown to be more significant for skew angles greater than 30° (Ebeido and Kennedy 1996; Gupta and Kumar 1983). Critical values for vertical deflections and bending moments within in-service skewed bridges have been shown to be lower when compared against those in similar right bridges (Aggour 1943; Aggour 1947; Ghali 1967; Ghali 1969; Hutter 1964). Conversely, torsional rotations, shears and moments have been shown to be larger for skewed bridges. In addition, studies have also demonstrated that interaction between main support girders and transverse bracing members (diaphragms and cross frames) influences skewed bridge load distribution due to an increase in torsional rotations at certain sections of the longitudinal girders (Aggour 1943; Aggour 1947; Ghali 1967; Ghali 1969; Hutter 1964). Additional work has shown that the magnitude of torsional shear rotations at skewed bridge supports are largest at the obtuse corners (Surana and Humar 1984).

While a number of studies dedicated to the response of in-service skewed bridges have been completed, as presented above, there are few studies that focus on the behavior of skewed bridges during construction. Torsional moments developed in steel bridges with large skews are difficult to predict during construction, as the alignment of the screed can result in an uneven distribution of wet concrete dead loads across the superstructure that increase the skew effects. There has been a lack of research studying the effects of the disproportionate distribution of dead loads on the superstructure during construction.

Coupled with the increase in the design and construction of skewed bridges has been an increase in the utilization of High Performance Steel (HPS) for bridge superstructure units and the use of integral or semi-integral abutments for the substructure. HPS offers improved toughness and weldability when compared to more conventional steels and, when produced with yield strengths of 70 or 100^{ksi} (482 to 689 MPa), it provides an attractive alternative to other materials for various bridge structures (Wasserman et. al. 1998).

While HPS has been available for a number of decades, its utilization by the bridge industry has begun relatively recently, beginning with the construction of two bridges in Tennessee and Nebraska in the late 1990s (Wasserman 2002; Van Ooyen 2002). Since these two initial projects, a number of other states, including Ohio, have recognized the economic benefits of using HPS and currently over 100 HPS bridges have been placed into service (AISI 2004).

Along with the increased implementation of HPS bridge structures in the U.S., there has been an increase in research related to the development of improved design and fabrication criteria for these structures. This research has included: (1) development of improved production and welding techniques for HPS (Nickerson and Wright 1996; Germanson 1998; Nickerson 1997); (2) experimental and numerical studies of HPS plate girder flexural strengths Earls and Shah 2002; Green et. al. 2002; Yakel et. al. 2002); (3) development of procedures for optimal design of HPS bridges (Wasserman 2002); and (4) cost-comparisons between HPS, conventional steel and concrete bridge designs (Barker and Schrage 2000). However, there has been no published information to date related to the response of completed HPS bridges under loads induced during construction or while in-service.

The use of semi-integral and integral abutments also continues to increase. For these types of structures, the superstructure and substructure are assumed to behave as a unit and expansion joints are eliminated. The girders act with the abutment and superstructure expansion is accommodated either through (1) an elastomeric pad placed underneath the abutment backwall for semi-integral abutments or (2) through movement of the entire abutment and foundation for integral abutments (Burke 1994).

A large amount of research related to semi-integral and integral abutments has also been completed, with work predominantly focusing on: (1) characterization of interaction between substructure units and the supporting soil (Abendroth and Greimann 1989; Ashour and Norris 2000; Lehan et. al. 1999); (2) development of analysis methods that predict stresses and deformations in superstructure and substructure units resulting from environmental, time-dependant and directly applied loads (Dicleli 2000; Hulsey and Emanuel 1978; Greimann and Yang 1986; Mourad and Tabsh 1998; Nicholuson 1994); (3) development of design criteria and procedures (Burke 1996; Girton et. al. 1991; Worlde-Tinsae and Greimann 1988; Husain 2000; Oesterle et. al. 1998); and (4) examination and assessment of the performance of in-service integral abutment bridges (Alampalli and Yannotti 1998; Ingram et. al. 2003; Emerson 1981; Thippeswamy and Ganga Rao 1995). While there have been a number of projects focusing on the qualitative examination of in-service semi-integral and integral abutment bridges, only a few studies have placed instrumentation onto actual structures and recorded their response and only two projects (Lawver et. al. 2000; Laman et. al. 2003) have involved study of actual structural response during construction.

Therefore, this manuscript attempts to add to the state-of-the-art related to skewed steel bridge response during construction by experimentally and numerically studying a continuous, skewed, HPS, semi-integral abutment bridge during placement of the concrete deck. Results from field-monitoring of the structure during deck placement are compared to numerical predictions to ascertain influence of various parameters on behavior and alternative methods for placing the deck are examined.

5.2 OBJECTIVES

The objective of the research described herein was to study environmental, material and concrete placement effects on girder response in a recently constructed, skewed, HPS, semi-integral abutment bridge. The study examined stresses in the exterior plate girders of the bridge and compared those stresses to the field data.

The environmental and material studies examined the effects of air temperature changes during the pour and of setting of the concrete on forces developed in the superstructure. The

accuracy with which numerical models predicted actual response when these effects were included or ignored is presented and discussed.

In addition, outer girder stresses were compared for two possible wet concrete placement schemes. The first was continuous placement of the wet concrete perpendicular to the girders, which was followed in the field, and the second was continuous placement of the wet concrete parallel to the skew (Figure 5-1). The deck pour method that resulted in the least detrimental response of the structure (i.e. lowest rotations and stresses) at the completion of the pour is identified and discussed.

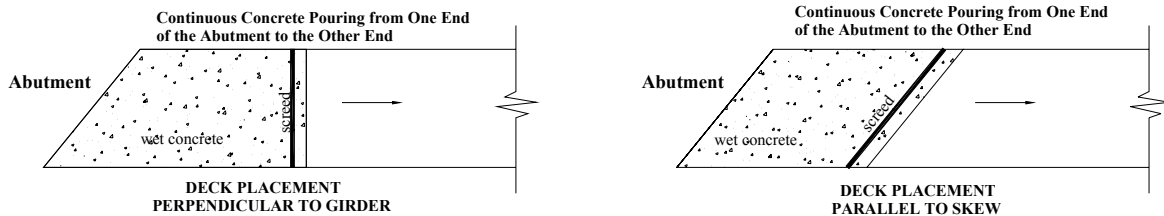


Figure 5-1: Deck Pouring Methods

5.3 STRUCTURE DESCRIPTION

The structure that was studied is a four-span continuous, HPS bridge with semi-integral abutments that was recently constructed in Ohio. Figure 5-2 details the framing plan and a typical cross section. Elastomeric bearings are located at Piers 1 and 3. Span lengths from south to north are 78'-5" (23.90 m), 130'-10" (39.88 m), 126'-10¹/₂" (38.67 m) and 82'-4¹/₂" (25.14 m) center-to-center of the bearings with a skew angle of 39°. Each girder is constructed with flanges ranging from 12" x ⁷/₈" (304.8 mm x 22 mm) to 13" x 2" (330 mm x 51 mm). The web plate is 48" x ¹/₂" (121.9 cm x 12.7 cm). The girders are braced with cross frames containing three ¹/₂" x 3¹/₂" x ³/₈" (89 mm x 89 mm x 9.5 mm) angles that are placed perpendicular to the webs as shown in Figure 5-2. The girders are hybrid sections composed of HPS70W Thermo-Mechanical Control Process (TMCP) HPS flanges and ASTM A588/A709 Grade 50 webs. Cross frames were also constructed of Grade 50 steel and were arranged in an X-shaped pattern. The use of hybrid HPS sections resulted in reduced cross sectional dimensions than what would have occurred if standard steel plate was used for the flanges. It can be inferred that, as a result,

the structure was more flexible than one that used Grade 50 steel everywhere and effects from varying concrete placement schemes on response would be more pronounced. However, other design decisions (e.g. semi-integral abutments) would also influence superstructure response during construction in a fashion that could make pour sequence effects less pronounced. It is the authors' opinion that, irrespective of the type of superstructure and substructure units that are designed, results discussed herein provide important information that should be considered during the design and construction of skewed, steel plate girder bridges.

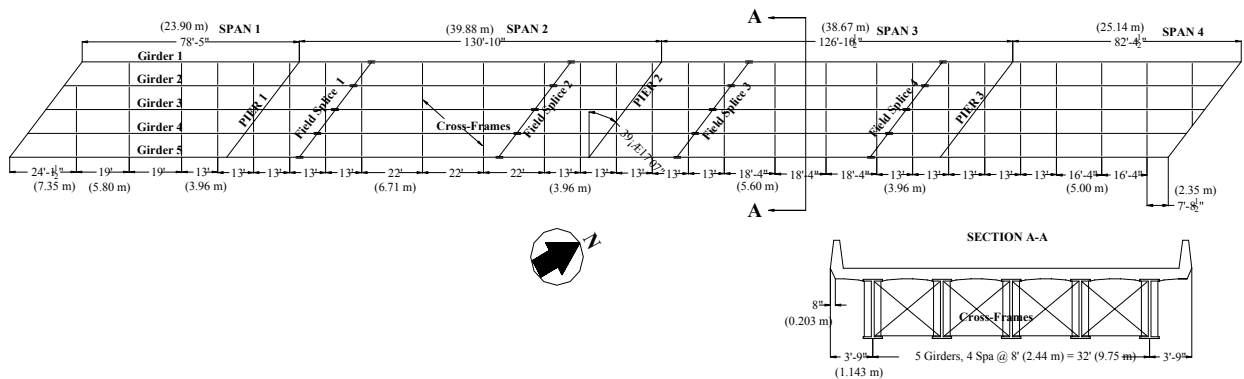


Figure 5-2: Framing Plan and Typical Cross Section

The concrete deck was placed during a single seven hour daytime pour initiating at the south abutment and proceeding to the north abutment. Retarders were placed into the concrete mix to theoretically prevent the concrete from setting until the pour was completed. A single screed was used for the pour and it was aligned so that the leading edge of the wet concrete would be placed perpendicular to the centerline of the roadway (Case (a) from Figure 5-1), as shown in Figure 5-3.



Figure 5-3: Deck-Pour Orientation – Perpendicular to Bridge Centerline

5.4 FIELD MONITORING

Nine Bridge Diagnostics, Inc. strain transducers were affixed to the exterior girder bottom flanges near their tips and on their webs approximately 3 ³/₄" (9.53cm) below the top flanges at locations G1A, G1B and G5A (Figure 5-4) to obtain strain data during the pour. These gages recorded data at 2.5 minute intervals throughout the deck placement process. Strains were converted to stresses assuming linear elastic behavior and stress variations during the deck pour were examined.

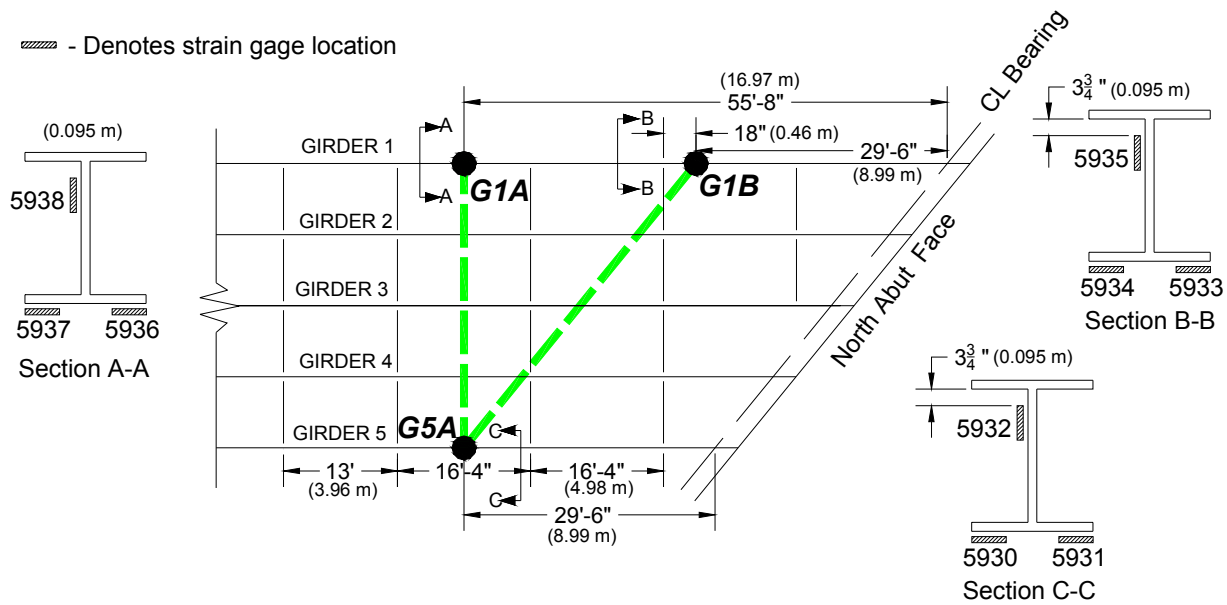


Figure 5-4: Location of Strain Gages

5.5 NUMERICAL PROGRAM

A three dimensional finite element model was developed from the design plans using SAP2000 Version 8. SAP2000 was selected because it is commonly used by practitioners and Version 8 offers a feature for staged (incremental) construction analysis.

The model consists of the girders and wet concrete being represented using either three or four-noded shell elements. All the girder shell elements are four-noded while the wet concrete elements consist of both three and four-noded shells. Shell elements were selected for the deck to provide an accurate distribution of the concrete dead load to the girders. Although it is understood that the use of four-noded shells provides a more accurate solution, since deck stresses were not examined three-noded shells were deemed acceptable for the deck. The shell elements were defined as elastic thin plates where the effect of transverse shear deformation was neglected.

Deck shell elements were connected to the girders using rigid links (frame elements) to transfer the wet concrete loads and to maintain compatibility between the deck and girders. Rigid link stiffness was established using a large modulus and a material density was assigned that would not contribute significantly to overall structure dead load. Three-dimensional frame

elements were used for the cross frames. A detail depicting the model and indicating boundary conditions after calibration is shown in Figure 5-5.

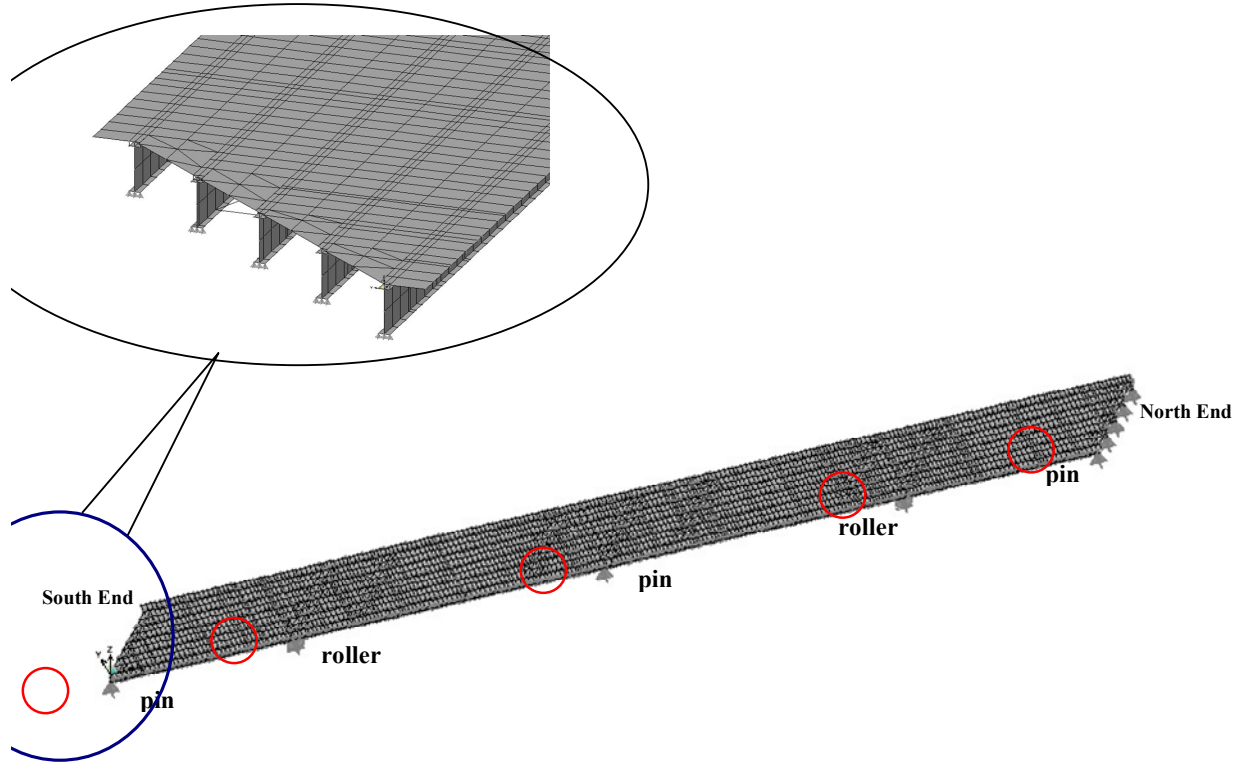


Figure 5-5: Three-Dimensional FE Model with Final Calibration Boundary Conditions

Loads placed onto the finite element model consisted of self-weights of the superstructure components (girders and cross frames) and the wet concrete. The model did not initially incorporate any additional loads caused by temperature changes that the structure experienced during the pour. In addition, any effects caused by setting of the concrete deck (i.e. change in deck stiffness) during the pour were not initially incorporated.

5.6 MODEL CALIBRATION

Stresses obtained from the finite element model were compared to measured values at strain gages on G1 and G5 (G1A, G1B and G5A, see Figure 5-4) obtained during the deck pour. The finite element model had nodes located at the top of the web and, therefore, linear

interpolation between nodes nearest to the transducer locations was used to perform any comparisons.

5.6.1 Boundary Conditions

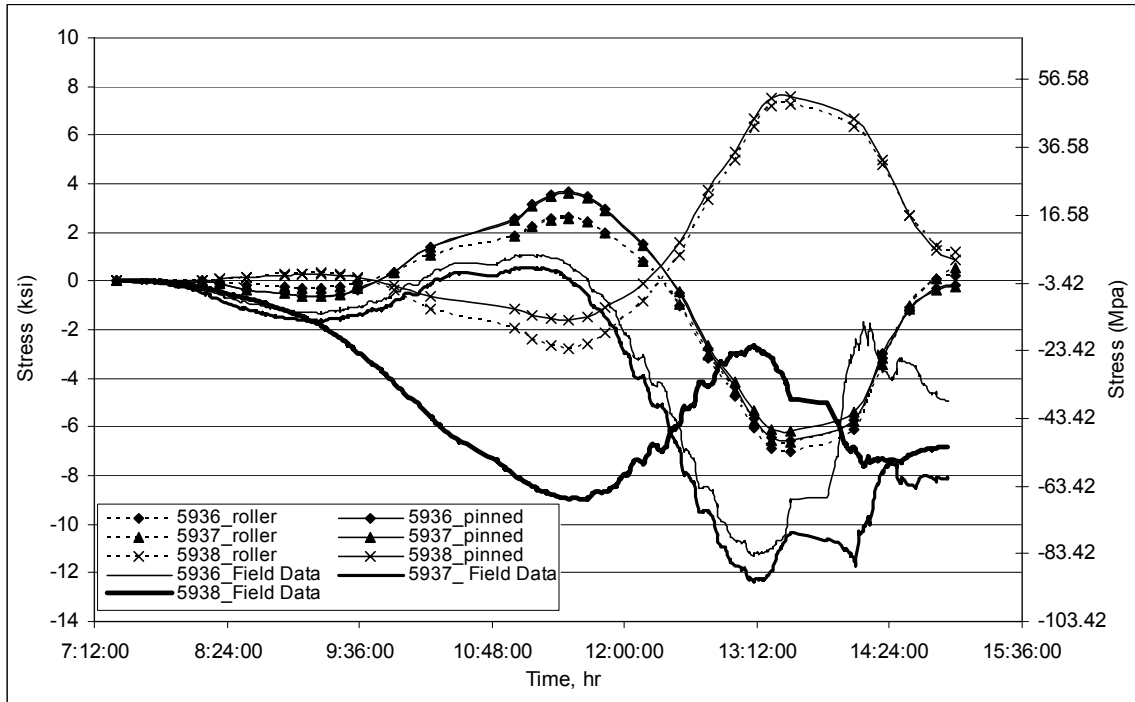
To accurately model the effects of the semi-integral abutments, detailed information regarding soil types and properties at the bridge site would need to be obtained. These properties would have helped establish the stiffness of the semi-integral abutments and the subsequent levels of restraint on the superstructure; however, insufficient information regarding actual soil conditions and properties was available. Examination of the field data indicated limited rotational restraint near the abutments. Therefore, girder abutment supports could initially be modeled using either rollers or pins. Girder response to deck placement for pinned abutment supports was considered to be one extreme for abutment restraint while roller supports were considered the other extreme. Finite element predictions for girder stresses at various instances during the deck pour were compared to field data to help assess which support conditions best mimicked actual behavior. Results from comparisons between measured and predicted flange stresses for the pinned and roller cases, plotted in Figure 5-6 for G1A and G5A, are summarized in Table 5-1. The table gives girder stresses for various extremes measured during the pour and after it was completed. The extremes occurred between the 8th and 10th hour of the pour (Extreme 1), between the 11th and 12th hour (Extreme 2), between the 13th and 14th hour (Extreme 3). It was observed that the percentage differences at end of pour were highest at G1A, a location furthest from the abutment, followed by G1B, the location nearer to the acute corner. The least percentage differences at end of pour were at G5A, a location nearer to the obtuse corner. While percentage differences indicated in the table were in some cases quite large, relative magnitudes for these differences were generally quite small. In addition, when both the figures and the table were examined and compared to the field data, results were largely inconclusive regarding the clear selection of one boundary condition set (pinned or roller) over the other. Roller supports appeared to provide more accurate predictions of response at intermittent points during the pour while pinned supports provided more accurate predictions of response at some of the extremes and at the completion of the pour. Therefore, pinned supports were chosen for the remainder of the calibration steps and pour sequencing studies. It is understood that more accurate modeling of the actual boundary conditions, such as the

incorporation of linear and/or nonlinear springs to mimic actual translational and rotational restraint at the semi-integral abutment, would influence the results. However, based upon the observed field data and boundary condition calibration work that was completed, support condition influence on trends that were observed from the parametric studies discussed in the sections that follow was assumed not to significantly affect the trends and results that were reported herein.

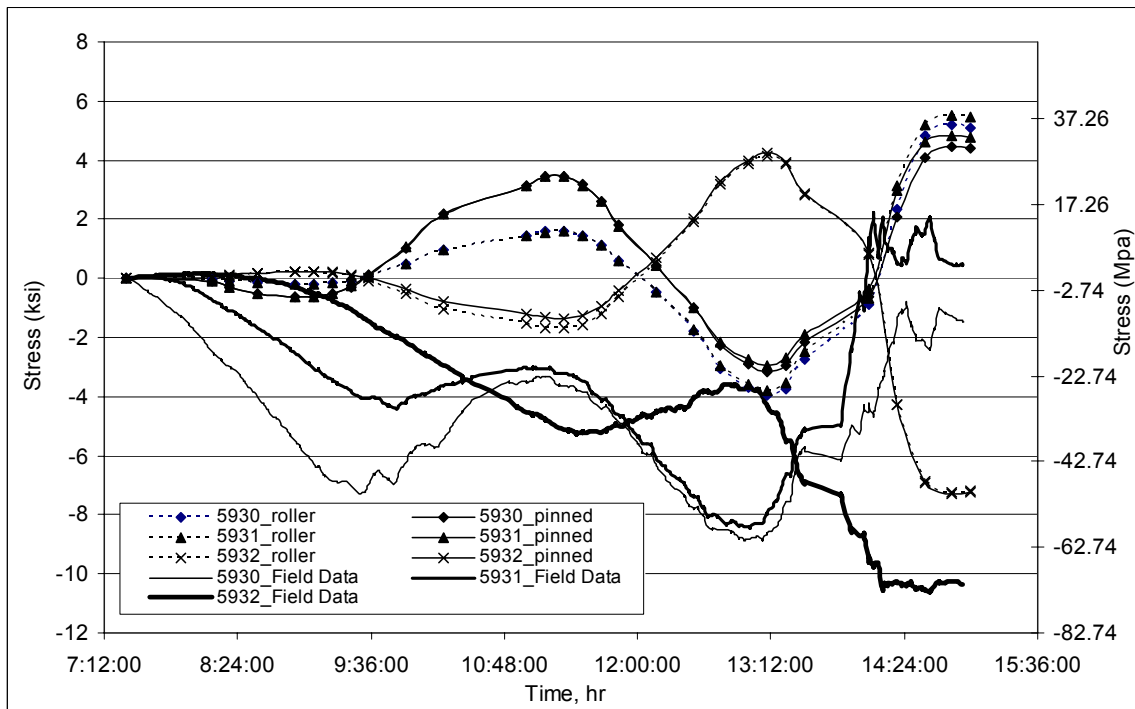
Table 5-1: Comparison between Numerical and Field Flange Stresses, Pinned and Roller Supports

Location		Extreme 1			Extreme 2			Extreme 3		
		Field (ksi)	Roller (ksi) (% diff)	Pin (ksi) (% diff)	Field (ksi)	Roller (ksi) (% diff)	Pin (ksi) (% diff)	Field (ksi)	Roller (ksi) (% diff)	Pin (ksi) (% diff)
G1A	5936	-1.304	-0.308 (76%)	-0.629 (52%)	1.051	2.259 (-115%)	3.544 (237%)	-10.705	-6.068 (43%)	-6.575 (39%)
	5937	-1.621	-0.286 (82%)	-0.624 (61%)	0.532	2.23 (-319%)	3.516 (-516%)	-11.778	-5.78 (51%)	-6.443 (45%)
	5938	-1.961	0.325 (117%)	0.035 (102%)	-8.356	-2.392 (71%)	-0.177 (98%)	-3.011	6.339 (311%)	3.788 (226%)
G1B	5933	-1.281	-0.159 (88%)	-0.561 (56%)	-1.669	1.203 (172%)	3.165 (290%)	-8.113	-3.236 (60%)	-2.855 (65%)
	5934	-0.024	-0.161 (-576)	-0.562 (-2267%)	-3.258	1.192 (137%)	3.157 (197%)	-9.494	-3.076 (68%)	-2.798 (71%)
	5935	-1.642	0.171 (110%)	0.002 (100%)	-5.656	-1.282 (77%)	0.004 (100%)	-4.845	3.376 (170%)	1.977 (141%)
G5A	5931	-6.886	-0.168 (98%)	-0.618 (91%)	-3.356	1.575 (147%)	3.363 (200%)	-8.722	-3.983 (54%)	-3.003 (66%)
	5930	-3.553	-0.164 (95%)	-0.616 (83%)	-3.057	1.569 (151%)	3.365 (210%)	-8.286	-3.807 (54%)	-3.085 (63%)
	5932	-0.826	0.177 (121%)	0.013 (102%)	-4.672	-1.675 (64%)	-0.067 (99%)	-3.77	4.16 (210%)	2.217 (159%)

Chapter 5 - Erection Study



(a) G1A

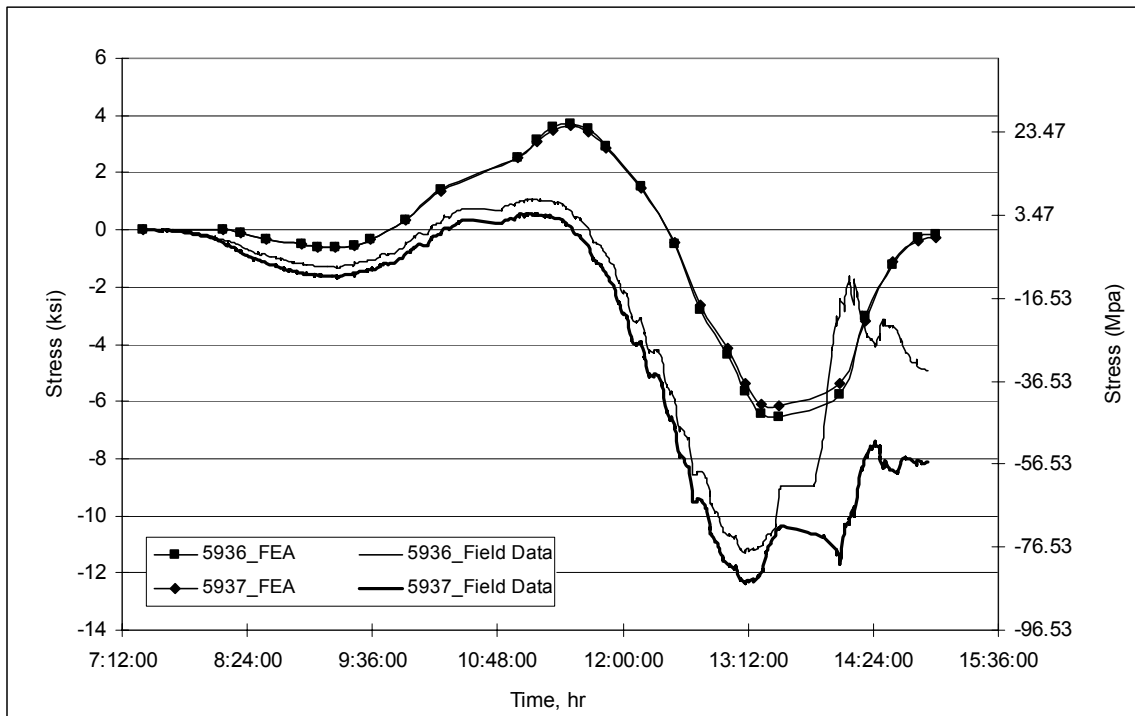


(b) G5A

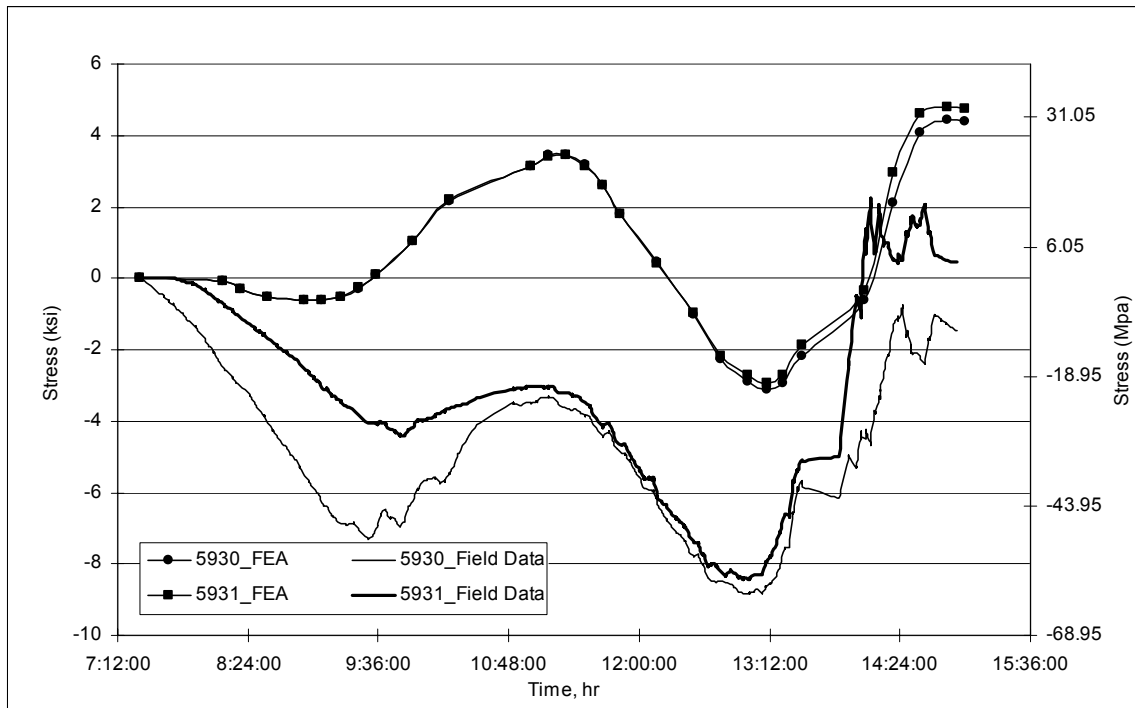
Figure 5-6: Comparing Girder Stresses, Pinned and Roller Abutment Supports

5.6.2 Incorporation of Temperature Effects

Representative comparisons between numerical predictions for flange stresses from the finite element model with pinned supports against the field data during the pour are provided in Figure 5-7. The figure indicates that, while the finite element models predicted trends for girder stresses quite well, as the pour progressed a general divergence between numerical and field results occurred. The field data generally experienced a gradual shift towards compressive stresses at all gage locations and this shift was not reproduced in the model.



(a) G1A



(b) G5A

Figure 5-7: Experimental and Numerical Bottom Flange Stress Variations, G1 and G5

To attempt to improve model accuracy prior to examining deck placement effects on response, air temperature changes that occurred during the pour were incorporated into the model. Values were recorded along the eastern side of the north abutment during the entire pour and, as is shown in Figure 5-8, the temperature varied from 36.0°F (2.2°C) to 63.7°F (17.6°C) during the seven-hour pour.

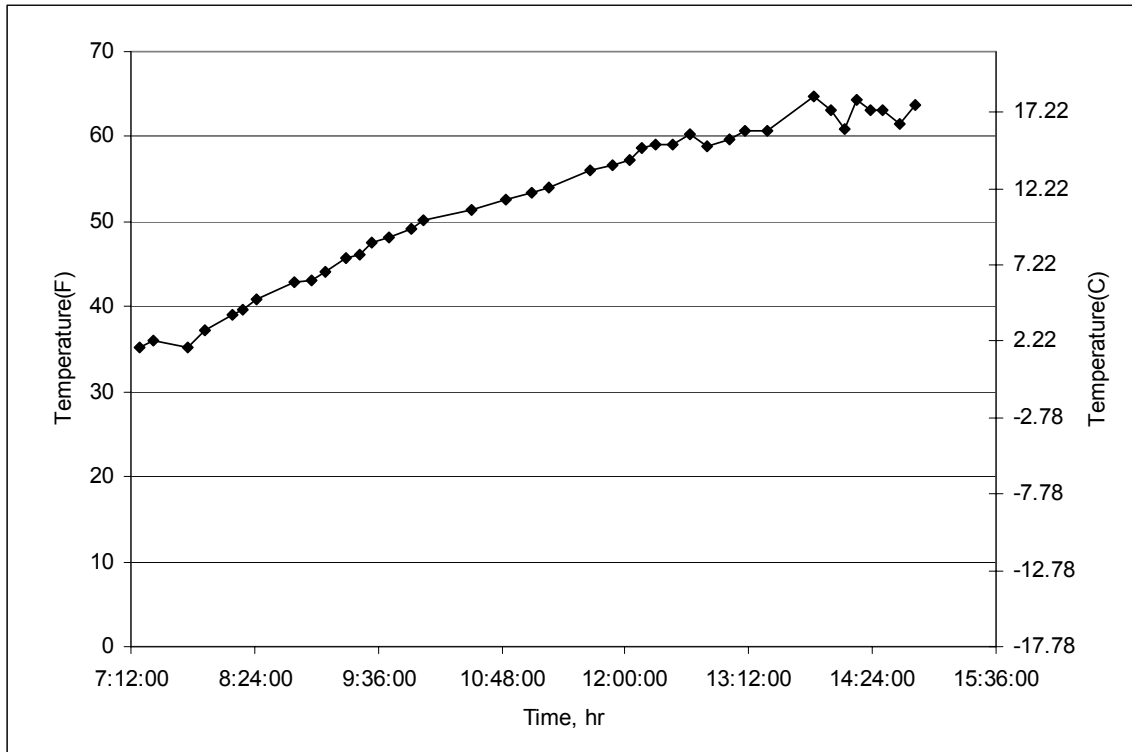
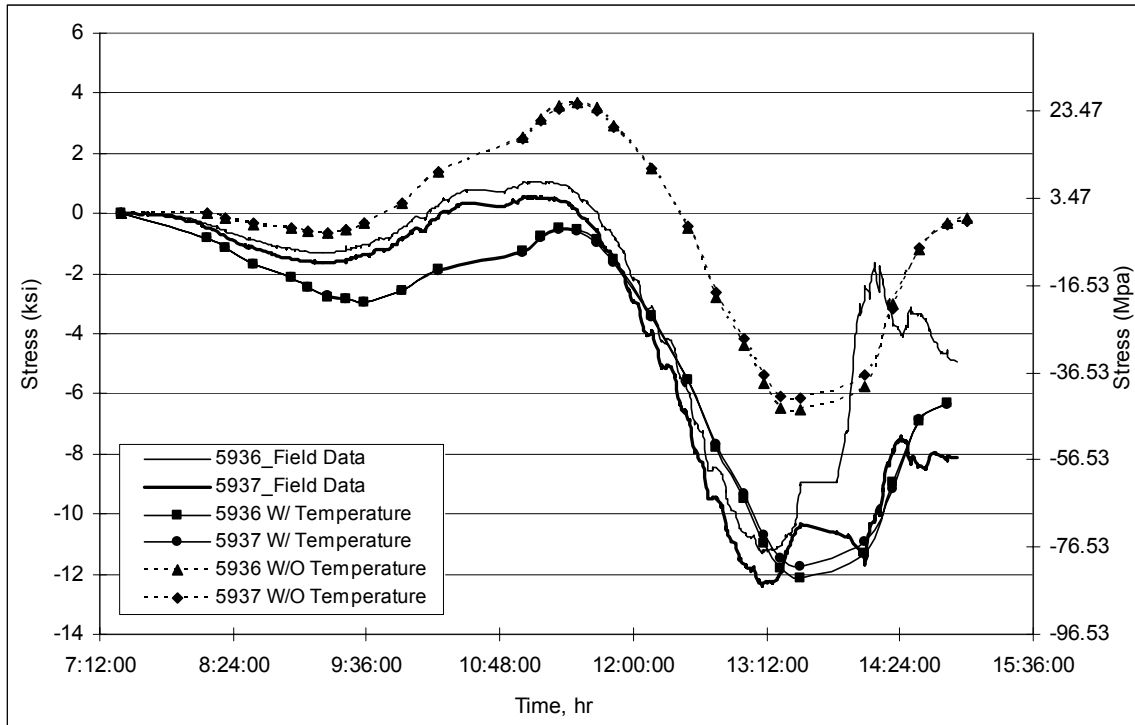
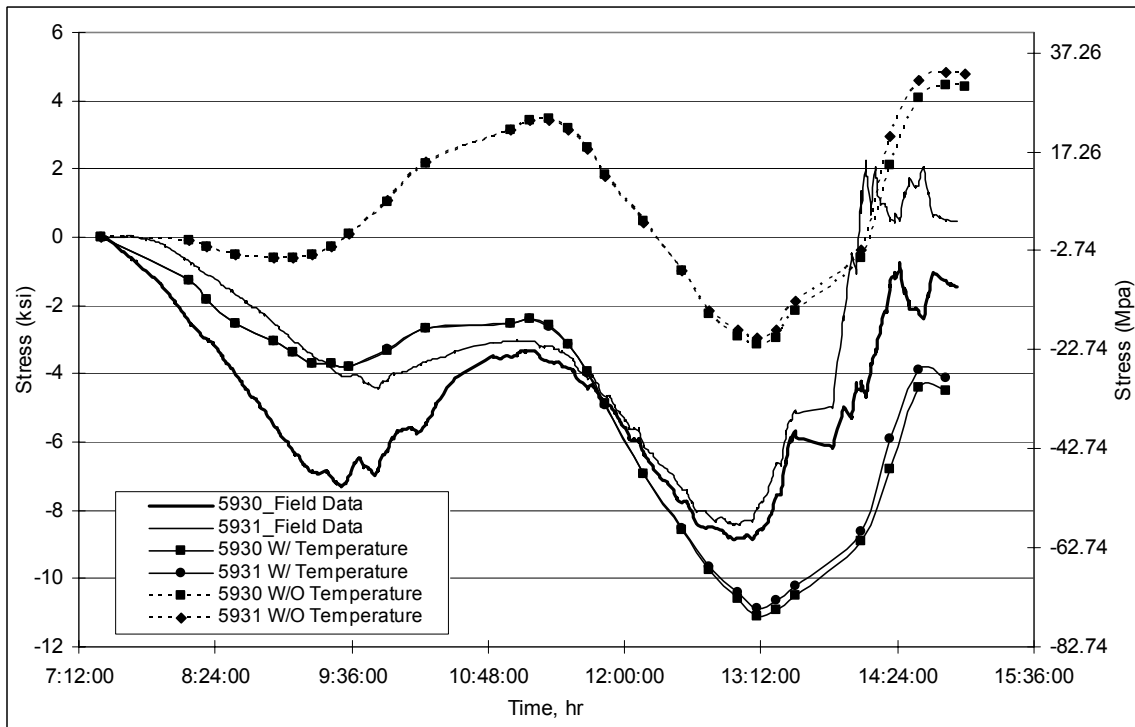


Figure 5-8: Measured Temperature Variation During Deck Pour

These temperature trends were incorporated into the finite element models by heating up the entire superstructure in a fashion that matched Figure 5-8. Results from the analysis including temperature and from the original analysis were again compared to the field data. Representative comparisons are shown in Figure 5-9 for each girder. The results clearly indicate an improvement in the numerical predictions, with errors in stress predictions being reduced from about 103% to 3% averagely in flanges.



(a) G1A



(b) G5A

Figure 5-9: Experimental and Numerical Bottom Flange Stress Variations, G1 and G5, Including Temperature

5.6.3 Incorporation of Concrete Stiffness

An additional attempt at improving numerical model accuracy was made prior to examining deck placement effects through the incorporation of changes in concrete stiffness. The contractor used a Master Builders Pozzoloth 200N retarder to prevent premature setting of the deck. However, recent research has shown that the development of composite action in steel-concrete systems with deck retarding agents can occur (Topkaya 2002). Therefore, the effects of premature composite action on the response of the system during construction were of interest.

Incorporation of the effects of formation of composite action during progression of the pour was examined through modifications to the concrete modulus for portions of the structure. Since time-dependant data regarding the concrete modulus was unavailable, incorporation of time-dependant modulus effects was conservatively accomplished as shown in Figure 5-10. The modulus of elasticity was increased to its full value for portions of the span as the pour progressed with the entire pour being divided into 29 steps. As the pour progressed, previous deck sections were assigned the fully matured concrete stiffness to simulate a fully cured section.

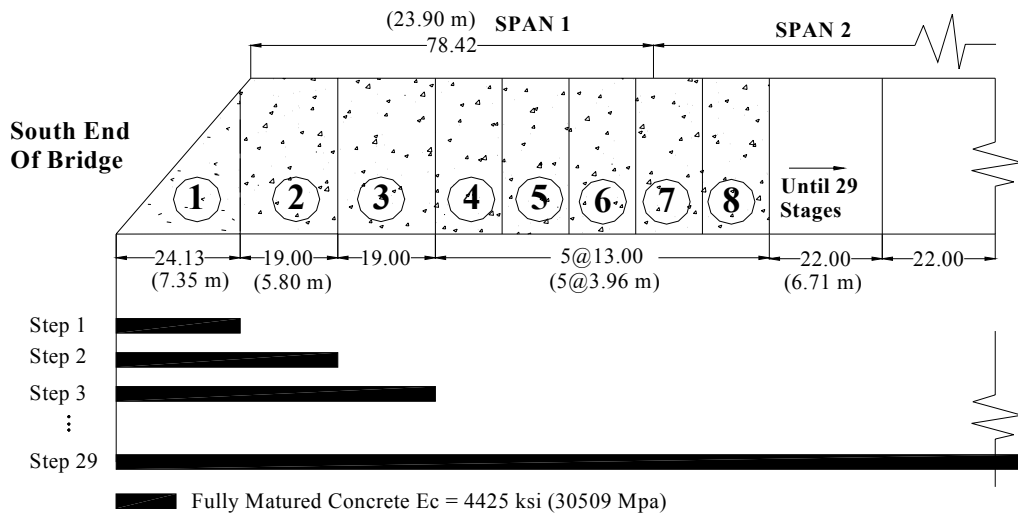
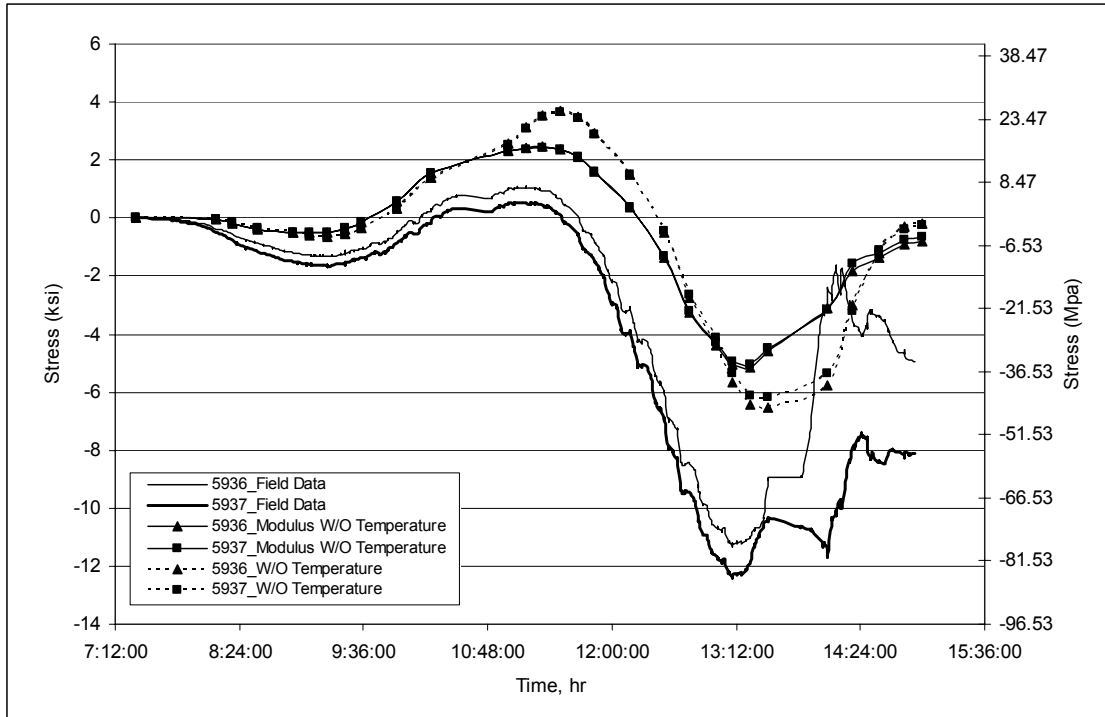


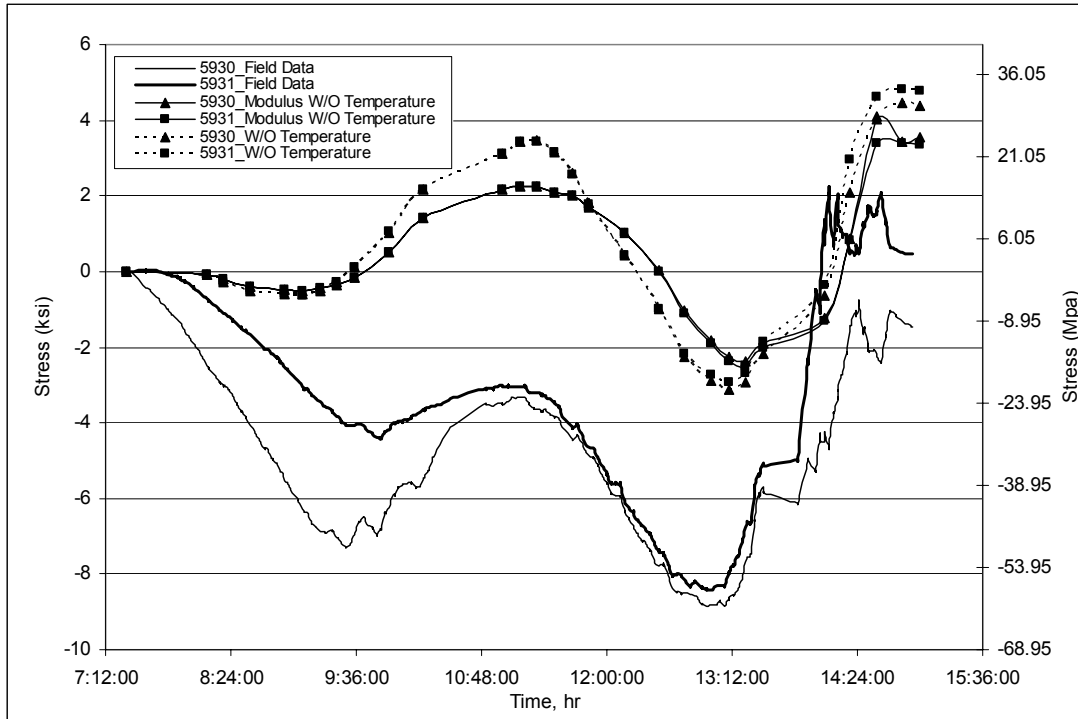
Figure 5-10: Incorporation of Time-Dependant Modulus into Numerical Models

Results from the analyses that included the effects of the formation of composite action are shown in Figure 5-11. These plots indicate that incorporation of the change in the modulus

and the subsequent incorporation of composite action has some small beneficial effects on the accuracy of the numerical predictions over a model that ignores these effects. The figure shows that an improvement of approximately 3% was achieved by incorporating a variable concrete stiffness.



(a) G1A

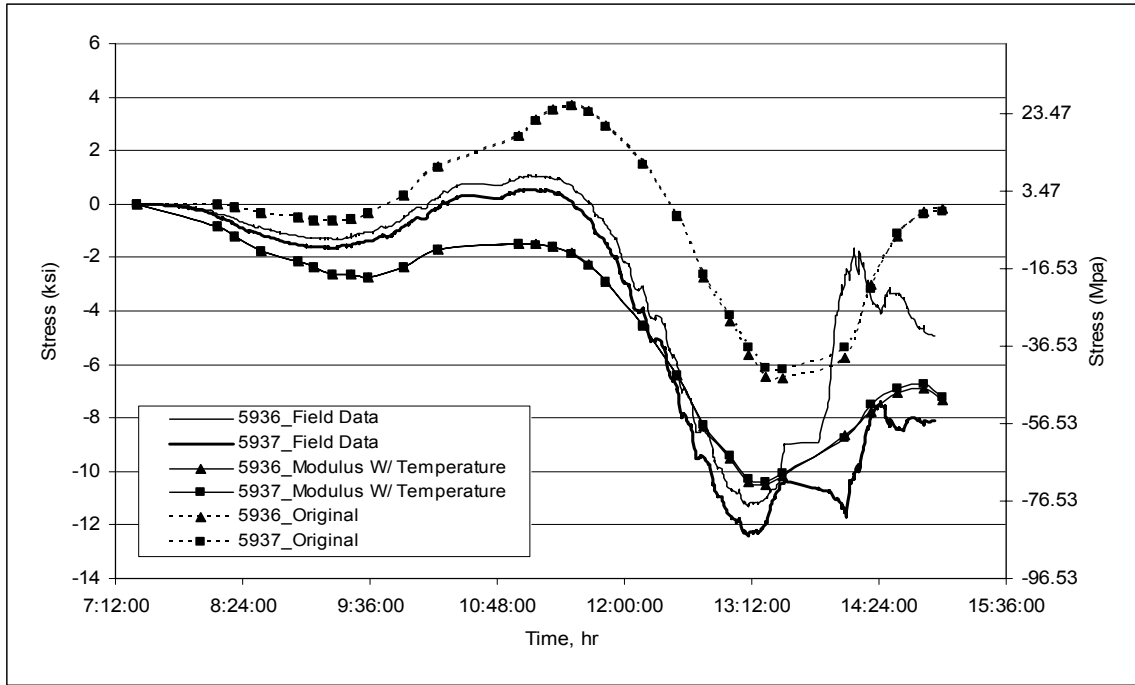


(b) G5A

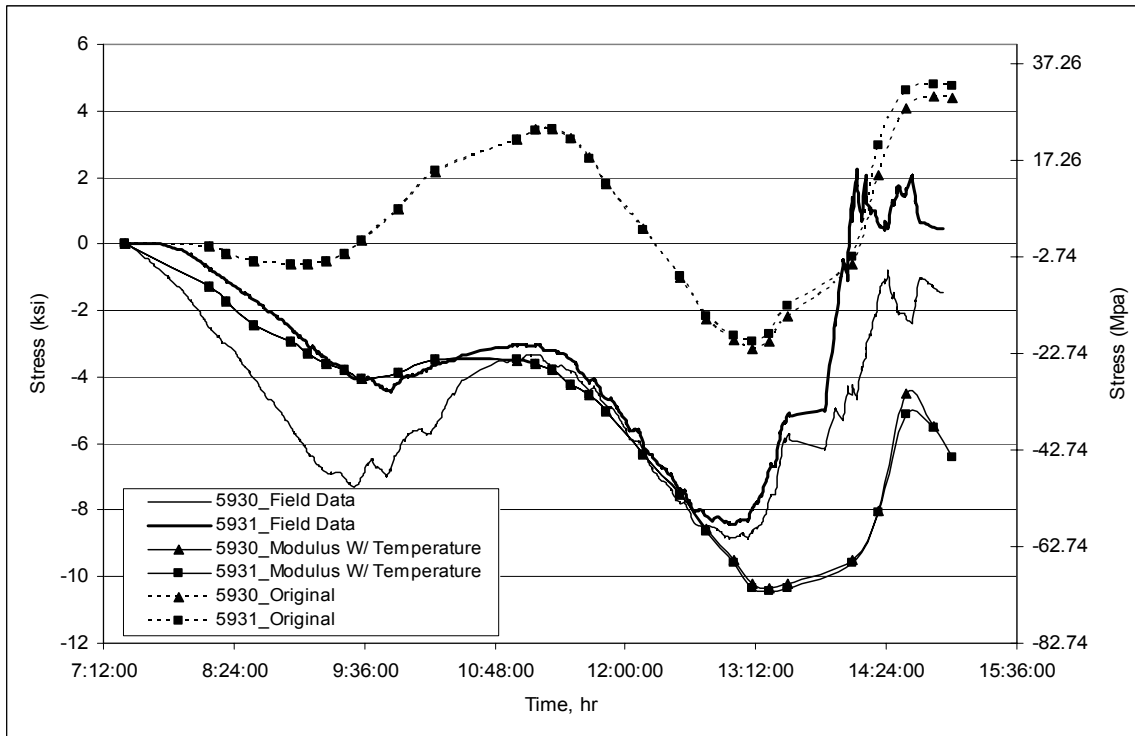
Figure 5-11: Experimental and Numerical Bottom Flange Stress Variations, G1 and G5, Including Time-Dependant Modulus

5.6.4 Combination of Calibration Results

A final calibration step involved examining the cumulative effects of incorporating the temperature changes and the time dependant modulus modifications into the model with the chosen boundary conditions. This comparison provided some insight into the total improvement in modeling accuracy that would be achieved. Results from this analysis, which included temperature and composite action, are shown in Figure 5-12 and are compared to field data and results from the original analysis that did not include temperature and time dependant modulus effects. This figure shows an appreciable improvement in behavioral predictions for a model including both temperature and modulus effects when compared to the original model, with differences between measured and predicted strains being reduced from 74% to 19%.



(a) G1A



(b) G5A

Figure 5-12: Experimental and Numerical Bottom Flange Stress Variations, G1 and G5, Including Temperature and Time-Dependant Modulus

5.7 POUR SEQUENCE STUDY

At the completion of the calibration phase, girder stresses and deflections generated from the original deck placement method (Case (a) from Figure 5-1) were examined numerically and compared against a method that placed the concrete parallel to the skew (Case (b) from Figure 5-1). These comparisons were used to establish if one method resulted in reduced stresses and deformations being induced into the structure during the deck pour.

For each of these analyses, a total of 29 separate sequential steps were used to apply the steel and wet concrete loads to the structure. The first step represented the self-weight of the steel superstructure being activated while the remaining steps represented a portion of the wet concrete load being placed either perpendicular to the centerline or parallel to the skew. Figure 5-13 provides a schematic detailing how the wet concrete loads were applied for Cases (a) and (b).

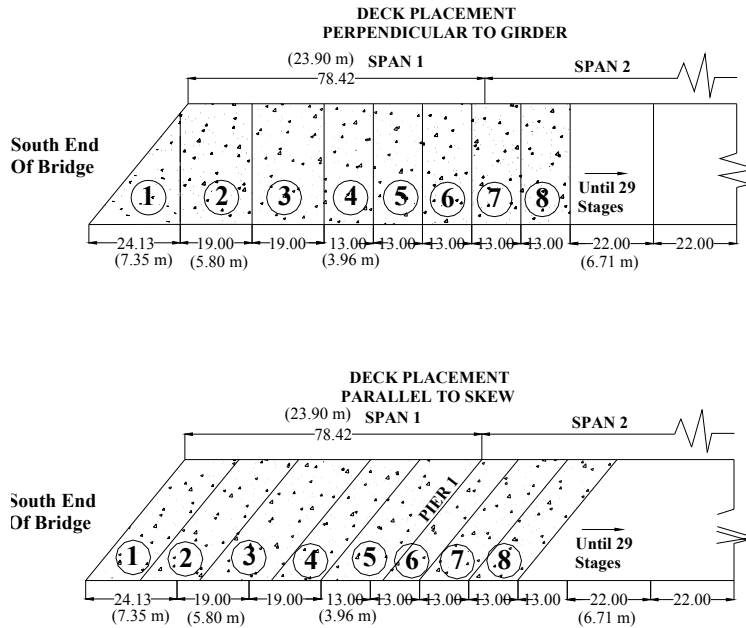
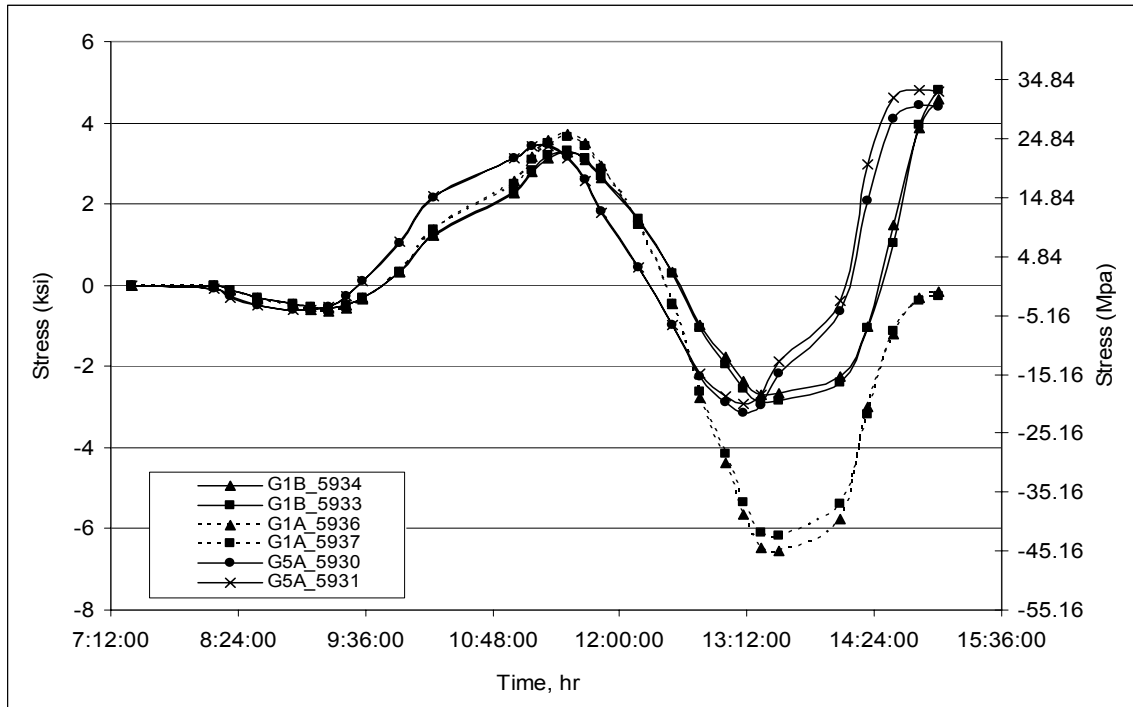


Figure 5-13: Deck Placement Sequence: (a) Perpendicular to Girder; (b) Parallel to Skew

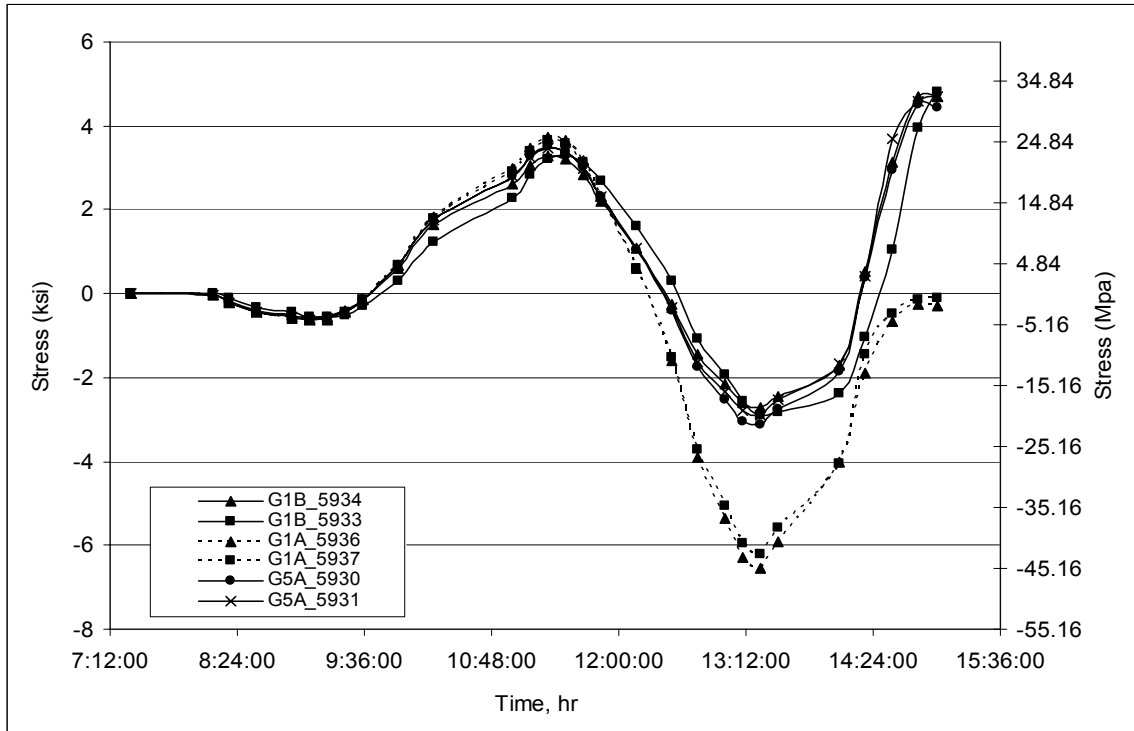
5.7.1 Study Results

Figure 5-14 details bottom flange stress variations at G1B and G5A (Figure 5-4) for Cases (a) and (b) throughout the duration of the pour. As the deck is placed perpendicular to the

roadway centerline, the bridge experiences the effect of differential girder deflections. The highest bottom flange stress differential observed between G1B and G5A is 4 ksi (27.6 MPa), a number that was representative of stress differentials observed at other locations within the superstructure and one that can not be considered insignificant. These differences indicate global rotation of the bridge during the pour.



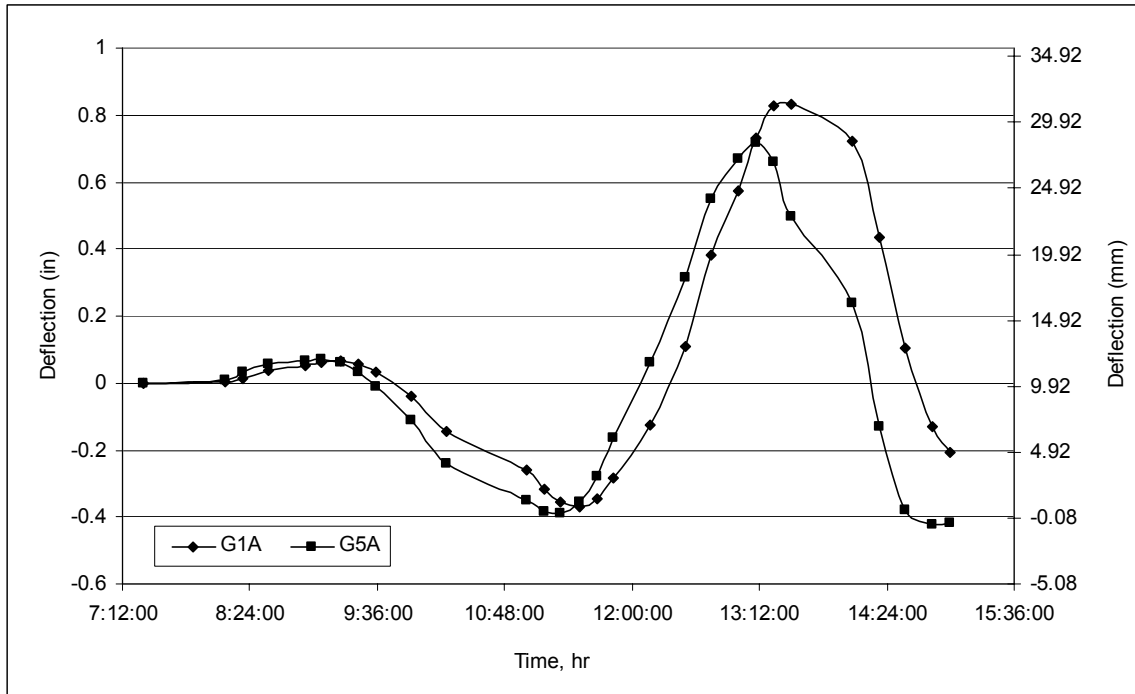
(a) Deck Placement Perpendicular to Centerline.



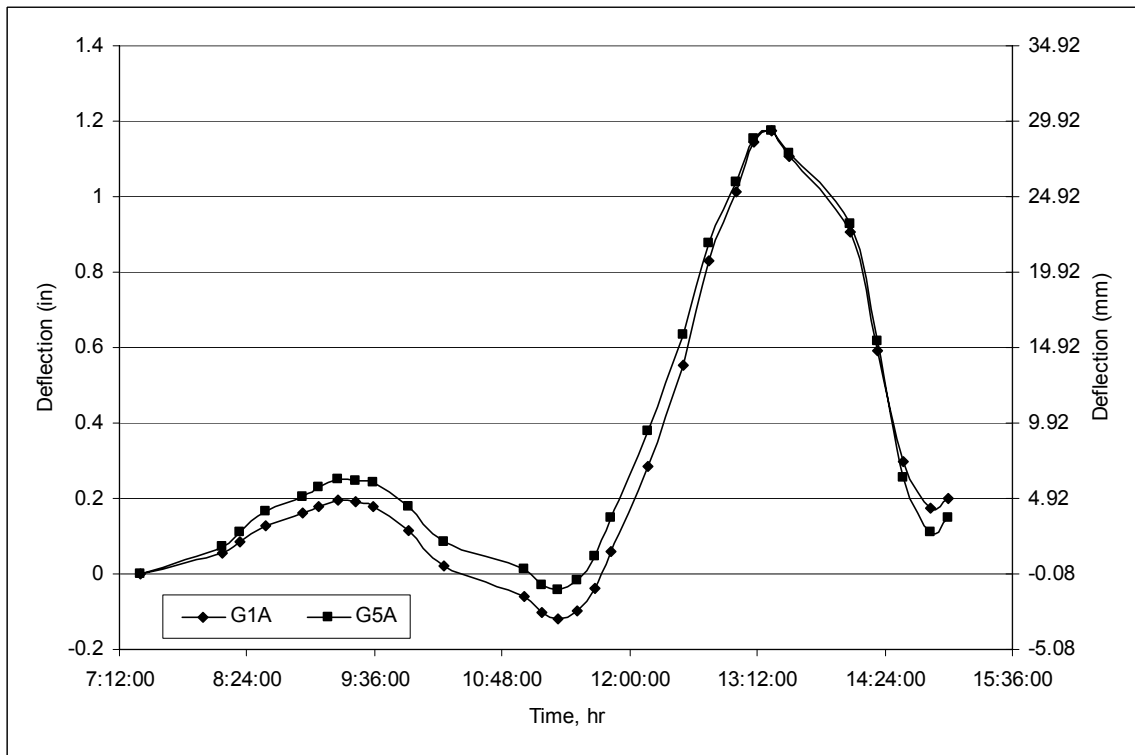
(b) Deck Placement Parallel to Skew
 Figure 5-14: Numerical Model Bottom Flange Stress Variations

When the pour sequence was changed to parallel to the skew, the maximum stress differentials observed between G1B and G5A were reduced to 0.42 ksi (2.9 MPa). This reduction indicated that only minor girder rotation was occurring as the pour progressed.

The influence of deck placement techniques on superstructure response is further reinforced in Figure 5-15, where vertical girder displacements are compared at G1B and G5A as the pour progressed. Figure 5-15(a) indicates a maximum differential deflection of 0.57” (14.5 mm) occurring at around the 14th hour between G1A and G5A, indicating some rotation of the superstructure. Figure 5-15(b) indicates differential deflection between G1A and G5A of 0.04” (0.91 mm), indicating that there is insignificant skew effect for deck placement parallel to skew.



(a) Deck Placement Perpendicular to Centerline



(b) Deck Placement Parallel to Skew

Figure 5-15: Numerical Model Girder Vertical Displacements

5.8 CONCLUSION

A finite element model was developed to study girder response during concrete deck placement for a continuous, skewed, steel, girder bridge. This model was calibrated against data recorded field monitoring of the structure's response during the actual deck pour.

During calibration, it was recognized that field data sustained an increasing, superimposed compressive effect during deck placement that was not reproduced in the numerical models. Replication of this effect in the numerical models was attempted through incorporation of air temperature and time-dependant concrete stiffness variations. Incorporation of these aspects during model calibration steps indicated that:

- Extreme changes in temperature during placement of the deck were of importance when attempting to accurately predict stress states in the superstructure at completion of the pour.
- Incorporation of time-dependant concrete modulus effects and the subsequent formation of premature composite action were of minor importance when attempting to accurately predict stress states in the superstructure at completion of the pour.

In addition, a numerical study investigating the effects of placing the wet concrete (1) perpendicular to the girders and (2) parallel to the skew was completed. These studies indicated that attempts to place the deck parallel to the skew would provide reduced differential deflections and stresses across the superstructure of the bridge that was studied. However, for this continuous structure the reductions were relatively small. Previous work by one of the authors (Norton et. al. 2003) indicates that deck placement parallel to the skew for simply-supported, steel structures with skew angles similar to those for the bridge studied herein provides a beneficial reduction of deformations and stresses that can result during construction. The combined results from that study and the current work indicate that, while continuity can possibly reduce the beneficial effects that can result from placing wet concrete parallel to the skew, bridge designers and builders should consider this placement method as a viable option when developed construction plans for skewed, steel I-girder bridges. It should be noted that results reported herein were limited to a single structure, however it can be inferred that they

would be representative of the response of skewed, multi-beam, composite steel-concrete bridges. However, additional studies, both experimental and numerical, would need to be performed to assess the ranges of parameters (e.g. skew angle, number of spans, number of girders, boundary conditions, etc.) over which the conclusions obtained herein would be applicable.

Chapter 6 - Field Testing of In-Service HPS-70W Bridge

6.1 INTRODUCTION

The American Association of State Highway and Transportation Officials (AASHTO) LRFD Bridge Design Specifications (2004) currently contains a simple procedure for analyzing and designing bridges. The typical procedures used for design require calculating the maximum bending moment and shear force based upon wheel loads from a design truck or lane loading on a one-dimensional beam, and then multiplying this bending moment and shear force by a wheel load distribution factor (DF) in order to obtain the moment and shear in an individual girder for design or evaluation. Therefore the load distribution factor is a key parameter in analyzing existing bridges and in designing new bridges.

The first AASHTO Standard Specifications for Highway Bridges was prepared in the late 1920s and published in 1931. Since then, numerous changes have been incorporated into every edition. Also, a great deal of research work has been conducted on the load distribution factor since then, including work done by Newmark and Siess (1954), Kostem and de Castro (1977), and Sander (1984), and some of these results were adopted by AASHTO.

The current AASHTO-LRFD Specification (2004) contains distribution factor formulas which have incorporated the results from National Cooperative Highway Research Program (NCHRP) Project 12-26, Distribution of wheel loads on highway bridges, by Zokaie, Osterkamp, and Imbsen (1991). This project was initiated in the mid-1980s in order to develop a comprehensive specification provisions for the distribution of wheel loads in highway bridges. The study was based on a database of actual bridges that included nearly 850 different bridges. Finally, a draft specification was prepared for determination of wheel load distribution factors. In the draft, several formulas were given to calculate DFs for several different bridge types, including beam-and-slab systems (reinforced concrete T-beams, prestressed concrete I-beams, and steel I-girders as the beam components), multi-cell box girders, side-by-side and spread box

beams, and slab bridges. Several follow-up research projects, such as work done by M. E. Mabsout (1998), were conducted to verify the accuracy of these formulas.

A new grade of High Performance Steel (HPS) has recently been developed through a cooperative research agreement between the Federal Highway Administration, the United States Navy, and the American Iron and Steel Institute, which lends itself to bridge applications. This new grade of steel, HPS-70W, has a higher yield strength, improved weathering characteristics, is much tougher than conventional steel, and is currently being used in bridge engineering. By using HPS engineers can use less material, span greater distances, and reduce the depth of bridge girders to achieve greater underpass clearances.

As of February, 2004, there were 201 HPS bridges in the United States. Among them, 109 were in service with the others under construction or in fabrication, design or planning. Among the 201 HPS bridges, 41 bridges are simple span, 46 have two spans, 30 have three spans, and 55 have four or more spans. Roughly 25% of the bridges are hybrid designs, which are defined as designs using both Grade HPS-70W and Grade 50W steel in the same cross section. The database used in NCHRP Project 12-26, which included nearly 850 different bridges, did not include HPS bridges. Therefore the AASHTO-LRFD distribution factors, which were based on NCHRP Project 12-26, should be validated for use with bridges incorporating high performance steel.

6.2 BACKGROUND

Numerous research studies have been conducted on the distribution of wheel loads on bridges. According to Sanders (1984), the majority of analytical approaches can be classified into one of four categories - orthotropic-plate theory, harmonic analysis and grillage analogies, folder-plate methods, and finite element or finite strip methods.

When orthotropic-plate theory is used, the structure is modeled as equivalent orthogonal anisotropic plates. The equivalent plates, which replace the bridge, including the girders and slab, have the same transverse and longitudinal flexural and torsional rigidities as the real structure. This method was widely used in beam and slab bridges and was first developed for

bridge analysis by Guyon (1946), whose results were valid for the no-torsion, full-torsion or isotropic conditions. Massonnet (1950) extended Guyon's analysis to include intermediate values of torsional rigidity by using an interpolation formula.

In the harmonic analysis and grillage analogy, the actual bridge structure is idealized as an assembly of girders or an equivalent grid system. Initial development of the harmonic analysis methods applied to bridge analysis was completed by Hendry and Jaeger (1956). This approach considers the same flexural and torsional rigidities as the orthotropic plate analysis, with the exception that torsional rigidity in the transverse direction is neglected.

The third general method of analysis, the folded plate method, can be divided into two categories: the ordinary method and the stiffness method. In the ordinary method, beam theory is used to determine the longitudinal behavior of the plate and one-way slab theory is applied to the transverse behavior. In the stiffness method, two-way slab theory and plane-stress theory are merged. In the second method, the actual bridge structure is idealized as an assembly of individual rectangular plate elements interconnected at the longitudinal joints and simply supported at the ends.

With advancements in desk-top computing and structural analysis software, the finite element and finite strip methods are becoming more common in the analysis of bridges. In these methods, the bridge is divided into a series of discrete elements or strips, where each element or strip has the same properties as the actual structure. The stiffness equations are then developed and solved. Loo and Cusens (1978) described the finite-strip method as applied to bridge engineering for several different types of bridges including curved and skew bridges, slab and pseudo-slab bridges, multi-span concrete box bridges and multi-span steel box-girder bridges. Since a general purpose finite element program usually involves labor intensive creation of input files, many engineers prefer to use commercially available programs such as SAP that incorporate preprocessors. Tarhini (1995) developed finite element models to represent the actual geometry of the bridge deck to analyze the elastic behavior of beam and slab bridges and used them in concert with field data to develop load distribution formulas for the AASHTO load distribution factor method. Mounir (1997) used two finite element programs, SAP90 and ICES-STRUDL, to idealize a typical one-span, simple support campsite bridge superstructure by

applying four finite-element modeling techniques. The wheel load distribution factors extracted from finite element method were compared with the results from AASHTO-LRFD formula. Also, a parametric study, varying span length and girder spacing, was conducted. Ahmet Turer (2000) modeled six typical steel stringer highway bridges with a 3D finite element strategy (SAP), and used test data to calibrate these models. Finally, the rating of bridges was conducted for calibrated models.

Besides these theoretical analyses, field tests are also important since without the investigation of the behavior of actual bridges, the accuracy of the analyses cannot be determined. Varney and Galambos (1965) provided a compilation of information for all of the highway bridge field tests from 1948 to 1965. The bibliography on load distribution, which was prepared by Lehigh University (1968, 1973), provided an excellent summary of the literature on related field tests, analytical methods, and model studies. Although not all these field tests resulted in load distribution, useful information can be extracted from each test.

6.2.1 Introduction of High Performance Steel

Since the application of HPS in bridge engineering began at the mid 1990's, the research of the behavior of HPS bridges was relatively limited. Sause (2001) tested two I-girders made from HPS-100W steel designed according to AASHTO-LRFD specifications (AASHTO 1996, 1998). His results showed that the AASHTO-LRFD specifications for the flexural strength of I-girders with compact or non-compact sections appear to be applicable to I-girders fabricated from HPS-100W steel.

Mans (2001) conducted several experiments to verify the safety of the 2000 interim version of the AASHTO-LRFD Bridge Design Specifications. The Design Specifications extended the applicability of the provisions for the design of composite plate girders in positive bending to include High-Performance Steel based on analytical work. He found that the code's current strength prediction equation with the proposed recommendation was adequate and the tension flange of composite flexural members constructed using HPS-70W steel could achieve large levels of tensile strain without fracture.

Greco (2003) applied experimentally verified nonlinear finite element modeling techniques for the study of hybrid high performance steel I-shaped beams to evaluate the appropriateness of using the current American building and bridge specification provisions for cross-sectional compactness within the context of applications involving A709 Gr. HPS-70W high performance steel.

Barth (2003) evaluated the influence of current AASHTO live-load deflection on the design of I-shaped steel girders, which were Grade 50W and HPS-70W.

Azizinamini (2004) summarized the major research studies on design issues related to application of high performance steel in bridge engineering. These design issues included: 1) flexural capacity of compact and non-compact HPS sections in negative bending; 2) ductility of HPS composite girders in the positive bending; 3) tensile ductility of HPS plates; 4) shear capacity of the hybrid steel plate girders; 5) live load deflections; 6) brief overview of the work that is underway to develop innovative bridge configurations capable of incorporating the advantages of HPS.

In 1994 AASHTO issued its first edition of bridge design specification based on LRFD. Since then, the Federal Highway Administration and the States have established a goal that the LRFD standards be used on all new bridge designs after 2007; only edits related to technical errors in the ASD version will be made thereafter. The ASD or Standard Specifications are applicable to new structure designs prior to 2007 and for the maintenance and rehabilitation of existing structures

The live load distribution formulas in the most recent edition of the AASHTO-LRFD Specification are based on the result from the National Cooperative Highway Research Program (NCHRP) research project 12-26 (Zokaie et. al., 1991). The project was performed in two phases: the first phase focused on beam and slab bridges and box girder bridges while the second phase concentrated on slab, multi-box beam, and spread box beam bridges. For each type of bridge, three levels of analysis were conducted. Level three was the most complex and accurate method, which involved detailed modeling of the bridge superstructure using the finite element method. Level two covered graphical methods, nomographs, influence surfaces, and other

simplified computer programs developed to apply such methods. Level one was the simplest method, which included simple formulas to predict the lateral response of a single girder by using the wheel load distribution factors. Zokaie found that girder spacing, span length, girder inertia and slab thickness have a profound effect upon the DF of bridges, especially for composite bridges. In the final report, Zokaie provided a draft specification for determination of wheel load distribution factors that was ultimately adopted by AASHTO.

6.3 OBJECTIVES AND SCOPE

This portion of the research work is focused on an HPS bridge that was constructed and opened to traffic in February, 2002. The objective of this part is to compare the load distribution factors extracted from bridge field tests with those values based on AASHTO-LRFD Bridge Design Specifications (2004) and then to verify the applicability these distribution factor formulas for HPS bridges.

The bridge to be investigated is designated as FAI-33-1309 (SFN: 2301067) and is located in Fairfield County, OH, south east of Columbus. The important dimensions from bridge plans are presented. The bridge is the first HPS Bridge to be constructed in Ohio, and thus serves as a demonstration bridge. It is an overpass structure on a new, divided by-pass highway around the city of Lancaster. As can be seen in Figures 6-1 through 6-3, the bridge has four-spans and a left-forward skew angle of $39^{\circ}-17'-06''$, and is supported by cap and column type piers on spread footings. The span lengths are $78'-5''$, $130'-10''$, $126'-10\frac{1}{2}''$ and $82'-4\frac{1}{2}''$. The bridge's abutments are integral and the $8\frac{1}{2}''$ thick, $39'-6''$ wide deck is supported by five girders which are spaced at $8'-0''$ center-to-center.

Chapter 6 - Field Testing

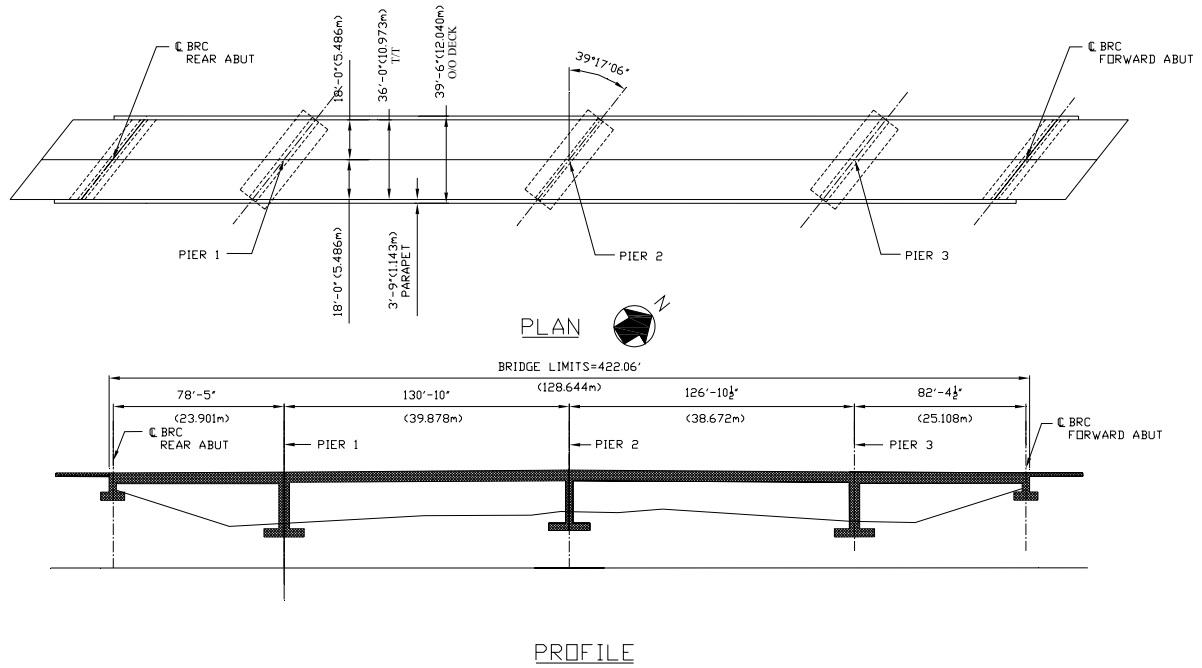


Figure 6-1: FAI-33-1309 Bridge Configuration

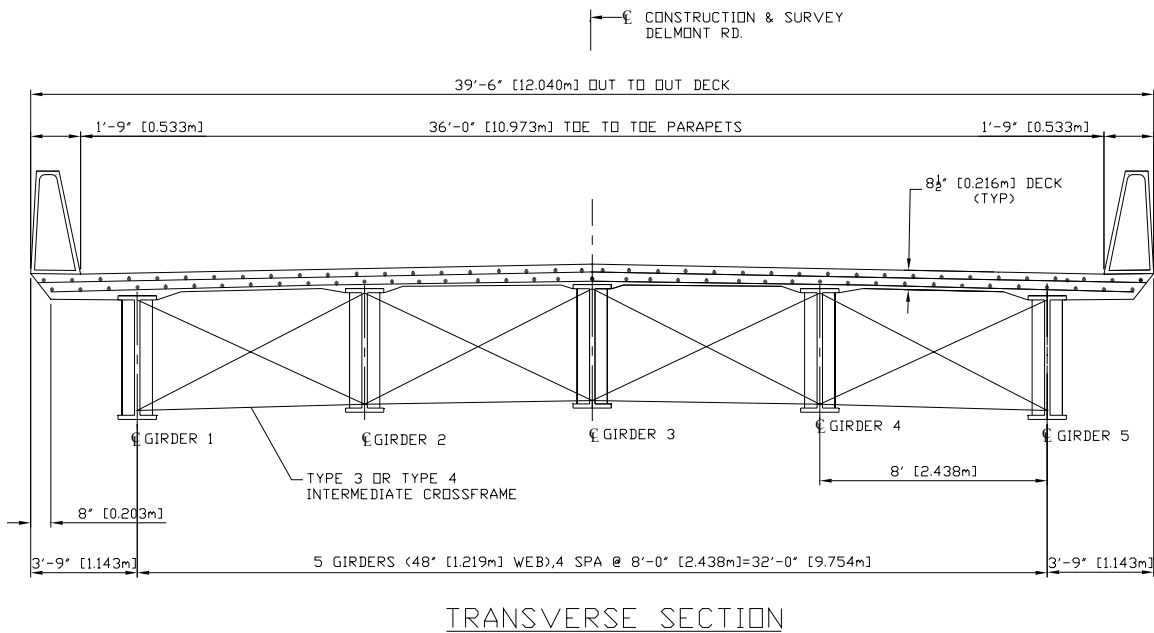


Figure 6-2: FAI-33-1309 Transverse Cross Section

Chapter 6 - Field Testing

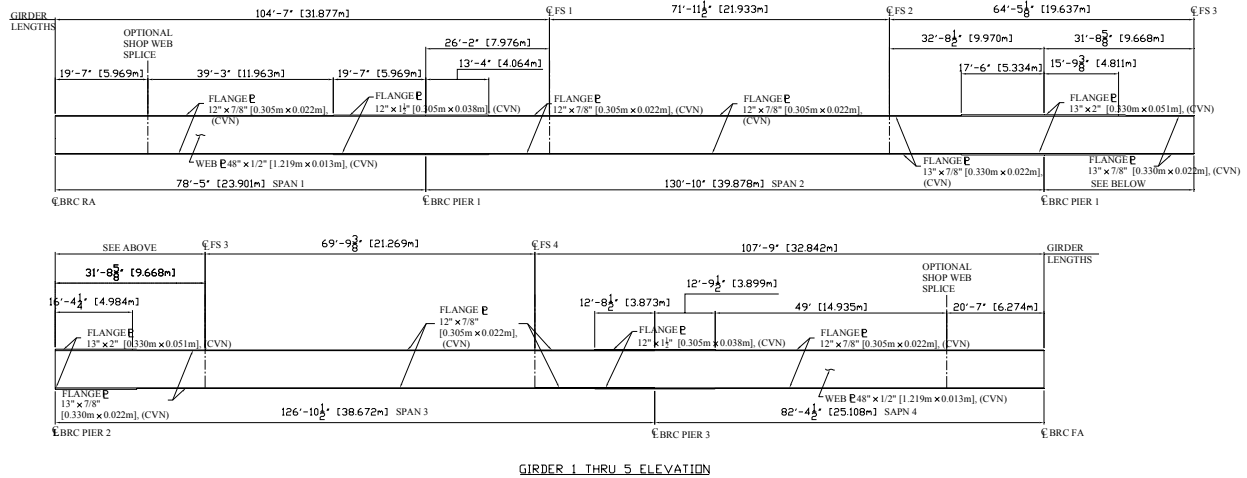


Figure 6-3: FAI-33-1309 Girder Details

6.4 FIELD TESTING PROCEDURES

Field testing is a real evaluation of bridge behavior, as it includes all the parameters that affect the bridge behavior. Strain gages and displacement transducers were installed at the bridge's critical locations and data was acquired while the bridge was loaded with one or more dump trucks. From the strain and deflection data collected during field tests, the distribution factors for moment will be determined. In this project, three field tests were performed over a period of 16 months. The first test was conducted in February, 2003, the second test was conducted in September, 2003, and the third test was conducted in June, 2004. The rationale for testing three times was to evaluate the bridge behavior under different conditions and to monitor the behavior of the bridge during the several months of service. Each bridge field test consisted of both moving load tests and static tests.

6.4.1 Instrumentation

The strain gages used in all bridge tests were BDI Strain Transducers (Figure 6-4) made by Bridge Diagnostics, Inc. Made of Aluminum, the gages have a strain range of -4000 to +4000 $\mu\epsilon$ and are based on a full Wheatstone bridge with 4 active 350 Ω foil gages using a 4-wire hookup. The accuracy of the gage is $\pm 2\%$, individually calibrated to NIST standards, and the sensitivity is approximately 300 $\mu\epsilon/mV/V$. This type of gage can be used for recording strains on highway bridges, railroad bridges, lock gates, amusement park rides, and other structures

without tedious work such as careful surface preparation and soldering which are usually required to install foil strain gages in the field. To prevent damage of the gage from installation and removal, the gages were attached to steel girder using special mounting tabs and adhesive, and were connected to the data acquisition system through cables with special quick-lock connectors.



Figure 6-4: Strain Transducers used for Field Testing

The DC-LVDT displacement transducers, which use the linear variable differential transformer (LVDT) sensing principle, were used to measure the girders' deflections. The gages have integral electronics for operation from simple, well-regulated DC power supplies of between -15 and +15 volts without the need for external instrumentation. The integral electronics includes an oscillator which energises the primary winding. The resulting signal from the secondary windings then passes through a demodulator converting the signal into a DC output. By multiplying by a calibration factor, the actual displacement can be read from the DC output. The LVDTs were mounting by using a modular and adjustable system that was constructed specifically for the purpose.

During the first of the three field experiments, the FHWA field survey team was invited to implement their laser deflection measurement system on the bridge. The team did in fact deploy their system but because of excessively cold temperatures, the system did not function correctly and no meaningful data was collected. The team was invited to again participate during the second and third field tests but was not able to because of scheduling conflicts with other summer work.

The strain gages and deflection gages were connected to the data acquisition system, a MegaDAC 3415AC, which is made by Optim Electronics Corporation. Powered by 110 AC, the MegaDAC can acquire up to 25,000 samples per second, has a 256 Megabyte memory storage capacity, 15 module slots, and can accommodate up to 512 input channels. By using the TCS software designed specially for the MegaDAC, strain and deflection data can easily be stored on the hard drive of a notebook computer in 'csv' format, which can then be processed by MS-Excel.

To obtain a complete understanding of the bridge's behavior under load, it would be ideal to know the strain and deflection at every position of bridge. But in fact, because of limitations on the number of gages, input channels of the data acquisition system, access to the girders, and efficiencies in gage installation, the gages are usually installed only at critical sections. For example, to obtain maximum positive moment, attaching the strain gages at the mid-span of the girders is obligated. On the other hand, installing the strain gages on girders near the piers will provide information about the negative moment of the continuous bridge under load. Since the maximum deflection of the bridge usually occurs at midspan or very close to midspan, the deflection gages are quite often there. For each bridge test, the gage layouts were slightly different, and details are shown in Figure 6-5 through Figure 6-8Figure 6-12.

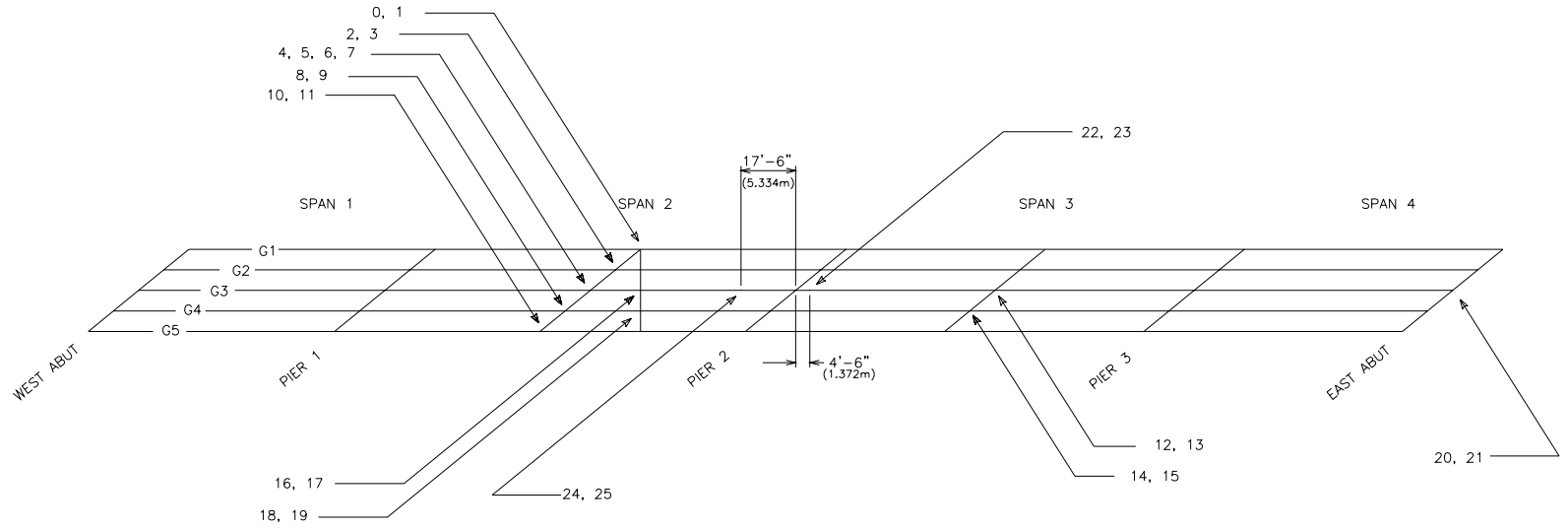


Figure 6-5: Field Test #1 Instrumentation Plan - Plan View

Chapter 6 - Field Testing

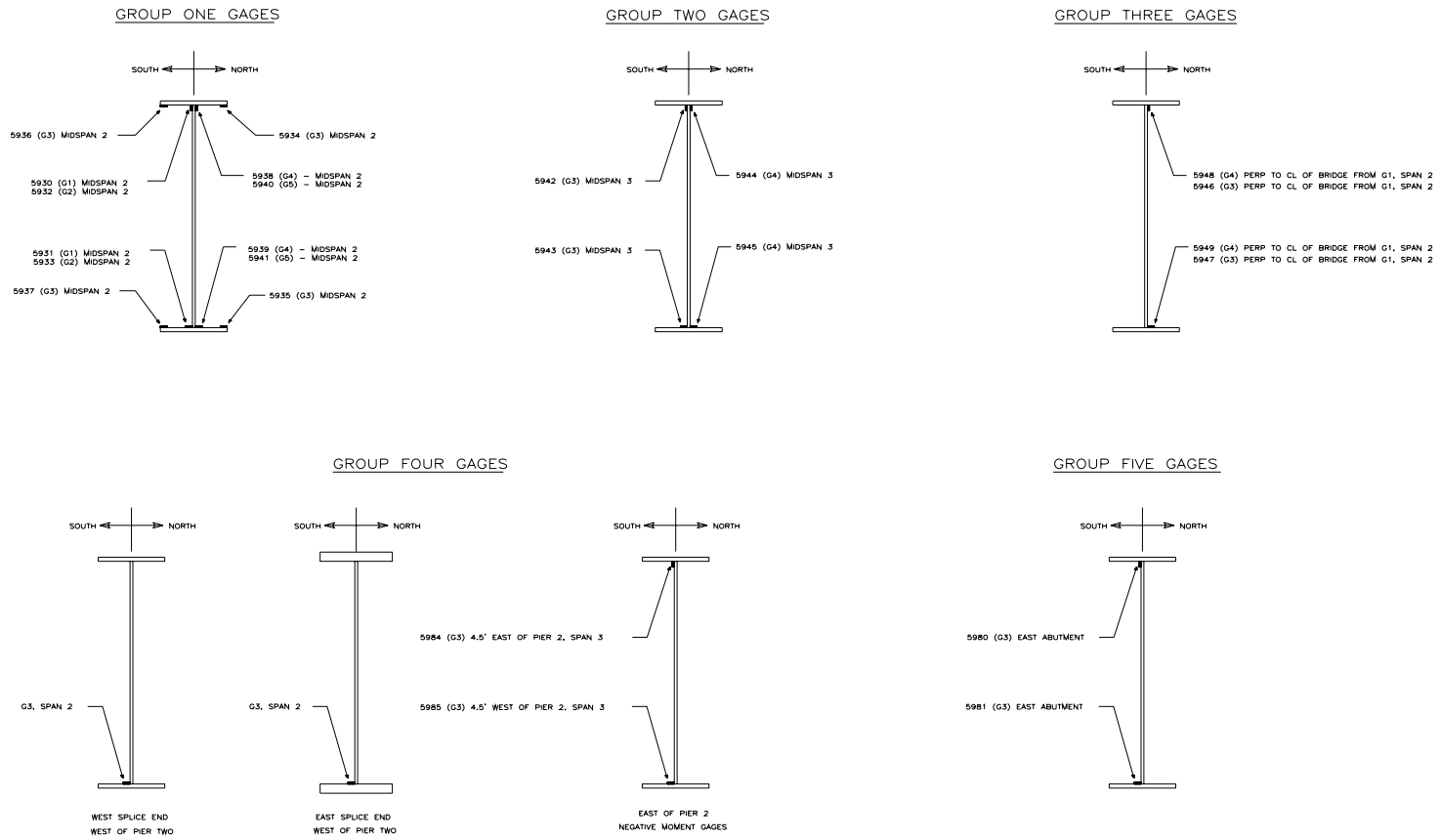


Figure 6-6: Field Test #1 Instrumentation Plan - Section View

Chapter 6 - Field Testing

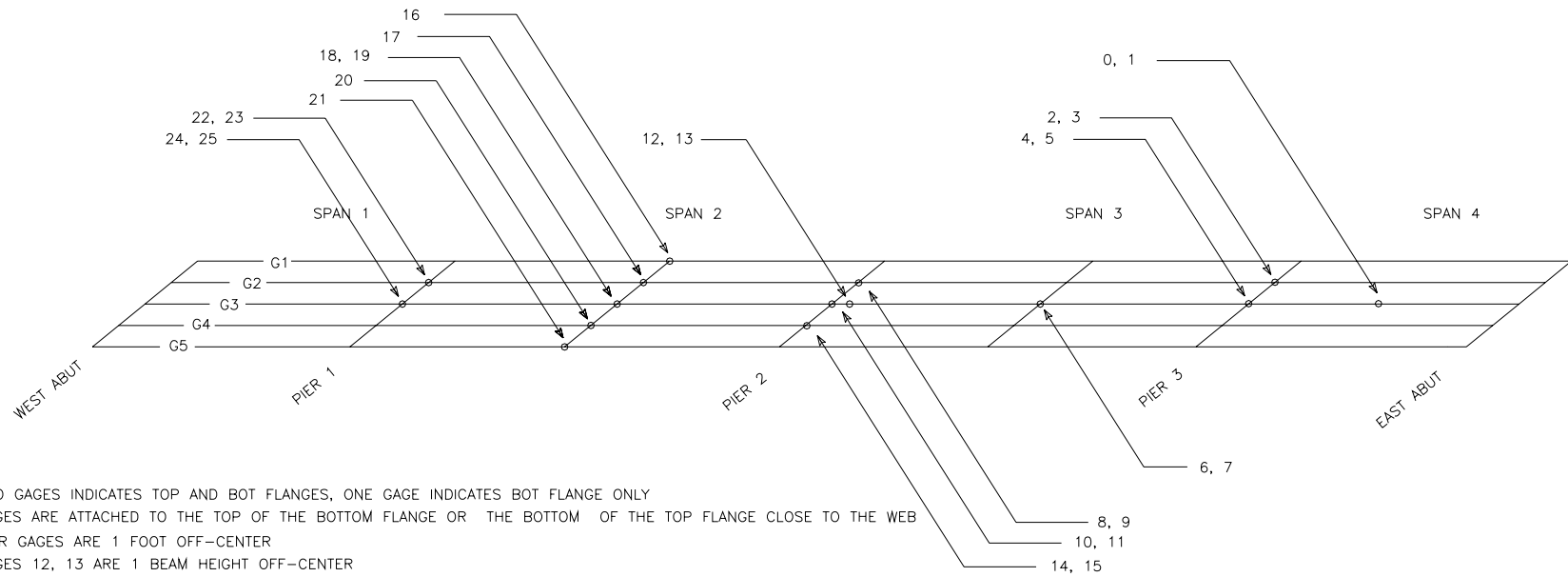
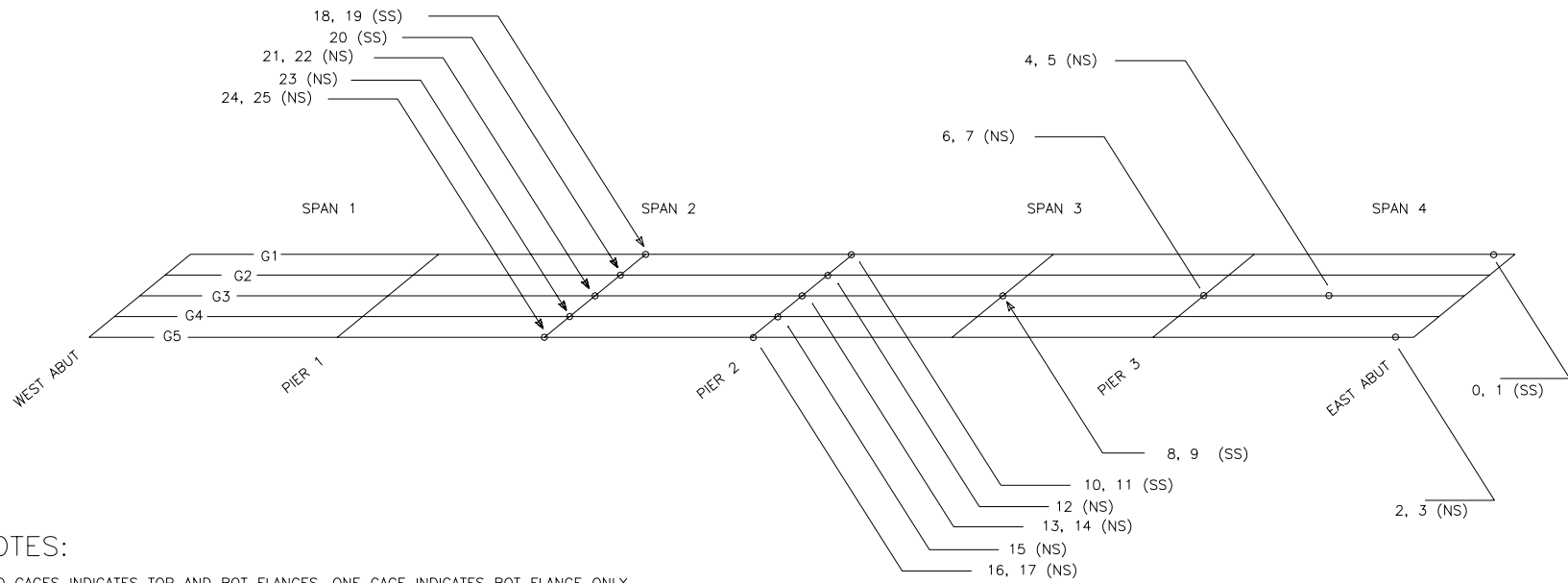


Figure 6-7: Field Test #2 Instrumentation Plan - Plan View

Chapter 6 - Field Testing



NOTES:

TWO GAGES INDICATES TOP AND BOT FLANGES, ONE GAGE INDICATES BOT FLANGE ONLY
 GAGES ARE ATTACHED TO THE TOP OF THE BOTTOM FLANGE OR THE BOTTOM OF THE TOP FLANGE CLOSE TO THE WEB
 NS = NORTH SIDE OF GIRDER; SS = SOUTH SIDE OF GIRDER

Figure 6-8: Field Test #3 Instrumentation Plan - Plan View

6.4.2 Trucks and Load Configurations

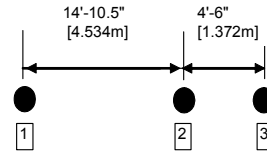
To have a series of consistent tests, the same type of truck was used in all bridge tests. In each test, the trucks, shown in Figure 6-9, were provided by the Ohio Department of Transportation and were loaded with either sand or salt. One typical loaded truck had a total weight of 48,000 lbs with axel spacings of 14'-7" and 4'-6". The trucks used in each test were not identical, however, and the weights and the axial spacings were slightly different for each test. The details of each truck are shown in Figure 6-10 through Figure 6-12 for each experiment.



Figure 6-9: Loaded Dump Trucks used for Truck-Load Testing

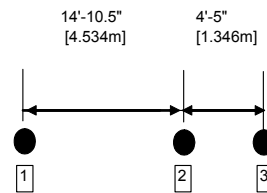
TRUCK 662

Axle	Left Wheel (lbs) [kg]	Right Wheel (lbs)[kg]	Total Axle (lbs) [kg]
1	7200 [3266kg]	7400[3357kg]	14600[6622kg]
2	9500 [4309kg]	10400[4717kg]	19900[9026kg]
3	9400[4264kg]	10000[4536kg]	19400[8800kg]
Gross Weight (lbs) [kg]			53900[24449kg]



TRUCK 832

Axle	Left Wheel (lbs) [kg]	Right Wheel (lbs)[kg]	Total Axle (lbs) [kg]
1	7000[3175kg]	7000[3175kg]	14000[6350kg]
2	9500[4309kg]	10200[4627kg]	19700[8936kg]
3	9600[4354kg]	10200[4627kg]	19800[8981kg]
Gross Weight (lbs) [kg]			53500[24267kg]



TRUCK 781

Axle	Left Wheel (lbs) [kg]	Right Wheel (lbs)[kg]	Total Axle (lbs) [kg]
1	6400[2903kg]	6300[2858kg]	12700[5716kg]
2	8800[3992kg]	9200[4173kg]	18000[8165kg]
3	8800[3992kg]	9100[4128kg]	17900[8119kg]
Gross Weight (lbs) [kg]			48600[22045kg]

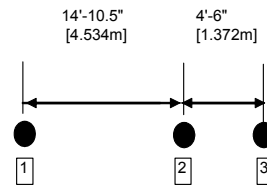
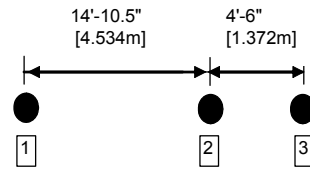


Figure 6-10: Data for Trucks used in Field Experiment #1

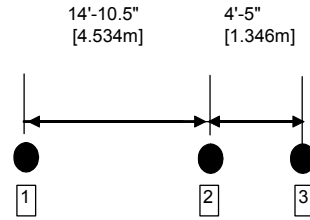
TRUCK 517

Axle	Left Wheel (lbs) [kg]	Right Wheel (lbs)[kg]	Total Axle (lbs)
1	6750[3062kg]	7300[3311kg]	14050[6373kg]
2	7500[3402kg]	9200[4173kg]	16700[7575kg]
3	7900[3583kg]	9100[4128kg]	17000[7711kg]
Gross Weight (lbs) [kg]			47750[21659kg]



TRUCK 781

Axle	Left Wheel (lbs) [kg]	Right Wheel (lbs)[kg]	Total Axle (lbs) [kg]
1	6700[3039kg]	6700[3039kg]	13400[6078kg]
2	8100[3674kg]	8900[4037kg]	17000[7711kg]
3	8050[3651kg]	8550[3878kg]	16600[7530kg]
Gross Weight (lbs) [kg]			47000[21319kg]



TRUCK 832

Axle	Left Wheel (lbs) [kg]	Right Wheel (lbs)[kg]	Total Axle (lbs) [kg]
1	6350[2880kg]	6450[2926kg]	12800[5806kg]
2	7850[3561kg]	8200[3719kg]	16050[7280kg]
3	7900[3583kg]	8250[3742kg]	16150[7326kg]
Gross Weight (lbs) [kg]			45000[20412kg]

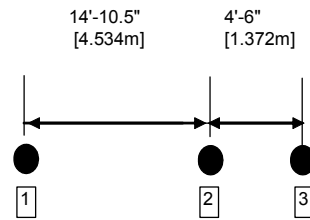
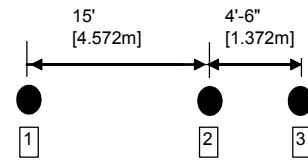


Figure 6-11: Data for Trucks used in Field Experiment #2

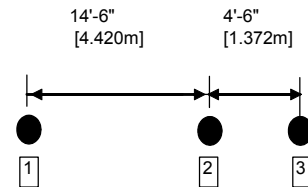
TRUCK 781

Axle	Left Wheel (lbs) [kg]	Right Wheel (lbs)[kg]	Total Axle (lbs) [kg]
1	7700[3493kg]	7700[3493kg]	15400[6985kg]
2	9600[4354kg]	10500[4763kg]	20100[9117kg]
3	9200[4173kg]	10400[4717kg]	19600[8890kg]
Gross Weight (lbs)[kg]			55100[24993kg]



TRUCK 858

Axle	Left Wheel (lbs) [kg]	Right Wheel (lbs)[kg]	Total Axle (lbs) [kg]
1	7100[3221kg]	7200[3266kg]	14300[6486kg]
2	9500[4309kg]	9500[4309kg]	19000[8618kg]
3	9200[4173kg]	9700[4400kg]	18900[8573kg]
Gross Weight (lbs)[kg]			52200[23678kg]



TRUCK 517

Axle	Left Wheel (lbs) [kg]	Right Wheel (lbs)[kg]	Total Axle (lbs) [kg]
1	6600[2994kg]	6900[3130kg]	13500[6123kg]
2	8400[3810kg]	9200[4173kg]	17600[7983kg]
3	8600[3901kg]	9200[4173kg]	17800[8074kg]
Gross Weight (lbs)[kg]			48900[22181kg]

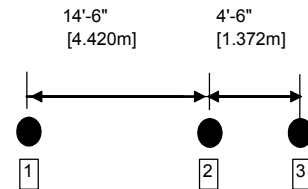


Figure 6-12: Data for Trucks used in Field Experiment #3

Two types of experiments were conducted during each field test — moving load tests and static tests. Compared with the static tests, moving load tests provide more information about the bridge under truckload. A strain gage only gives one meaningful data point during each static test, but numerous data points are collected from the same gage when a moving load test is performed. In essence, the test data from one gage during a moving load test are the strain

responses for the position where the gage is attached. In some cases, if the same pattern of the trucks is used, the data from the static test is only one point of the data from the moving load test. Since the pattern of the trucks during the moving load test is restricted, static tests serve as supplementary test for the moving-load data.

During moving load tests, a single truck or train of three trucks was driven over the bridge while strain and displacement data at critical locations was collected. To reduce the dynamic effects, the speed of the trucks was held at or below 5 mph.

Three field experiments were conducted, during which five types of moving load tests were designated, but not all of them were conducted during each experiment. The five types of moving load tests are described below:

- Moving Load Type #1: Three trucks moving east to west along the west-bound lane of the bridge, as is shown in Figure 6-13.
- Moving Load Type #2: Three trucks moving west to east along the east-bound lane of the bridge, as is shown in Figure 6-14.
- Moving Load Type #3: Three trucks moving east to west along the centerline of the bridge, as is shown in Figure 6-15.
- Moving Load Type #4: One truck moving east to west along the middle of the west-bound lane of the bridge, as is shown in Figure 6-16.
- Moving Load Type #5: One truck moving west to east along the middle of the east-bound lane of the bridge, as is shown in Figure 6-17.

Table 2-1 shows which type of moving load test was conducted during each of the three FAI-33 Bridge field tests. Truck information (weights and axle spacings) is tabulated in Figures 2-12, 2-33, and 2-40 for three field tests.

Chapter 6 - Field Testing

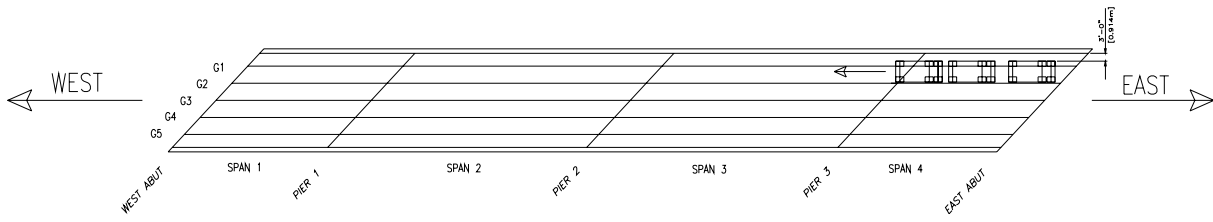


Figure 6-13: Moving Load Type #1

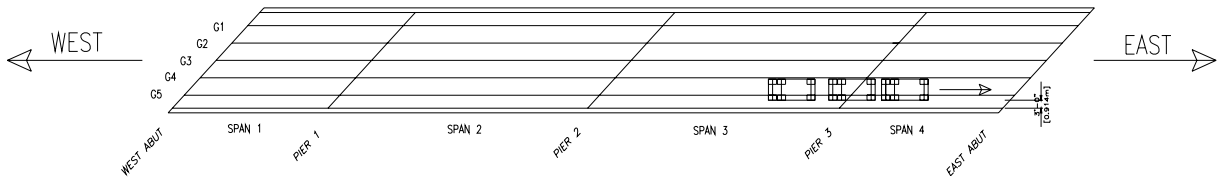


Figure 6-14: Moving Load Type #2

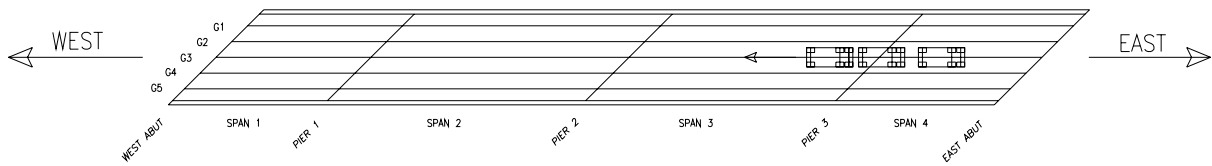


Figure 6-15: Moving Load Type #3

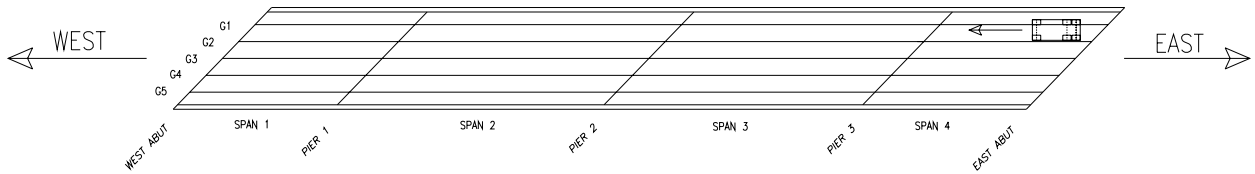


Figure 6-16: Moving Load Type #4

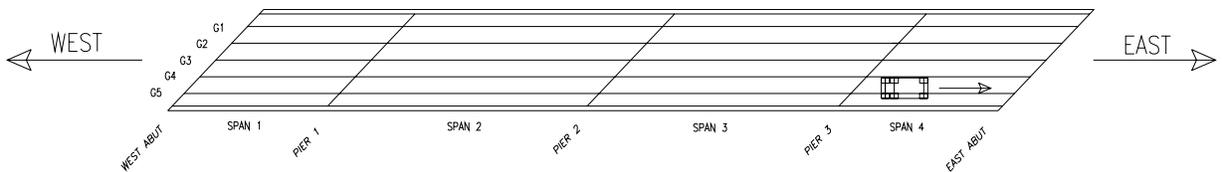


Figure 6-17: Moving Load Type #5

Table 6-1: Moving Load Tests of the FAI-33-1309 Bridge

	ML Type #1-3	ML Types #4-5
Field Experiment #1	1 st Truck: #662	N/A
	2 nd Truck: #832	
	3 rd Truck: #781	
Field Experiment #2	1 st Truck: #781	Truck #517
	2 nd Truck: #517	
	3 rd Truck: #832	
Field Experiment #3	1 st Truck: #781	Truck #781
	2 nd Truck: #858	
	3 rd Truck: #517	

Although moving load tests provide an enormous amount of information about bridge behavior under load, static tests are still needed to provide supplemental data. During static tests, one or more trucks were placed at critical locations on the bridge while strain and deflection data were measured.

There were 14 static tests conducted during field experiment #1, (as shown in Figure 6-18 through Figure 6-31), five static tests conducted during field experiment #2 (as is shown in Figure 6-32 through Figure 6-36), and three static tests conducted during field experiment #3 (as is shown in Figure 6-37 through Figure 6-39).

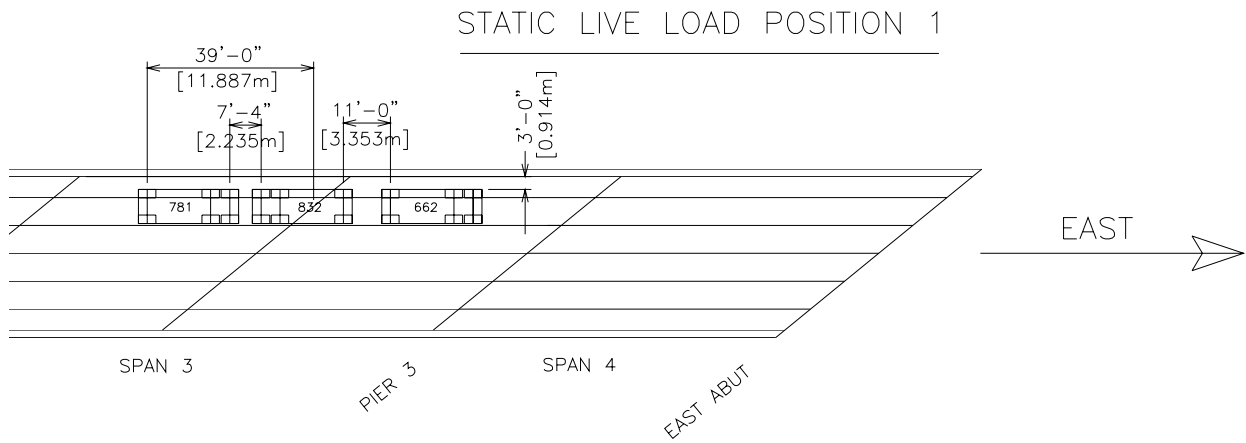


Figure 6-18: Field Experiment #1, Static Position 1

Chapter 6 - Field Testing

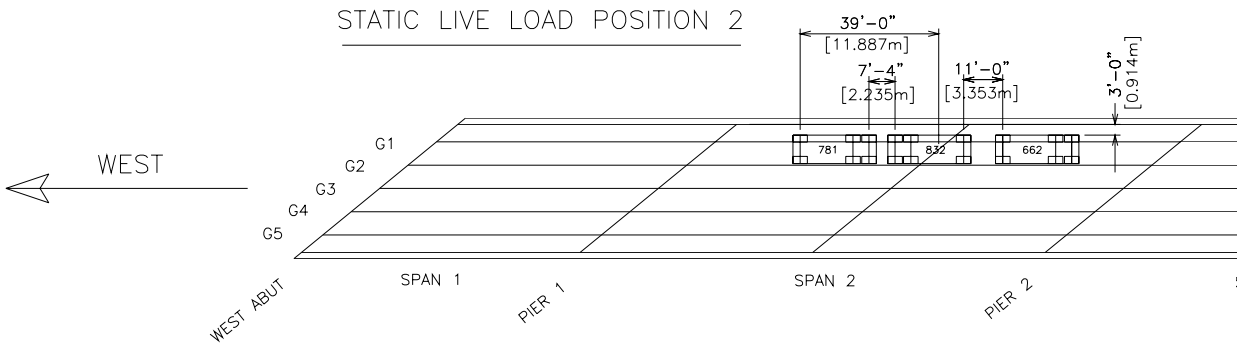


Figure 6-19: Field Experiment #1, Static Position 2

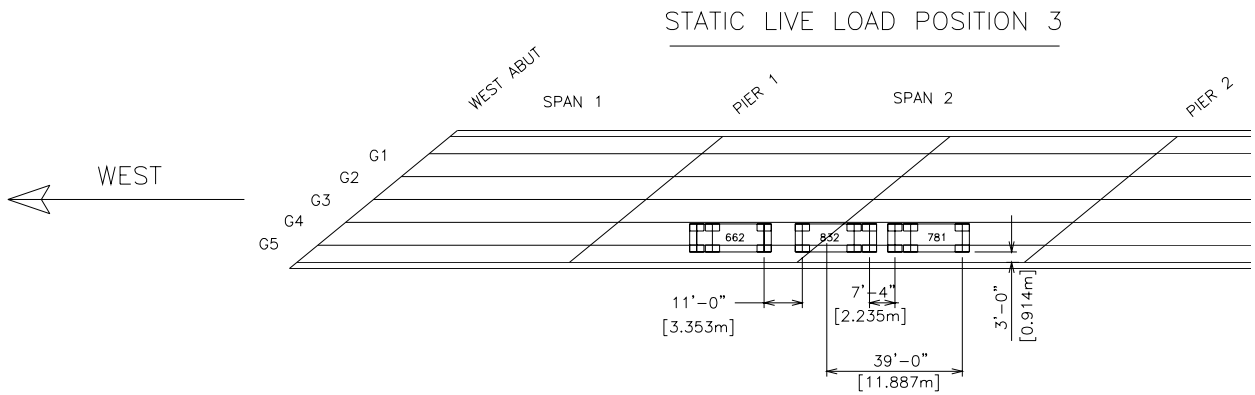


Figure 6-20: Field Experiment #1, Static Position 3

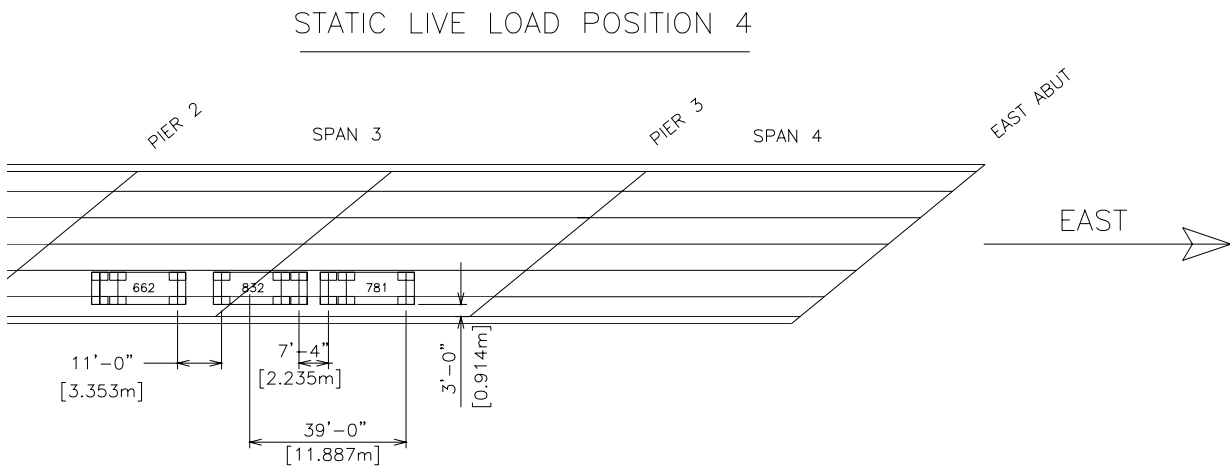


Figure 6-21: Field Experiment #1, Static Position 4

STATIC LIVE LOAD POSITION 5

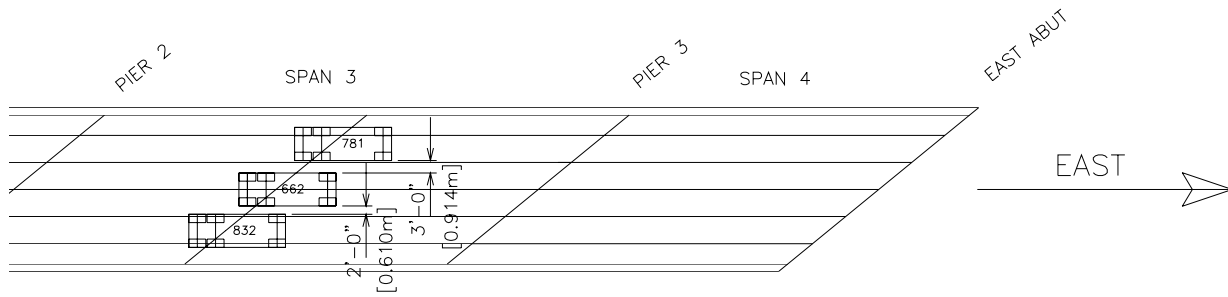


Figure 6-22: Field Experiment #1, Static Position 5

STATIC LIVE LOAD POSITION 6

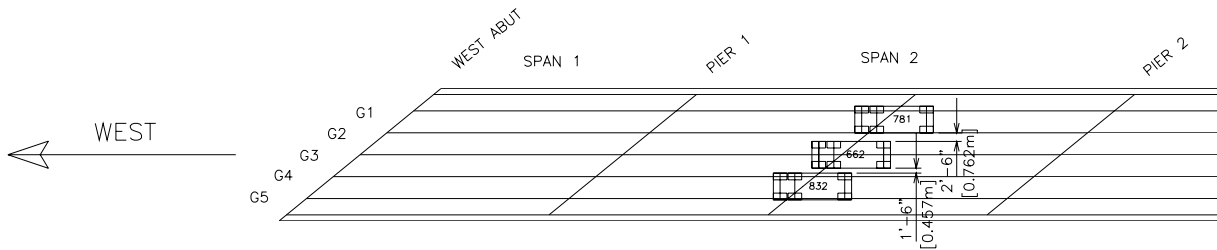


Figure 6-23: Field Experiment #1, Static Position 6

STATIC LIVE LOAD POSITION 7

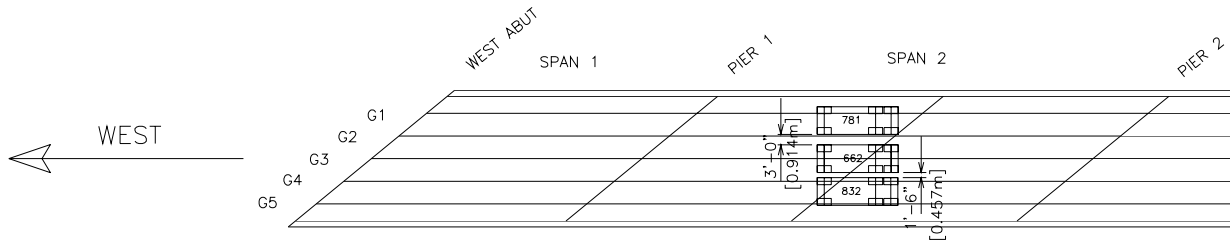


Figure 6-24: Field Experiment #1, Static Position 7

Chapter 6 - Field Testing

STATIC LIVE LOAD POSITION 8

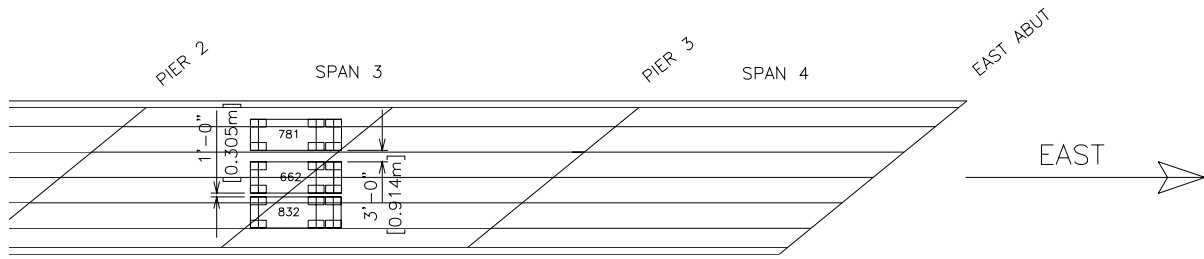
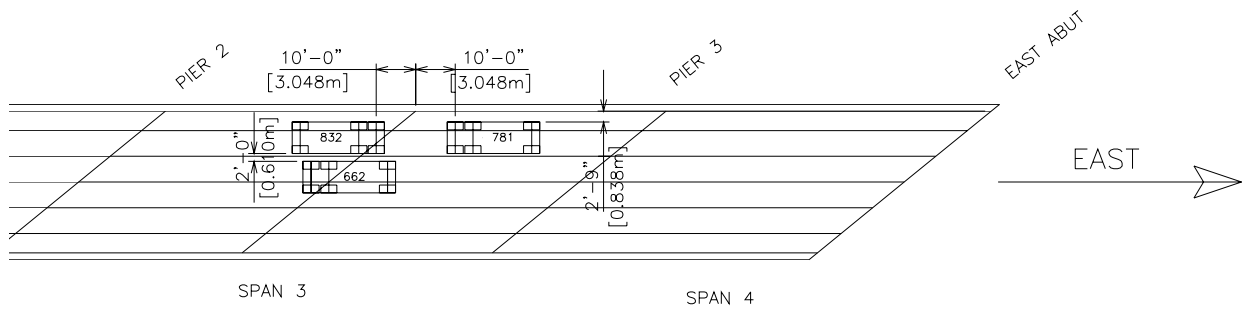


Figure 6-25: Field Experiment #1, Static Position 8

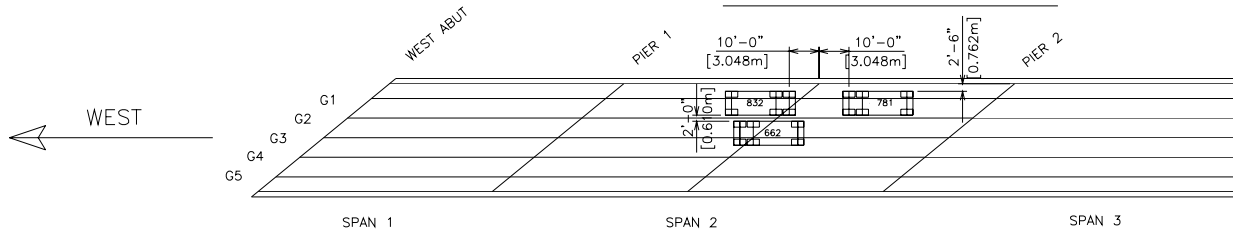
STATIC LIVE LOAD POSITION 9



N.B. - THE CG OF 662 WAS APPROXIMATELY PLACED OVER THE SKEW LINE BY LETTING THE CENTER AXLE ROLL UP TO THE SKEW LINE

Figure 6-26: Field Experiment #1, Static Position 9

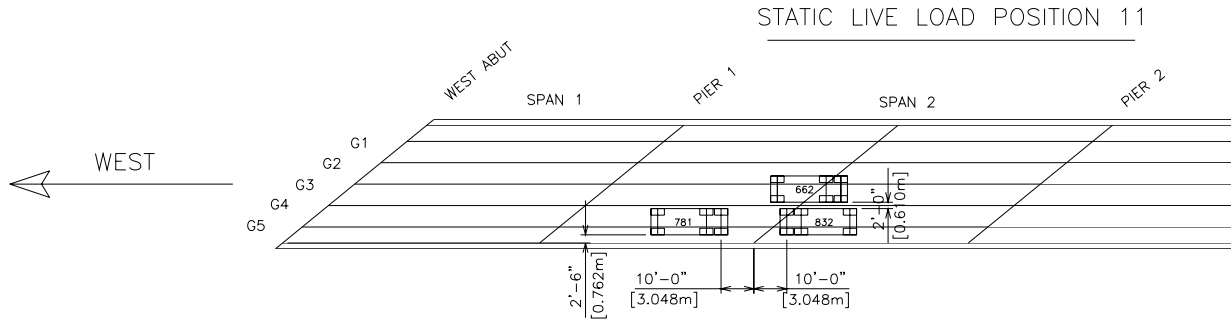
STATIC LIVE LOAD POSITION 10



N.B. - THE CG OF 662 WAS APPROXIMATELY PLACED OVER THE SKEW LINE BY LETTING THE CENTER AXLE ROLL UP TO THE SKEW LINE

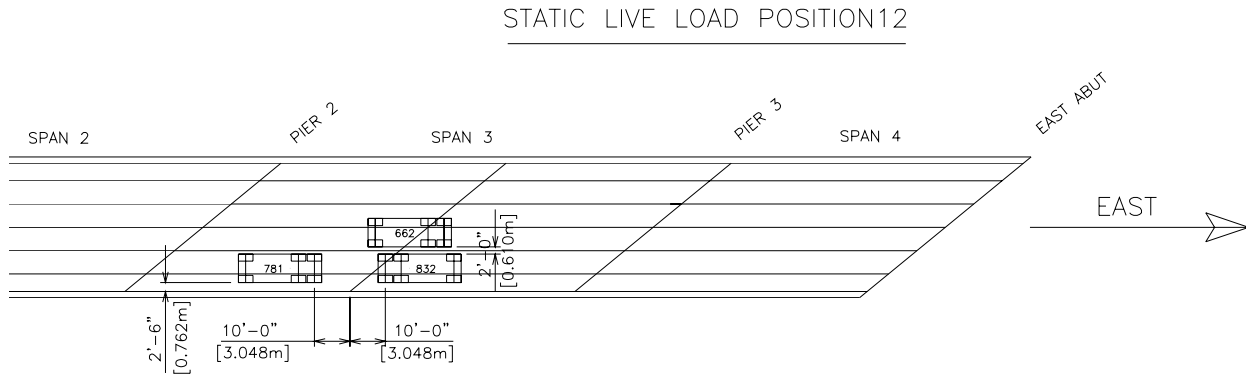
Figure 6-27: Field Experiment #1, Static Position 10

Chapter 6 - Field Testing



N.B. - THE CG OF 662 WAS APPROXIMATELY PLACED OVER THE SKEW LINE BY LETTING THE CENTER AXLE ROLL UP TO THE SKEW LINE

Figure 6-28: Field Experiment #1, Static Position 11



N.B. - THE CG OF 662 WAS APPROXIMATELY PLACED OVER THE SKEW LINE BY LETTING THE CENTER AXLE ROLL UP TO THE SKEW LINE

Figure 6-29: Field Experiment #1, Static Position 12

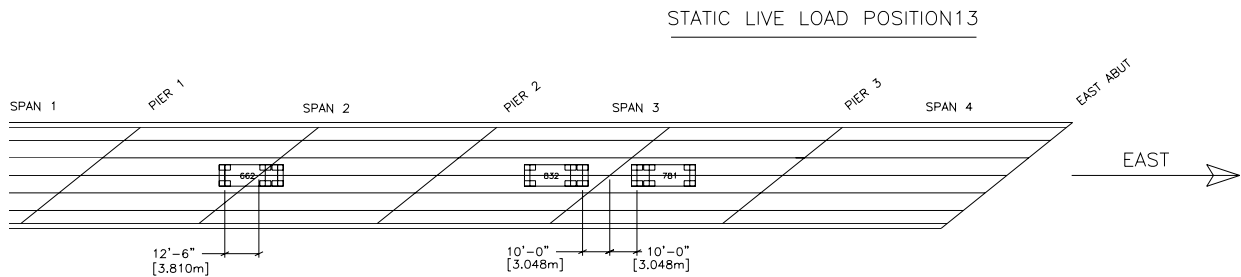


Figure 6-30: Field Experiment #1, Static Position 13

Chapter 6 - Field Testing

STATIC LIVE LOAD POSITION 14

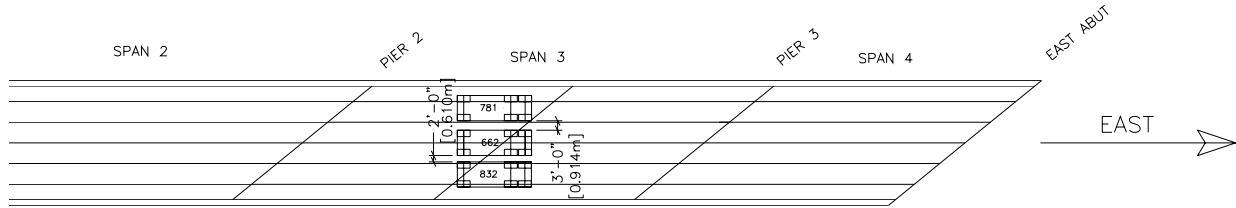


Figure 6-31: Field Experiment #1, Static Position 14

STATIC LIVE LOAD POSITION 1

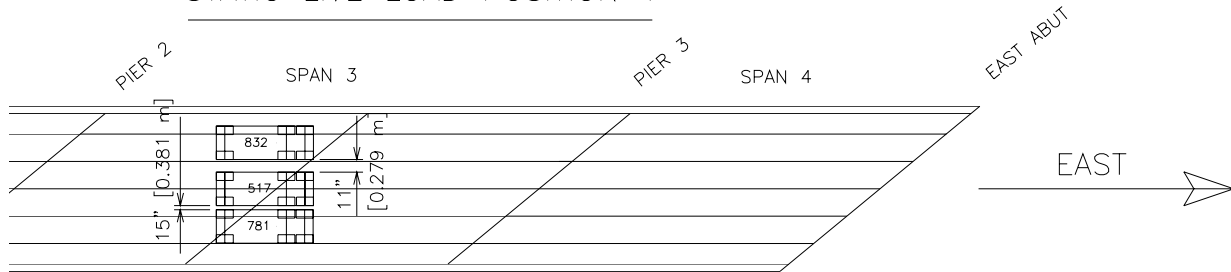


Figure 6-32: Field Experiment #2, Static Position 1

STATIC LIVE LOAD POSITION 2

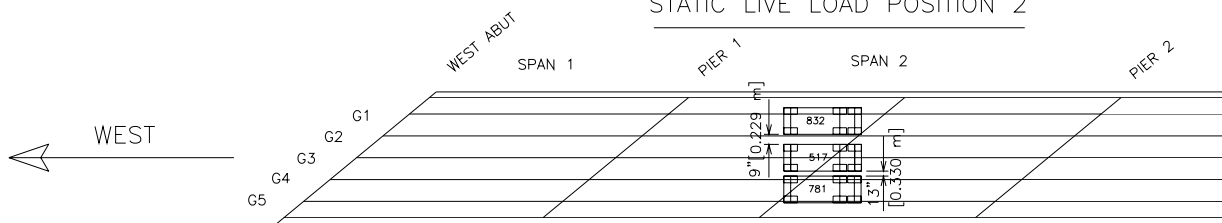


Figure 6-33: Field Experiment #2, Static Position #2

Chapter 6 - Field Testing

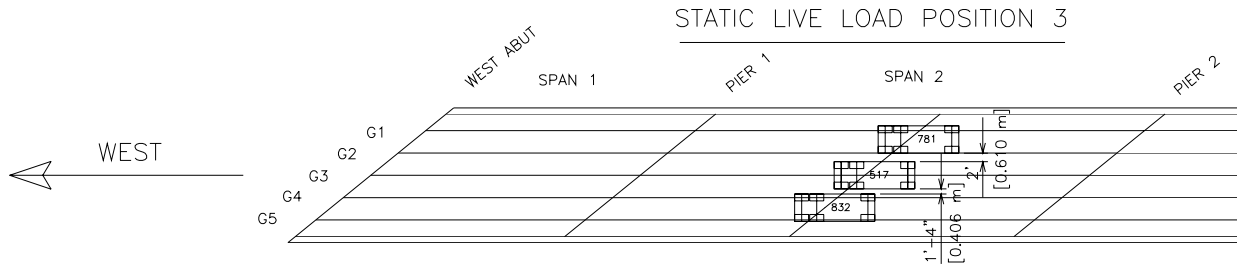


Figure 6-34: Field Experiment #2, Static Position #3

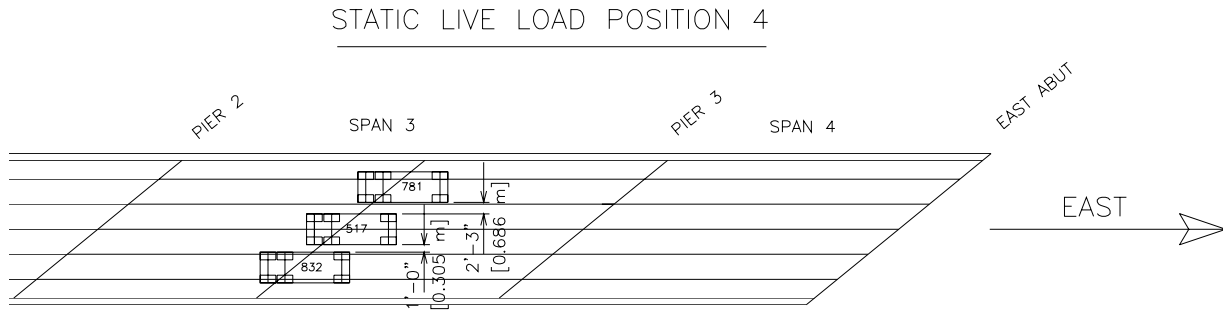


Figure 6-35: Field Experiment #2, Static Position #4

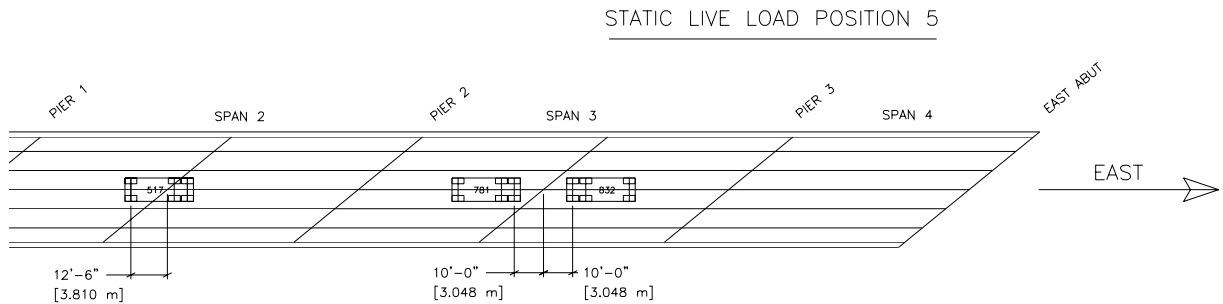


Figure 6-36: Field Experiment #2, Static Position #5

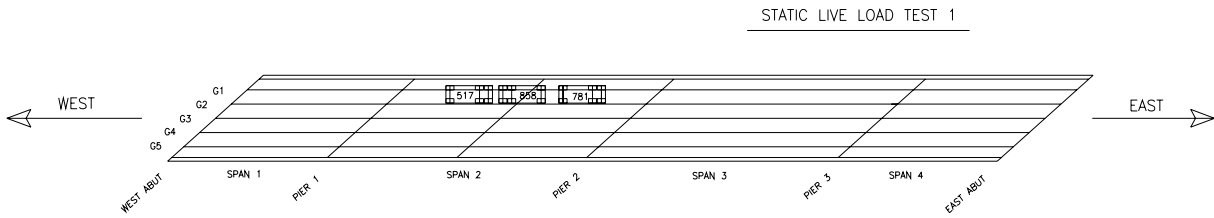


Figure 6-37: Field Experiment #3, Static Position #1

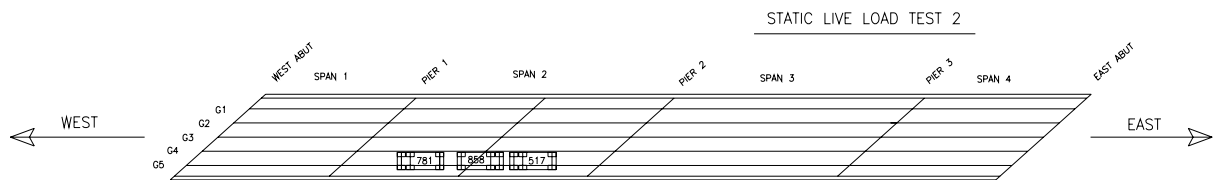


Figure 6-38: Field Experiment #3, Static Position #2

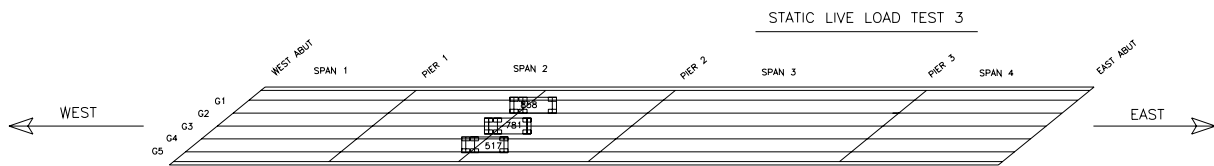


Figure 6-39: Field Experiment #3, Static Position #3

6.5 POST-PROCESSING OF FIELD EXPERIMENT DATA

This section explains how the original strain and displacement data collected from field experiments were processed in order to obtain clean and usable results. Despite the fact that during the moving load tests, the trucks were driven over the bridge at crawl speed, there was still some dynamic ‘noise’ noted in the acquired data. Additionally, since the data acquisition system needs electric power to operate, electronic noise is unavoidable (this is particularly true in field experiments where gas-powered generators are used). To obtain the pseudo-static

component or “true” data, a low-pass filter based on a series of Fast Fourier Transforms (FFTs) is used to filter out the noise.

The strain data obtained from bridge field tests are discrete-time signals. Every discrete-time signal can be approximated by a sum of Fourier series formed by a discrete-time exponential and its harmonics, each at a different frequency. The more series included in the sum, the better the approximation. Each of the harmonic frequencies is defined by a magnitude (amplitude) and a phase. The phase indicates how to shift the harmonic before adding it to the sum. Plotting the harmonic magnitudes on the y-axis and the frequency of the harmonic on the x-axis generates a Frequency Spectrum. The spectrum is a set of vertical lines or bars because harmonics can only have frequencies that are integer multiples of the original signal frequency. In theory, the spectrum includes frequencies up to infinity but in practice, the magnitude of very high frequency harmonics are usually insignificant.

The FFT is a very efficient way to generate a frequency spectrum, in other words, to transform the strain data from the time-domain to the frequency-domain. In the frequency-domain, the noise can be filtered out by applying an ideal low-pass filter. The noise will be filtered out since noise signals are usually at higher frequencies than signals resulting from the pseudo-static truck response. The filter is implemented by selecting a cutoff frequency and setting the magnitude and phase components of the frequency-domain data whose frequency is higher than cutoff frequency to zero. Taking the Inverse Fast Fourier Transform (IFFT) of the results yields the filtered truck-load response. By selecting different low-pass cutoffs, the strain data can be filtered by different frequencies (Ramirez, 1985). Figure 6-40 shows a comparison of the raw field data with the filtered data.

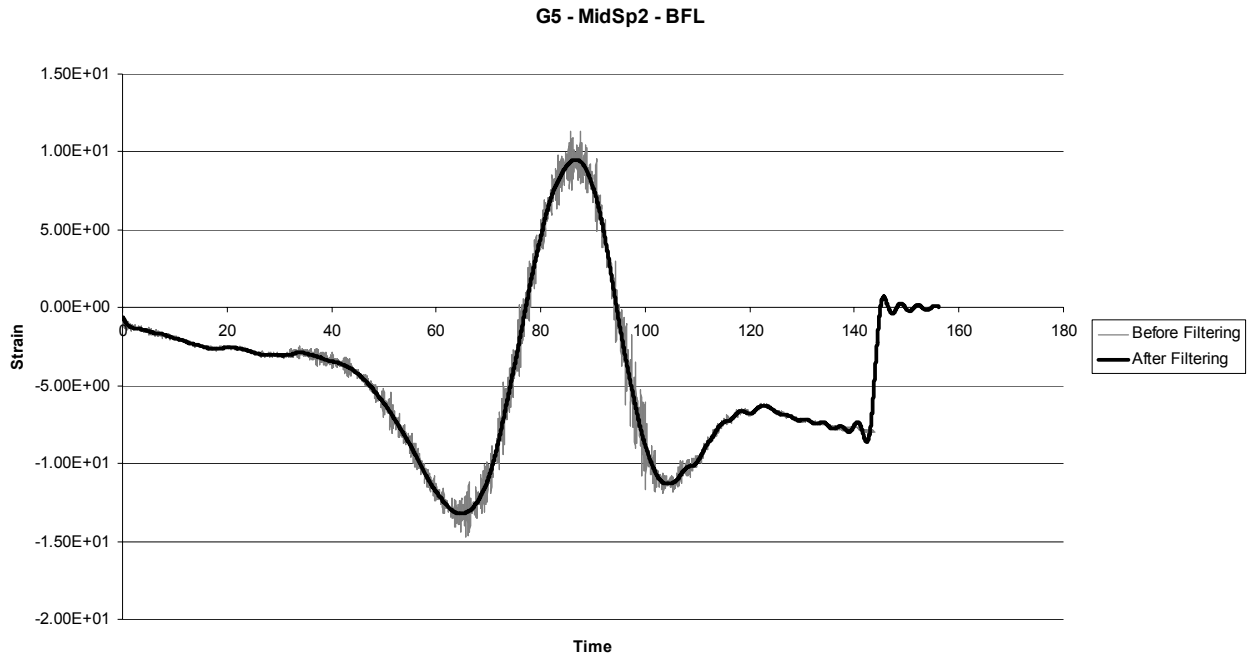


Figure 6-40: Comparison Between Raw Field Data and Filtered Truck-Load Response

6.5.1 Distribution Factor Calculation

Two methods of determining the distribution factors from field data were used. Using the first method, the bending moment in each girder was calculated by using an effective composite cross-section. The distribution factor for each girder was then obtained by dividing the girder moment by the total moment in all girders. Using the second method, the distribution factors were evaluated using the strains in the bottom flange of each girder. For example, the distribution factor of a girder was calculated by dividing the strain at that girder by the sum of the strains in all girders. The differences between these two methods was negligible, since the difference between the moments inertias of girders are negligible due to the uniform girder spacing and girder dimensions. Because of the negligible difference and the relative simplicity associated with the second method, it was chosen for use in evaluation of the AASHTO distribution factors.

6.6 DISTRIBUTION FACTOR EVALUATION

In this section, the AASHTO-LRFD (2002) method for the calculation of distribution factors is illustrated and the results are presented. The DFs extracted from bridge field test data are tabulated and compared with DFs from the AASHTO-LRFD method.

The AASHTO-LRFD Specification has different formulas for different types of bridges. Following the procedures outlined in the specification, the DFs can be easily computed. The FAI-33- Bridge is a slab-on-steel-stringer bridge with 5 parallel, identical HPS steel girders. The concrete deck is width constant with 1.979' overhangs, which is smaller than 3'. Therefore, AASHTO-LRFD Tables 4.6.2.2.2b-1 and 4.6.2.2.2d-1 are applicable for calculating the distribution of live loads per lane for moments in interior and exterior girders (AASHTO-LRFD, 2002).

6.6.1 Distribution of Live Loads per Lane for Moment in Interior Beams:

6.6.1.1 One Design Lane Loaded:

$$\begin{aligned}
 DF &= 0.06 + \left(\frac{S}{14}\right)^{0.4} \left(\frac{S}{L}\right)^{0.3} \left(\frac{K_g}{12.0Lt_s^3}\right)^{0.1} \\
 &= 0.06 + \left(\frac{8ft}{14}\right)^{0.4} \left(\frac{8ft}{130.8ft}\right)^{0.3} \left(\frac{458600in^4}{12.0 * 130.8ft * (8.5in)^3}\right)^{0.1} \\
 &= 0.3809
 \end{aligned}$$

where:

S is the spacing of beams (ft)

$$3.5 \leq S = 8ft \leq 16.0$$

t_s is the depth of concrete slab (in)

$$4.5 \leq t_s = 8.5in \leq 12.3$$

L is the span of beam (ft)

$$L = 130.8 \text{ ft}$$

K_g is the longitudinal stiffness parameter, shall be taken as:

$$\begin{aligned}
 K_g &= n(I + A * e_g^2) \\
 &= 7.131 * (17150in^4 + 45in^2 * (32.38in)^2) \\
 &= 458600in^4
 \end{aligned}$$

In which:

n is the ratio of the modulus of elasticity of beam material (E_B psi) to the modulus of elasticity of deck material (E_D psi)

$$n = \frac{E_B}{E_D} = \frac{29,000,000psi}{33 * \omega_c^{1.5} \sqrt{f'_c}} = \frac{29,000,000psi}{33 * (150)^{1.5} * \sqrt{4500psi}} = \frac{29,000,000psi}{4,067,000psi} = 7.131$$

ω_c is the concrete unit weight (pcf)

f'_c is the concrete strength (psi)

I is the moment of inertia of beam (in^4)

$$I = 17150in^4$$

A is the area of beam (in^2)

$$A = 45in^2$$

e_g is the distance between the center of gravity of the basic beam and deck (in)

$$e_g = 32.38in$$

6.6.1.2 Two or More Design Lanes Loaded :

$$\begin{aligned}
 DF &= 0.075 + \left(\frac{S}{9.5}\right)^{0.6} \left(\frac{S}{L}\right)^{0.2} \left(\frac{K_g}{12.0Lt_s^3}\right)^{0.1} \\
 &= 0.075 + \left(\frac{8ft}{9.5}\right)^{0.6} \left(\frac{8ft}{130.8ft}\right)^{0.2} \left(\frac{458600in^4}{12.0 * 130.8ft * (8.5in)^3}\right)^{0.1} \\
 &= 0.5539
 \end{aligned}$$

6.6.2 **Distribution of Live Load per Lane for Moment in Exterior Beams:**

6.6.2.1 One Design Lane Loaded:

The lever rule is used to calculate the distribution factor for exterior beams. The lever rule assumes that the interior supports are hinged and the reactions at the other outer girders are used to define the DFs (Figure 6-41).

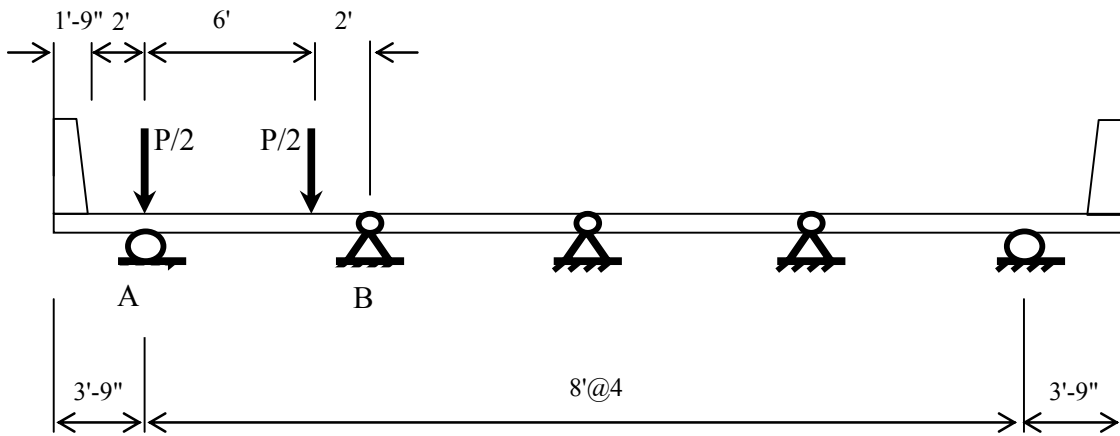


Figure 6-41: Illustration of Lever Rule for Exterior Girder Distribution Factors

The reaction of support A is $R_A = 0.625P$. Thus the distribution factor is $DF = (1.2)(0.625) = 0.75$ where 1.2 is the multiple presence factor.

6.6.2.2 Two or More Design Lanes Loaded:

$$\begin{aligned} DF &= eDF_{interior} \\ &= 0.9875 * 0.5539 \\ &= 0.5470 \end{aligned}$$

Where e is the correction factor,

$$\begin{aligned} e &= 0.77 + \frac{d_e}{9.1} \\ &= 0.77 + \frac{1.979 \text{ ft}}{9.1} \\ &= 0.9875 \end{aligned}$$

in which:

d_e is the distance from exterior web of exterior beam and the interior edge of curb or traffic barrier (ft)

$$-1.0 \leq d_e = 1.979 \text{ ft} \leq 5.5$$

6.6.2.3 Skew Reduction Factor

When the bridge supports are skewed, the bending moment in the beams should be reduced in accordance with AASHTO-LRFD Table 4.6.2.2.2e-1. The skew reduction factors should be used to both exterior and interior girders. The skew reduction factor is calculated as:

$$\begin{aligned} SF &= 1 - C_1 * (\tan \theta)^{1.5} \\ &= 1 - 0.0513 * (\tan 39.29^\circ)^{1.5} \\ &= 0.9620 \end{aligned}$$

where:

$$\begin{aligned} C_1 &= 0.25 * \left(\frac{K_g}{12.0 * L * t_s^3} \right)^{0.25} \left(\frac{S}{L} \right)^{0.5} \\ &= 0.25 * \left(\frac{458600 \text{ in}^4}{12.0 * 130.8 \text{ ft} * (8.5 \text{ in})^3} \right)^{0.25} \left(\frac{8 \text{ ft}}{130.8 \text{ ft}} \right)^{0.5} \\ &= 0.0513 \end{aligned}$$

The DFs calculated above should be multiplied by the skew reduction factor to obtain the final DFs.

According to the AASHTO-LRFD Specification, exterior girders of multi-girder bridges shall not have less resistance than an interior beam. Therefore, the DF of exterior girders shall not be less than that of interior girders. The distribution factors obtained by using the AASHTO-LRFD Specification formula are tabulated in Table 6-2. For the exterior girders, the DF from one lane loaded governs, however, for interior girders, the DF from two or more lanes loaded governs.

Table 6-2: AASHTO LRFD Distribution Factors for FAI-33

Girder	# Lanes Loaded	Distribution Factor
Interior Girders	1 Lane Loaded	0.3664
	2 or More Loaded	0.5329
Exterior Girders	1 Lane Loaded	0.7215
	2 or More Loaded	0.5262 < 0.5329

6.6.3 Comparison of Experimental Results with AASHTO LRFD Specifications

6.6.3.1 Field Experiment #1

Three moving load tests were conducted on the FAI-33 Bridge in Feb. 2003. Using the methodology described in Chapter 3, the moment distribution factors were evaluated from the field test data. The comparison of the field test results with AASHTO-LRFD Specification is shown in Figure 4-5. Fourteen static load tests were also conducted in Feb. 2003, including one lane loaded and two lanes loaded. The moment distribution factors evaluated from test data are compared with DFs obtained from the AASHTO method in Figures 4-6a and 4-6b.

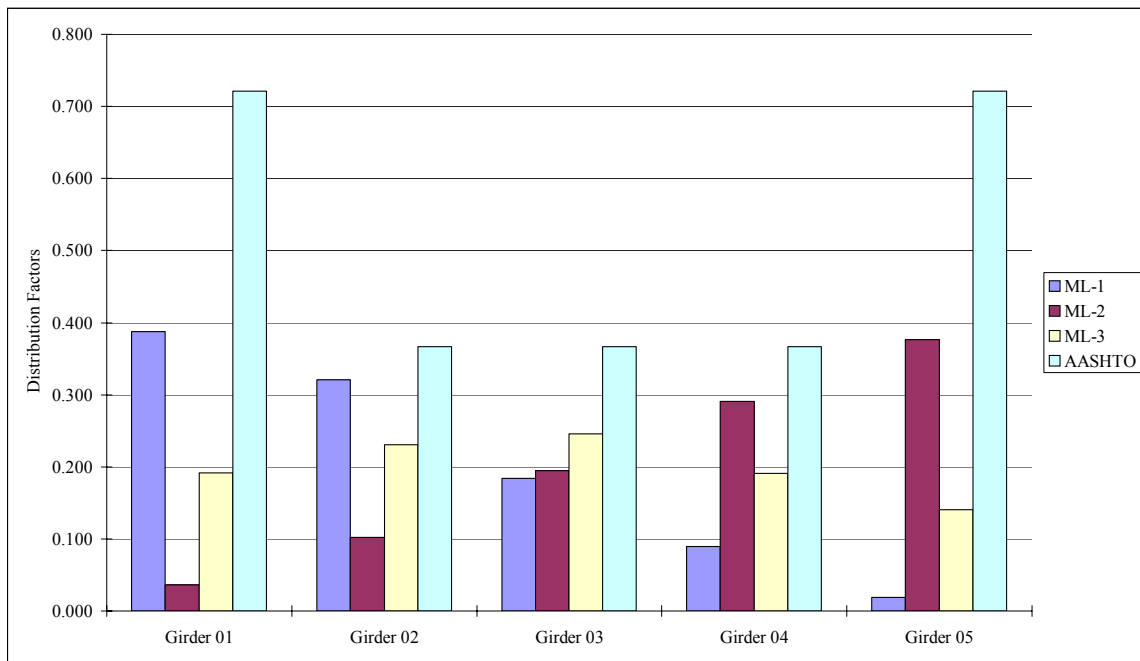


Figure 6-42: Field Experiment #1, Moving Load Tests

Chapter 6 - Field Testing

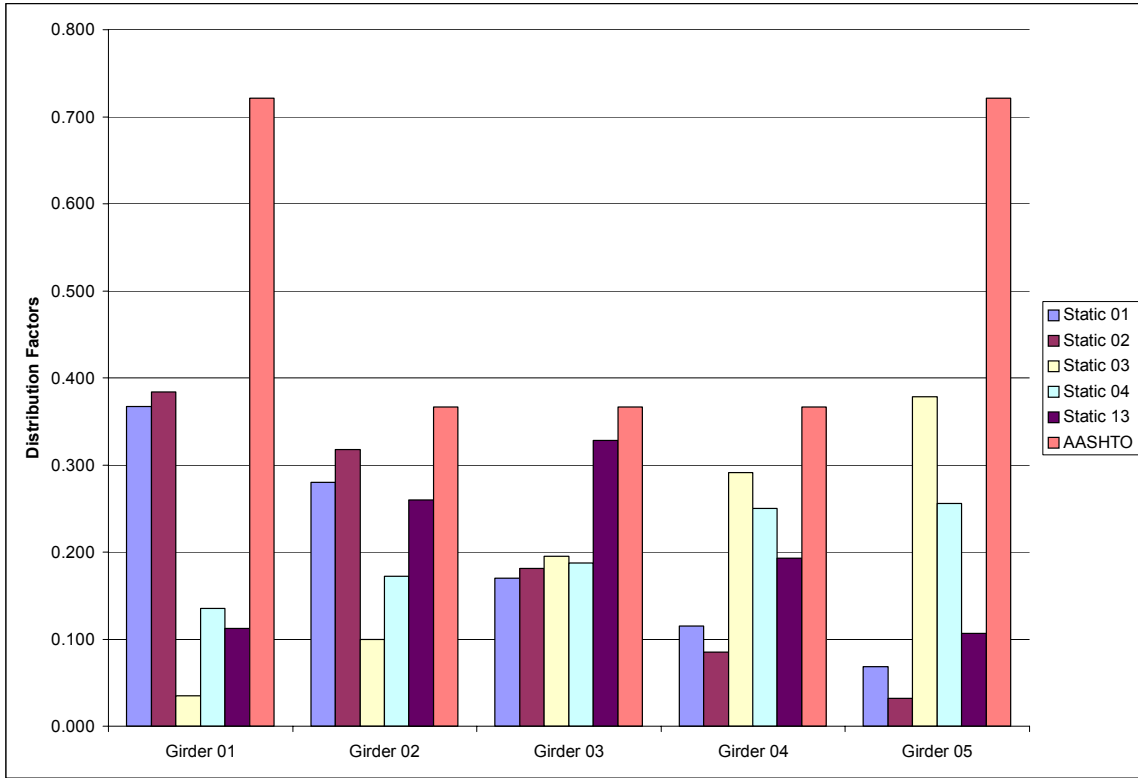


Figure 6-43: Field Experiment #1, Static Tests, One Lane Loaded

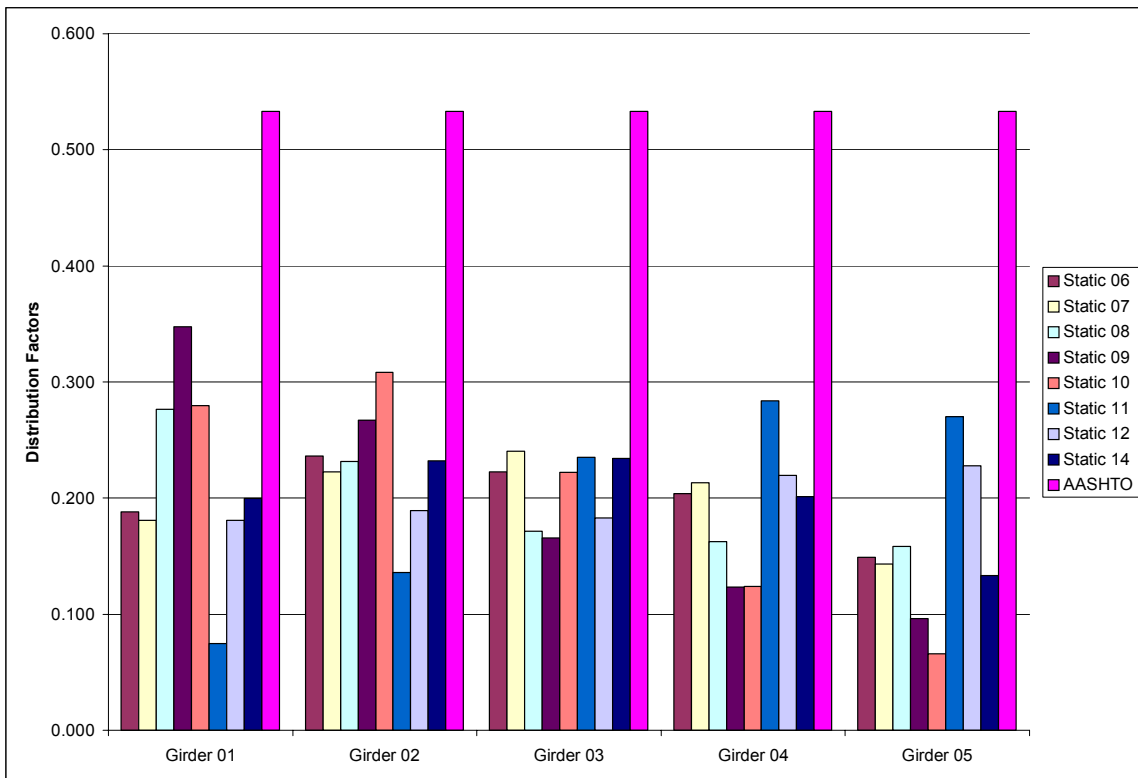


Figure 6-44: Field Experiment #1, Static Tests, Two Lanes Loaded

6.6.3.2 Field Experiment #2

In September, 2003, five moving load tests were completed and Figure 6-45 and Figure 6-46 show the moment distribution factors evaluated from test data compared with AASHTO-LRFD Specification. Meanwhile, five static loads were conducted, among them four tests with two lanes loaded and one test with one lane loaded. The moment distribution factors obtained from test data are compared with DFs using the AASHTO method in Figure 6-47 and Figure 6-48.

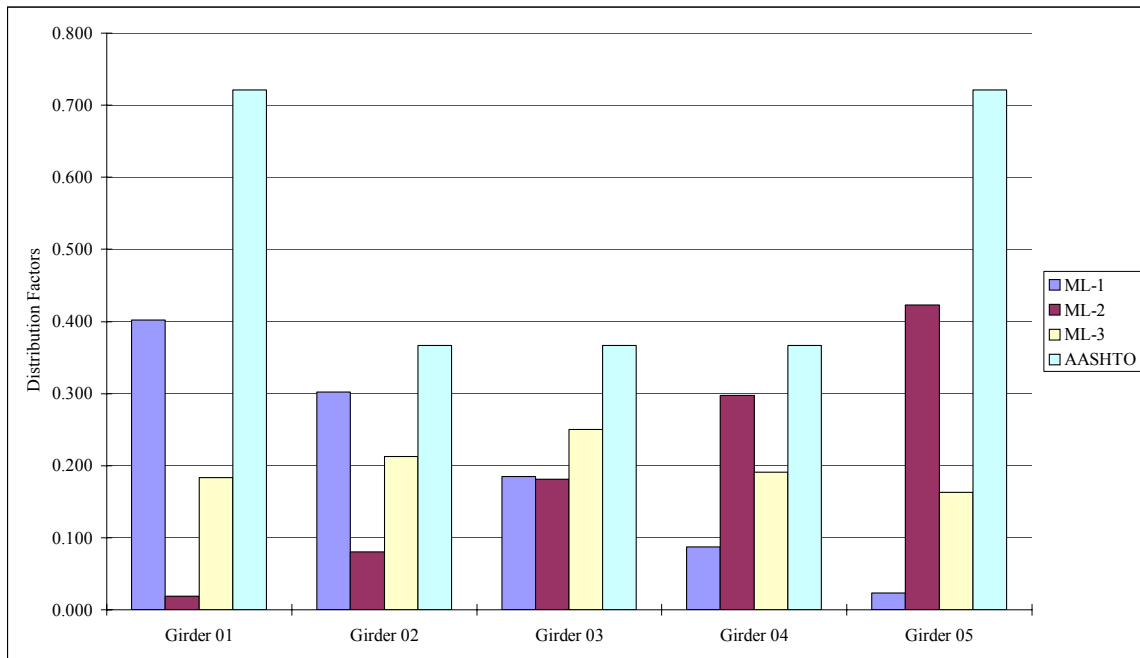


Figure 6-45: Field Experiment #2, Moving Load Tests

Chapter 6 - Field Testing

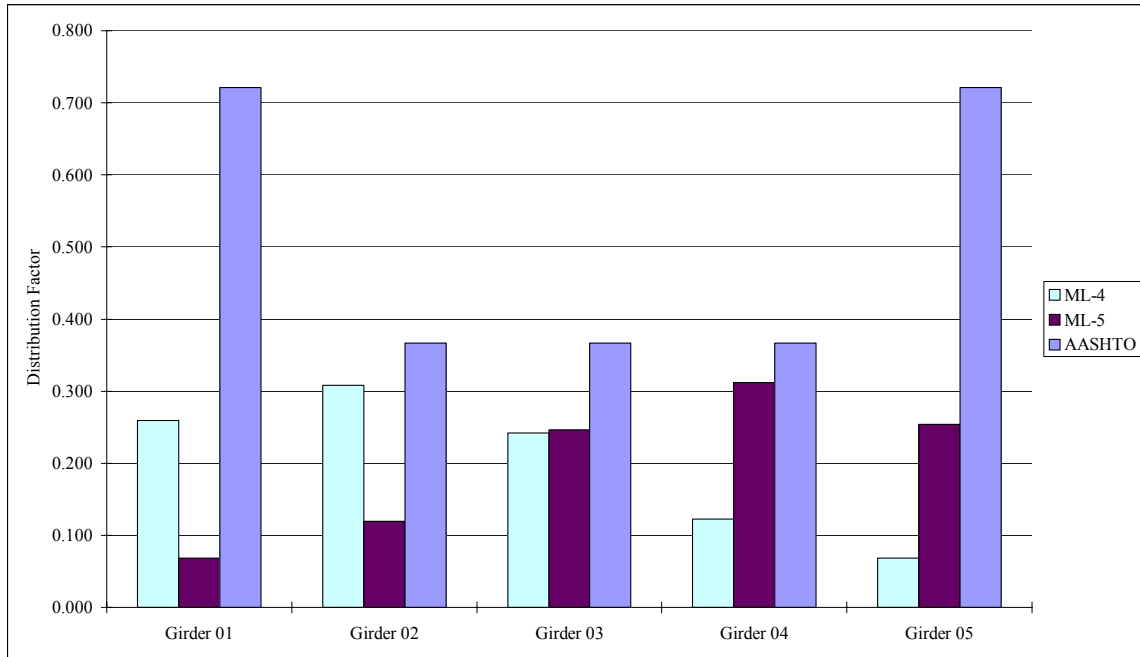


Figure 6-46: Field Experiment #2, Moving Load Tests

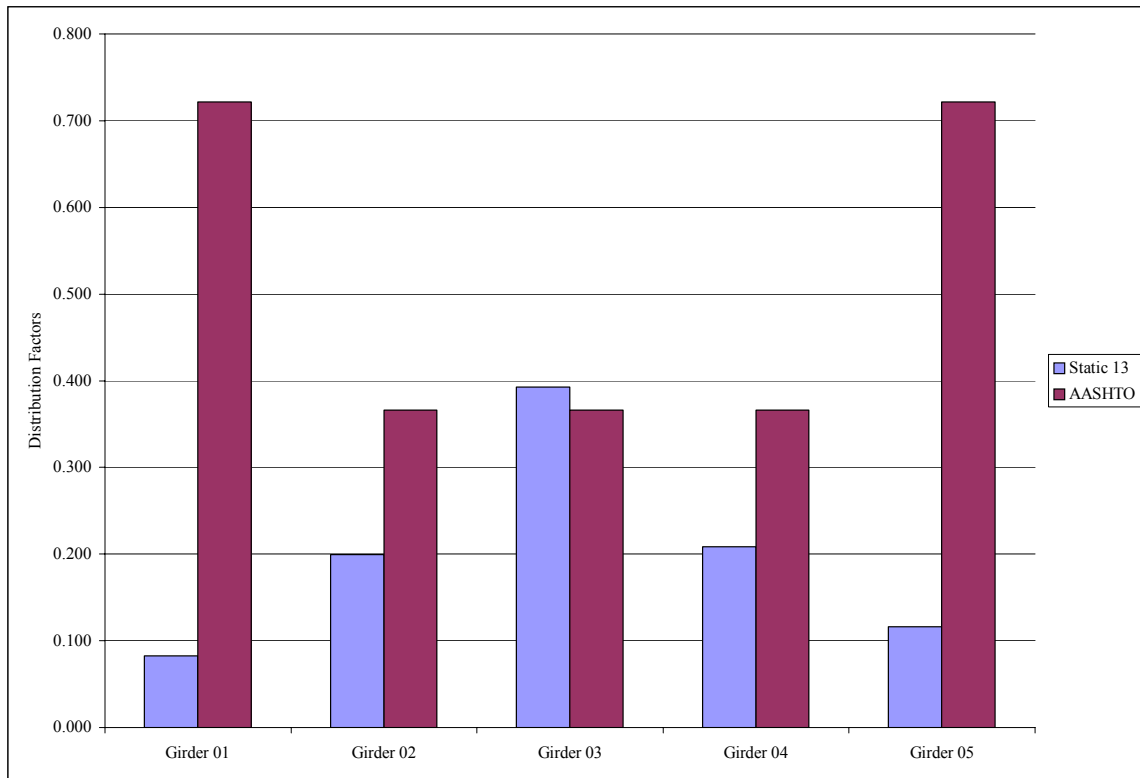


Figure 6-47: Field Experiment #2, Static Tests, One Lane Loaded

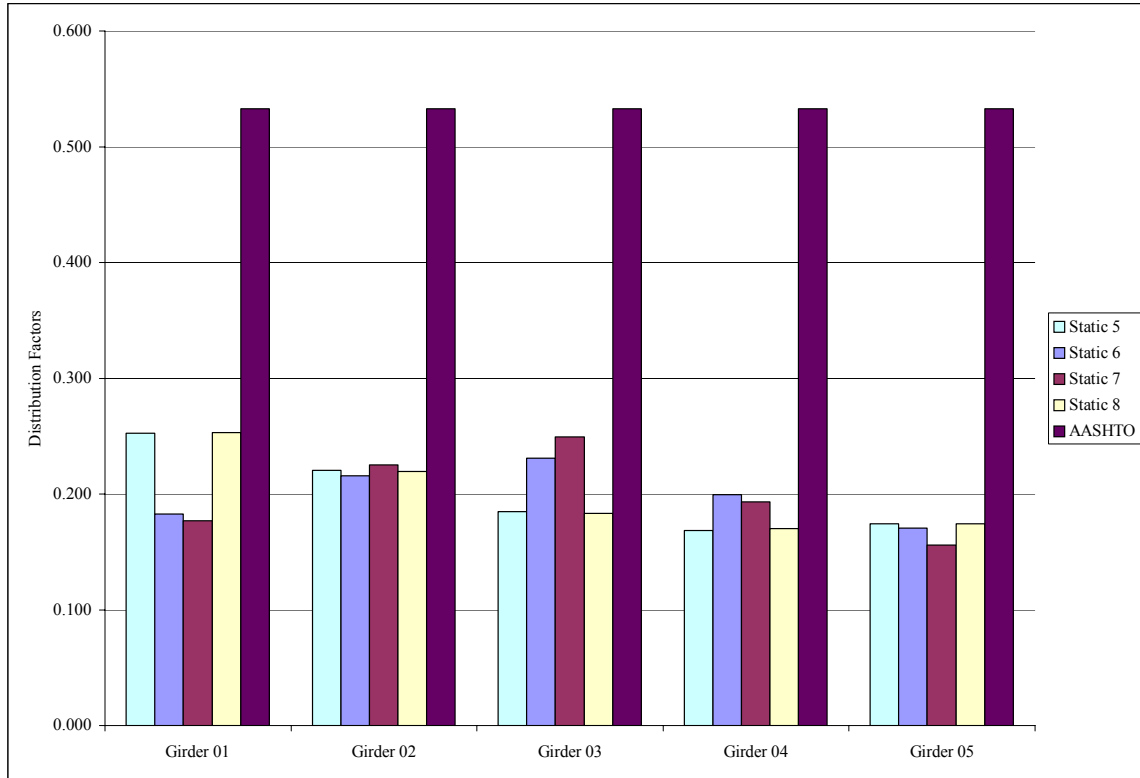


Figure 6-48: Field Experiment #2, Static Tests, Two Lanes Loaded

6.6.3.3 Field Experiment #3

The moment distribution factors calculated from field experiment #3 are shown in Figure 6-49 and Figure 6-50. Only three static load tests were conducted during this bridge field test. One test included two loaded lanes and two tests included a single loaded lane. The moment distribution factors obtained from the test data are compared with DFs using AASHTO method in Figure 6-51 and Figure 6-52.

Chapter 6 - Field Testing

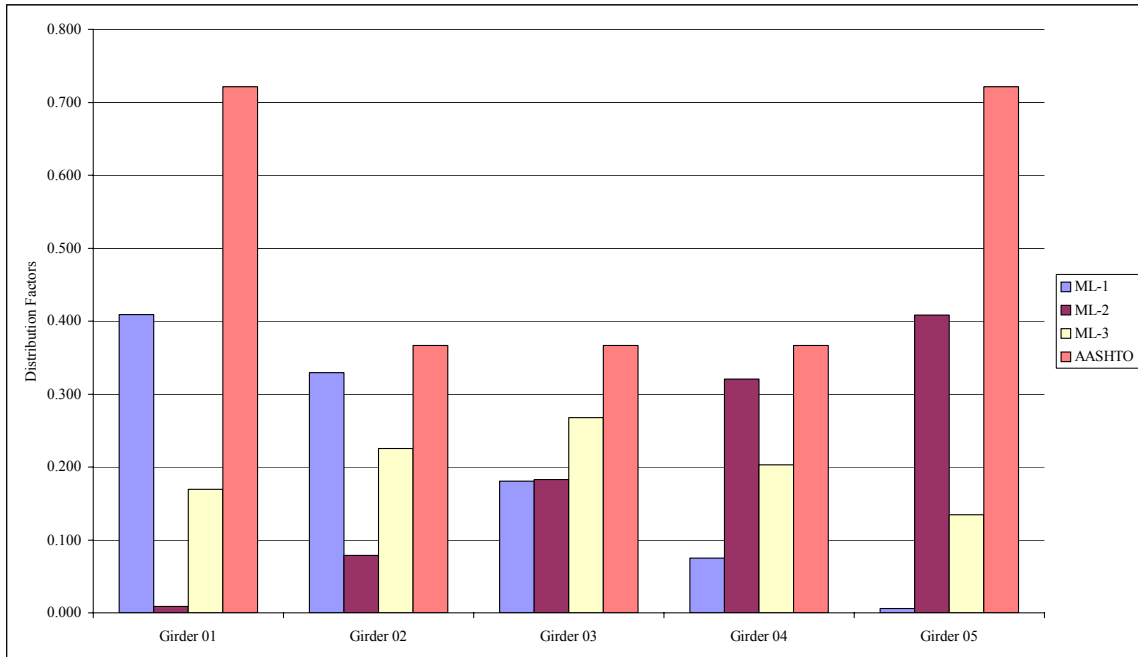


Figure 6-49: Field Experiment #3, Moving Load Tests

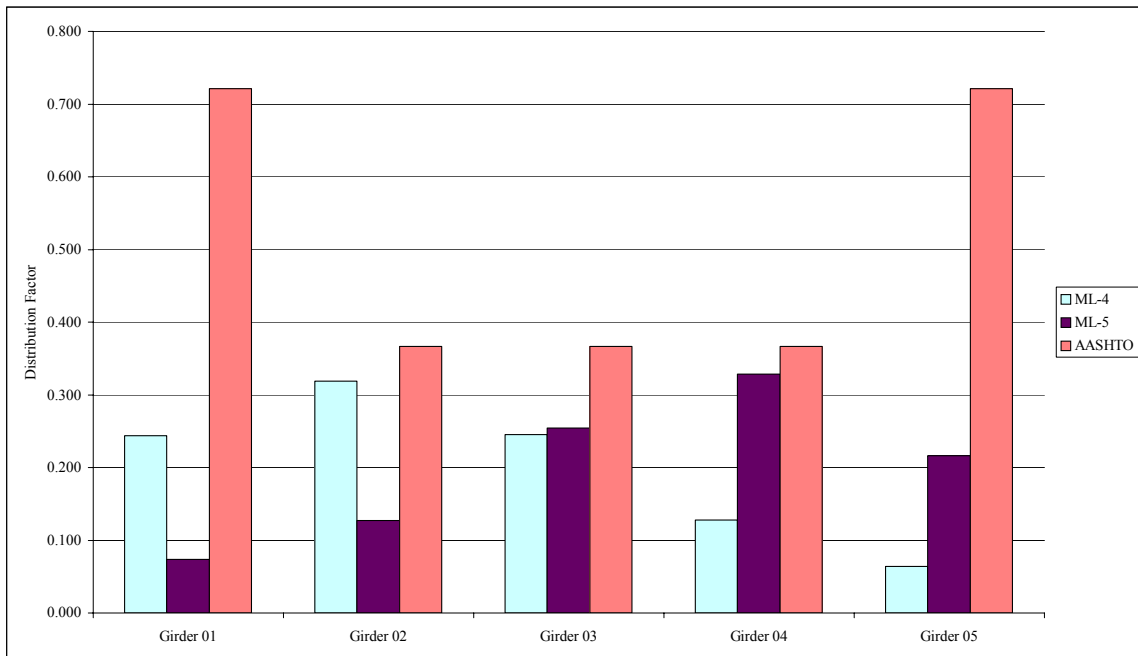


Figure 6-50: Field Experiment #3, Moving Load Tests

Chapter 6 - Field Testing

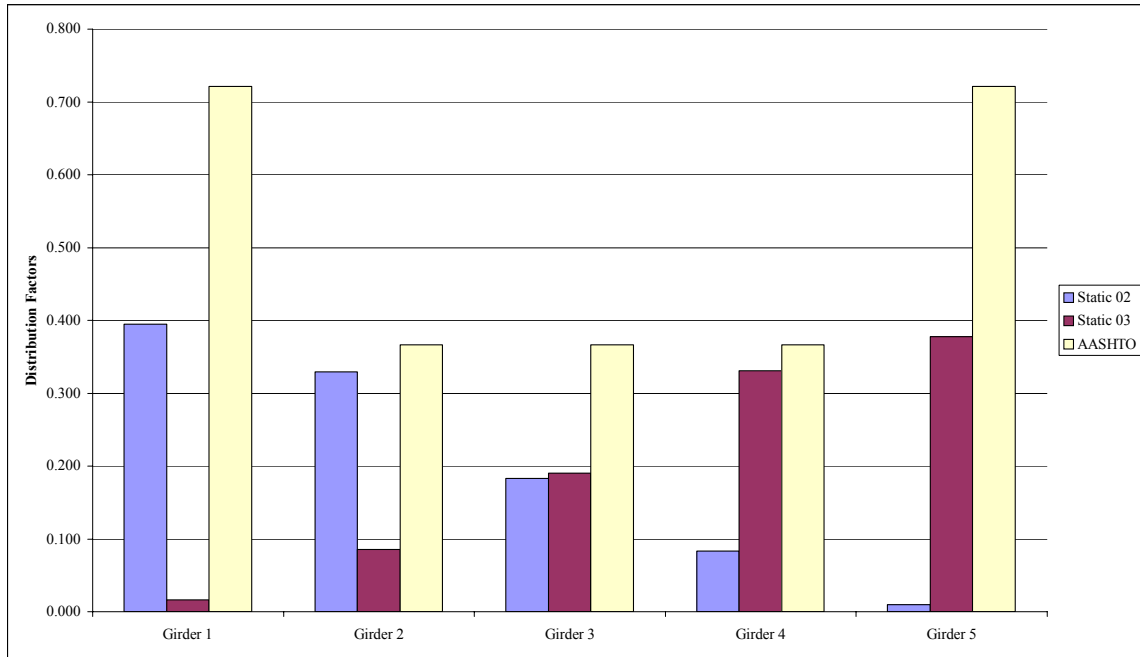


Figure 6-51: Field Experiment #3, Static Tests, One Lane Loaded

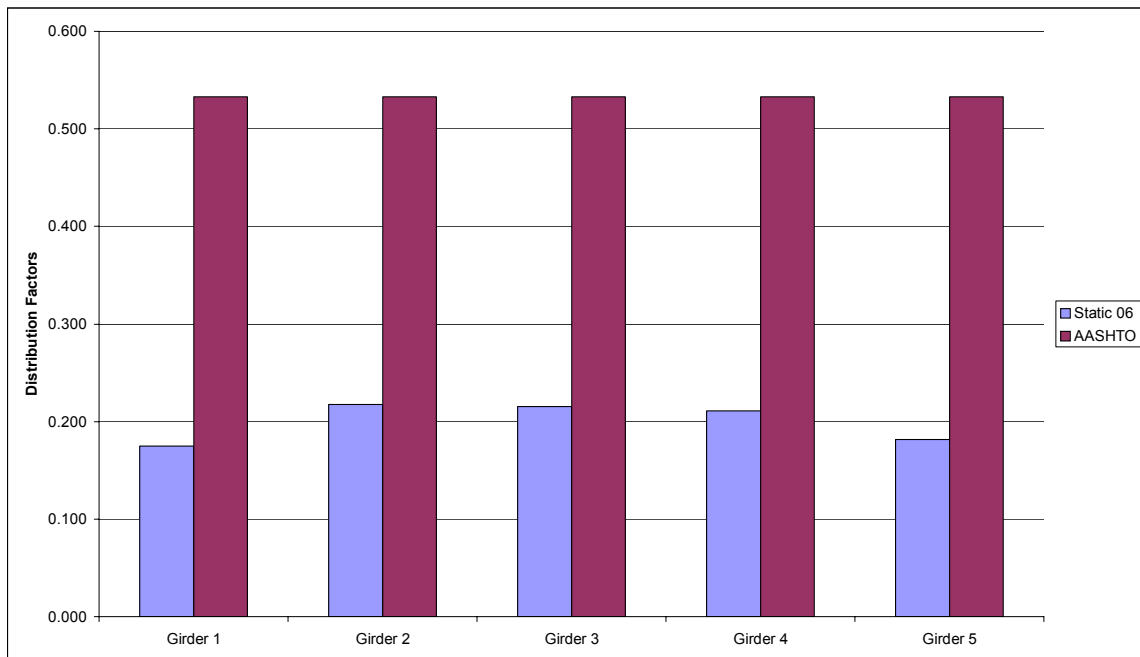


Figure 6-52: Field Experiment #3, Static Tests, Two Lanes Loaded

6.6.3.4 Summary

As described before, during the moving load tests, a single truck or train of three trucks was driven over the bridge, so moving load tests were considered as one lane loaded. Although many static tests were conducted, according to the trucks' locations they were classified into two categories — one lane loaded, two or more lanes loaded. The DFs extracted from experimental data correctly reflect the trucks' locations on the bridge. For instance, the DFs calculated from moving load test #1 showed Girder 1 had the highest DF compared with the other 4 girders, which were expected given the fact that trucks were positioned along the west-bound lane of the bridge over Girder 1. Also the comparison of DFs indicated that AASHTO-LRFD formulas gave more conservative results for two or more lanes loaded than one lane loaded. For one lane loaded, AASHTO-LRFD gave more conservative DFs to exterior girders than interior girders.

6.7 SUMMARY AND CONCLUSIONS

This study is focused on the verification of AASHTO-LRFD live load distribution formulas for high performance steel (HPS) bridges through bridge truckload test data. Three field experiments were conducted on the bridge to evaluate its behavior under different conditions. After the field experiments, the original strain data that was collected was processed to filter out the dynamic and electronic noise by applying a low pass filter. Finally, live-load distribution factors (DFs) were extracted from the filtered strain data, and compared with the results from AASHTO-LRFD formulas.

The comparison of the DFs obtained from field test data with the DFs calculated from AASHTO-LRFD formulas shows the AASHTO-LRFD formulas are applicable to design beam-and-slab bridges with girders fabricated from HPS. Also the AASHTO-LRFD formulas give conservative results. Compared with beam-and-slab bridges made with traditional steel, HPS bridges usually use less steel because of its higher yield strength, which reduces the depth of the girders and therefore the decreased moment inertia of the girders will make the HPS bridges more flexible. This results in uniform transverse distribution of loads when compared with the stiffer traditional beam-and-slab bridges.

Chapter 7 - Summary of Conclusions and Recommendations

7.1 INTRODUCTION

This report has been arranged into seven chapters that each discuss a separate aspect of the experimentation that was conducted during the course of the research project. Each of the chapters was conceived such that any could be read and understood without the need to read the others. As a result, this chapter is simply a summary of the conclusions and recommendations contained in Chapters 1 through 6.

In Chapter 1, the material characteristics of HPW-70W TMCP were investigated. It was found that its material properties – yield strength, tensile strength, and toughness – may fail to meet minimum requirements for thicker plates. Experimentally, it meets or exceeds many of the required properties for the Q&T grade described in ASTM A709, regardless of plate thickness. It certainly meets the requisites for toughness and ultimate strength, and the intra-plate variability of tensile strength and toughness for the thicknesses tested does not seem to be a great concern. However, HPS-70W TMCP does not meet the same yield strength criterion as is posed for the HPS-70W Q&T when examining the 2” plate. The experimentally found average dynamic yield strength of 68.2^{ksi} (470 MPa) is below the required 70^{ksi} (485 MPa), and this should be recognized by designers and dealt with in the steel-making industry. Despite the exhaustive depth of the material testing documented herein, whether these findings are representative of HPS-70W TMCP as a product or if these findings hold for only the heats of steel included in the study remains undetermined. Further research should be conducted to determine the cause of the roundhousing phenomena in thicker plates and to see if this phenomenon is isolated or endemic.

In Chapter 2, it was found that HPS-70W fatigue samples with drilled and sub-punched and reamed specimens rated at or above AASHTO (2004) Category B details, while the punched specimens rated between a Category C and D. This leads to conclusions that current provisions restricting punching holes in thicker plate are justified, the fatigue strength of the specimens

having punched holes seems to be more dependent upon plate thickness than hole diameter, and current AASHTO (2004) fatigue design specifications appear to be applicable to HPS-70W bolted splice connections. Overall, the HPS-70W fatigue samples with drilled and sub-punched and reamed holes exhibited fatigue resistance at least as good as is required by AASHTO (2004), and in many cases, slightly better. This finding reinforces the applicability of HPS-70W to bridge girder applications.

In Chapter 3, the fatigue performance joints in HPS-70W made with submerged arc welding (SAW) and narrow gap improved electrosag welding (NGI-ESW) was evaluated. The results indicate that HPS-70W welded butt-splices created with NGI-ESW performed at least as well as similar connections created using SAW, NGI-ESW and SAW HPS-70W welded butt-splices exhibited improved performance over the predicted fatigue life calculated using the AAHTO fatigue life equation, and that NGI-ESW seems to be an appropriate method for joining HPS-70W in welded butt-splice connections. As a result, it is suggested by the researchers that HPS-70W welded butt-splices created using NGI-ESW be included in AWS D1.5 since significant economic gains may be realized by utilizing this innovative welding technique.

A discussion of automated ultrasonic evaluation of full penetration butt welds in presented in Chapter 4. Currently, radiographic testing is required for all butt welds in flange material of plate girders or rolled beams. Ultrasonic testing offers economic advantages over radiography because radiography requires isolation of the part being examined to avoid exposing workers to radiation. Ultrasonic testing can be conducted without moving the part from welding station. Unfortunately, due to factors outside of the control of the UC research team, this study did not reveal much about the potential of this emerging technology.

In Chapter 5, different construction schemes for skewed slab-on-steel-stringer bridges were evaluated analytically. A finite element model was developed to study girder response during concrete deck placement for a continuous, skewed, steel, girder bridge. This model was calibrated against data recorded field monitoring of the structure's response during the actual deck pour. During calibration, it was recognized that field data sustained an increasing, superimposed compressive effect during deck placement that was not reproduced in the numerical models. Replication of this effect in the numerical models was attempted through

incorporation of air temperature and time-dependant concrete stiffness variations. Incorporation of these aspects during model calibration steps indicated that extreme changes in temperature during placement of the deck were of importance when attempting to accurately predict stress states in the superstructure at completion of the pour and that incorporation of time-dependant concrete modulus effects and the subsequent formation of premature composite action were of minor importance when attempting to accurately predict stress states in the superstructure at completion of the pour.

In addition, a numerical study investigating the effects of placing the wet concrete (1) perpendicular to the girders and (2) parallel to the skew was completed. These studies indicated that attempts to place the deck parallel to the skew would provide reduced differential deflections and stresses across the superstructure of the bridge that was studied. However, for this continuous structure the reductions were relatively small. Previous work by one of the authors indicates that deck placement parallel to the skew for simply-supported, steel structures with skew angles similar to those for the bridge studied herein provides a beneficial reduction of deformations and stresses that can result during construction. The combined results from that study and the current work indicate that, while continuity can possibly reduce the beneficial effects that can result from placing wet concrete parallel to the skew, bridge designers and builders should consider this placement method as a viable option when developed construction plans for skewed, steel I-girder bridges. It should be noted that results reported herein were limited to a single structure, however it can be inferred that they would be representative of the response of skewed, multi-beam, composite steel-concrete bridges. However, additional studies, both experimental and numerical, would need to be performed to assess the ranges of parameters (e.g. skew angle, number of spans, number of girders, boundary conditions, etc.) over which the conclusions obtained herein would be applicable.

Finally, in Chapter 6 of this study, the appropriateness of AASHTO-LRFD live load distribution formulas for high performance steel (HPS) bridges was evaluated through the use of bridge truckload test data. Three field experiments were conducted on the bridge to evaluate its behavior under different conditions. After the field experiments, the original strain data that was collected was processed to filter out the dynamic and electronic noise by applying a low pass filter. Finally, live-load distribution factors (DFs) were extracted from the filtered strain data,

and compared with the results from AASHTO-LRFD formulas. The comparison of the DFs obtained from field test data with the DFs calculated from AASHTO-LRFD formulas shows the AASHTO-LRFD formulas are applicable to design beam-and-slab bridges with girders fabricated from HPS. Also the AASHTO-LRFD formulas give conservative results. Compared with beam-and-slab bridges made with traditional steel, HPS bridges usually use less steel because of its higher yield strength, which reduces the depth of the girders and therefore the decreased moment inertia of the girders will make the HPS bridges more flexible. This results in uniform transverse distribution of loads when compared with the stiffer traditional beam-and-slab bridges.

7.2 CLOSURE

The results summarized above and contained herein support the continued use of HPS-70W in bridge construction within the state of Ohio. While there are still areas in need of further study, this project has demonstrated that the product can provide benefits not possible with conventional grades of steel.

References

- AASHTO (2004). *LRFD Bridge Design Specifications, 3rd Ed.*, American Association of State Highway and Transportation Officials, Washington, D.C.
- AASHTO (2004). *Standard Specification for Highway Bridges, 17th Ed.*, American Association of State Highway and Transportation Officials, Washington, D.C.
- AASHTO (2003). *Guide Specification for Highway Bridge Fabrication with HPS 70W (HPS 485W) Steel, 2nd Ed.*, American Association of State Highway and Transportation Officials (AASHTO), Washington, D.C.
- AASHTO. (1998). *LRFD Bridge Design Specifications, 2nd Ed.*, American Association of State Highway and Transportation Officials, Washington, D.C.
- AASHTO, (1994) *LRFD Bridge Design Specifications, 1st Ed.*, American Association of State Highway and Transportation Officials, Washington, D.C
- Abendroth, R.E., Greimann, L.F. (1989). “A Rational Design Approach for Integral-Abutment Bridge Piles,” *Transportation Research Record: Journal of the Transportation Research Board*, Vol. 1223, pp. 12–23.
- Adonyi, Y. (2000). “Weldability of High Performance Steels,” *Proc., Steel Bridge Design and Construction for the New Millennium with Emphasis on High Performance Steel*, FHWA and NABRO, Baltimore, MD.
- Aggour, MS. (1947). *Theoretical and Experimental Study of Space Frame Action and Load Distribution in Square and Skew Bridges*, Thesis, Cairo University, Egypt.
- Aggour, MS. (1943). *Treatment of Skew Truss Bridges as Space Frames*, Thesis, Cairo University, Egypt.
- AISI. (2004). “HPS Scoreboard,” *AISI*, <<http://www.steel.org/infrastructure/>>, (Accessed 2004)
- Alampalli, S., Yannotti, A.P. (1998). “In-Service Performance of Integral Bridges and Jointless Decks,” *Transportation Research Record: Journal of the Transportation Research Board*, Vol. 1624, pp. 2–7.
- Anderson, T. (2002), “Inspection Connection: Radiographic and Ultrasonic Weld Inspection - Establishing Weld Integrity without Destroying the Component,” *The Fabricator.Com*, <http://www2.thefabricator.com/Articles/Welding_Article.cfm?ID=492> (Accessed 2005)
- Ashour, M., Norris, G. (2000). “Modeling Lateral Soil–Pile Response Based on Soil–Pile Interaction,” *Journal of Geotechnical and Geoenvironmental Engineering*, Vol. 126, No. 5, pp. 420–428.

References

- ASTM A370 (2002). "Standard Test Methods and Definitions for Mechanical Testing of Steel Products," *American Society for Testing and Materials*
- ASTM A709 (2001). "Standard Specification for Carbon and High-Strength Low-Alloy Structural Steel Shapes, Plates, and Bars and Quenched-and-Tempered Alloy Structural Steel Plates for Bridges," *American Society for Testing and Materials*
- ASTM E8 (2001). "Standard Test Methods for Tension Testing of Metallic Materials," *American Society for Testing and Materials*
- ASTM G101 (1997). "Standard Guide for Estimating the Atmospheric Corrosion Resistance of Low-Alloy Steels," *American Society for Testing and Materials*
- Azizinamini, A., Barth, K., Dexter, R. and Rubeiz C. (2004) "High Performance Steel: Research Front—Historical Account of Research Activities" *Journal of Bridge Engineering*, Vol. 9, No. 3, pp. 212-217
- Barker, M.D., Schrage, S.D. (2000). "High Performance Steel: Design and Cost Comparisons," *Modern Steel Construction*, Vol. 46, No. 6, pp. 35.
- Barsom, J.M., (1997), "Properties of High Performance Steels and Their Use in Bridges," *Proc., Building to Last: Structures Congress XV*, ASCE, New York, NY, pp. 140-145.
- Barth, K. E., Roeder, C. W., Christopher, R. A. and Wu H. (2003). "Evaluation of Live-Load Deflection Criteria for I-Shaped Steel Bridge Girders" *Proc. International Conference*, July 29-August 3, 2001, Kona, Hawaii, pp.193-208
- Better Roads, (2003). "Better Roads 2003 Bridge Inventory," *Better Roads*, Vol. 73, No. 11, p. 26.
- Bodnar, R.L. (1995). *Progress in the Development of an As-Rolled Nb-V Weathering Steel for Bridge Applications*, Final Report under ONR-AISI No. N00014-94-2-0002, Bethlehem Steel Corp., 714-2785, TPO-71-94055, June 15, 1995.
- Burke, M.P. (1996). "The Design of Integral Bridges," *Concrete International*, Vol. 15, No. 6, pp. 37-42.
- Burke, M.P. (1994). "Semi-Integral Bridges: Movements and Forces," *Transportation Research Record: Journal of the Transportation Research Board*, Vol. 1460, pp. 1-7.
- Chen, H., Grondin, G., and Driver, R. (2003). "Fatigue Properties of High Performance Steel." *Proc., First International Conference on Fatigue Damage of Materials*, WIT Press, Toronto, Ontario, pp. 181-191.
- Chilton, J. and Manganello, S.J. (1996). "Material Development for High-Performance Bridge Steels." *Proc., Building an International Community of Structural Engineers: Structures Congress XIV*, ASCE, New York, NY, pp. 100-107.

References

- Densmore, D. (2000), "INFORMATION: Narrow-Gap Electroslag Welding for Bridges," *Technical Memorandum*, FHWA, March 20, 2000. < <http://www.fhwa.dot.gov/bridge/esw.htm>>
- Dicleli, M. (2000). "Simplified Model for Computer-Aided Analysis of Integral Bridges," *Journal of Bridge Engineering*, Vol. 5, No. 3, pp. 240–248.
- Dues, E., Hattin, J., Kesler, S. (2002). *Tensile Testing of HPS-70W TMCP Plate Material*, Final Report under NSF Grant ID No. EEC 9820102, University of Cincinnati, August 16, 2002.
- Earls, C.J., Shah, B.J. (2002). "High Performance Steel Girder Compactness," *Journal of Constructional Steel Research*, Vol. 58, pp. 859–880.
- Ebeido T, and Kennedy, JB. (1996). "Girder Moments in Simply Supported Skew Composite Bridges," *Canadian Journal of Civil Engineering* Vol. 23, No. 4, pp. 904–16.
- Emerson, M. (1981). "Thermal Movements of Concrete Bridges—Field Measurements and Methods of Prediction," *Publication SP—American Concrete Institute*, pp. 77–102.
- FHWA. (2003), "Narrow Gap Improved Electroslag Welding of Bridge Steels," *FHWA*, <http://www.fhwa.dot.gov/bridge/ngiesw.htm>, (Mar. 9, 2005).
- Focht, E.M. and Manganello, S.J. (1996). "Stress-strain behavior of high-performance 70W bridge steel." *Proc., Materials for the New Millennium, Vol. 2: Fourth Materials Engineering Conference*, ASCE, New York, NY, pp. 1541-1550.
- Germanson, T. (1998). "Working with HPS 70W Steel," *Presented at the 77th Annual Meeting of the Transportation Research Board*.
- Ghali, A. (1967). "Analysis of Continuous Skew Concrete Girder Bridge," *Proc., First International Symposium on Concrete Bridge Design, American Concrete Institute*.
- Ghali, A. (1969). "Field Measurement of End Support Reactions of a Continuous Multi-Girder Skew Bridge," *Proc., Second International Symposium on Concrete Bridge Design, American Concrete Institute*, pp. 260–271.
- Girton, D.D., Hawkinson, T.R., Greimann, F.F. (1991). "Validation of Design Recommendations for Integral-Abutment Piles," *Journal of Structural Engineering*, Vol. 117, Np. 7, pp. 2117–2134.
- Greco, N. and Earls, C. J. (2003) "Structural Ductility in Hybrid High Performance Steel Beams" *Journal of Structural Engineering*, Vol. 129, No. 12, pp. 1584-1595.
- Green, P.S., Sause, R., Ricles, J.M. (2002). "Strength and Ductility of HPS Flexural Members," *Journal of Constructional Steel Research*, Vol. 58, pp. 907–941.
- Greimann, L.F., Yang, P.S., Wolde-Tinsae, A.M. (1986). "Nonlinear Analysis of Integral Abutment Bridges," *Journal of Structural Engineering*, Vol. 112, No. 10, pp. 2263–2280.

References

- Gupta YP, and Kumar A. (1983). "Structural Behavior of Interconnected Skew Slab–Girder Bridges," *Journal of the Institution of Engineers (India)* Vol. 64, pp. 119–24.
- Guyon, Y. (1946). "Calcul des Ponts Larges a Poutres Multiples Solidarisees par les Entretoises" *Annales des Ponts et Chausees*, Paris, Vol. 116, pp. 663-612.
- Hendry, A. W., and Jaeger, L. G. (1956). "Load Distribution in Highway Bridge Decks." *Proc.*, ASCE, 82, No. ST4, pp. 1023-1—1023-48.
- Hulsey, J.L., Emanuel, J.H. (1978). "Environmental Stresses in Flexibility Supported Bridges," *Transportation Research Record: Journal of the Transportation Research Board*, Vol. 664, pp. 262–270.
- Husain, I., Bagnariol, D. (2000). *Performance of Integral Abutment Bridges*, Ministry of Transportation Bridge Office Report BO-99-04, Ontario, Canada.
- Hutter, G. (1964). "Skew and Curved Box-Girders: Theory and Research," *Proc.*, *Seventh Congress of the International Association for Bridges and Structural Engineering*, pp. 615–623.
- Ingram, E.E., Burdette, E.G., Goodpasture, D.W., Deatherage, J.H. (2003). "Evaluation of Applicability of Typical Column Design Equations to Steel H-Piles Supporting Integral Abutments," *Engineering Journal*, Vol. 40, No. 1, pp. 50–58.
- ISG. (2003). "High Performance Steels for Bridges: HPS-70W," *International Steel Group, Inc.*, < <http://www.intlsteel.com/PDFs/bridges.pdf> > (Sep., 2003).
- Jata, G. (2003), "14 Bridges in Region to Get Safety Updates," *The Pittsburgh Post*, August 14.
- Kostem, C. N., and deCastro, E. S. (1977). "Effect of Diaphragms on Lateral Load Distribution in Beam–Slab Bridges." *Transportation Research Record 645*, Transportation Research Board, National Research Council, Washington, D.C.
- Krouse, D. (1999). "High Performance Steel; Material Development." *Proc.*, *Materials and Construction – Exploring the Connection: Fifth ASCE Materials Engineering Congress*, ASCE, Reston, VA, 566-575.
- Kulicki, J.M. (2000), "The Shape of Things to Come," *Civil Engineering*, Vol. 70, No. 2
- Laman, J.A., Linzell, D.G., Leighty, C.A., Fennema, J.L. (2003) *Methodology to Predict Movement and Stresses in Integral Abutment Bridges*, Pennsylvania Department of Transportation.
- Lawver, A., French, C., Shield, C.K. (2000). "Field Performance of an Integral Abutment Bridge," *Transportation Research Record: Journal of the Transportation Research Board*, Vol. 1740, pp. 108–117.

References

- Lehane, B.M., Keogh, D.L., O'Brien, D.J. (1999). "Simplified Elastic Model for Restraining Effects of Backfill Soil on Integral Bridges," *Computers and Structures*, Vol. 73 (1-5), pp. 303-313.
- Loo, Y. C. and Cusens, A. R. (1978) *The Finite-Strip Method in Bridge Engineering*, Viewpoint Publications, London.
- Mabsout, M. E., Naddaf, I. Y., Tarhini, K. M., and Frederick, G. R. (1998). "Load Reduction in Steel Girder Bridges," *Practice Periodical of Structural Design and Construction*, Vol. 7, No. 1, pp. 37-43.
- Mabsout, M.E., Tarhni, K.M. (1997). "Influence of Sidewalks and Railings on Wheel Load Distribution in Steel Girder Bridges," *Journal of Bridge Engineering*, Vol. 2, No. (88)
- Massonnet, C. (1950). "Contribution to the Calculation of Multiple Beam Bridges." *Annales des Travaux Pub de Belgique*, Vol. 103, No. 3,5 and 6, pp. 377-422, 749-796, 927-964.
- Massonnet, C. (1950). "Method of Calculation of Bridges with Several Longitudinal Beams, Taking into Account Their Torsional Resistance." *International Association of Bridge and Structural Engineers Publications*, Zurich, Vol. 10, pp 147-182.
- Malin, V, "Electroslag Welding For Bridges Program," http://www.iti.northwestern.edu/research/a_projects/malin_electroslag_welding2.html (Mar. 9, 2005).
- Manganello, S.J. (1995). *AISI/FHWA High-Performance Bridge-Steel Screening Study*, Final Report under AISI Cooperative Agreement ONR-AISI No. N00014-94-2-0002, March 31, 1995.
- Mans, P., Yakel, A. J. and Azizinamini, A. (2001) "Full-Scale Testing of Composite Plate Girders Constructed Using 485-MPa High-Performance Steel" *Journal of Bridge Engineering*, Vol. 6, No. 6, pp. 598-604
- Miller, D. (2000), "Welding HPS-70W Steel," *Proc., Steel Bridge Design and Construction for the New Millennium with Emphasis on High Performance Steel*, FHWA and NABRO, Baltimore, MD.
- Mourad, S., Tabsh, S.W. (1998). "Pile Forces in Integral Abutment Bridges Subjected to Truck Loads," *Transportation Research Record: Journal of the Transportation Research Board*, Vol. 1633, pp. 77-83.
- Newmark, N. M., and Siess, C. P. (1954). "Research on Highway-Bridge Floors." *Proc., Highway Research Board Processing, 33rd Annual Meeting*, NCHRP, Washington, D.C., pp. 30-53.
- Nicholoso, B.A. (1994). "Effects of temperature, shrinkage and creep on integral bridges," *Proc., Henderson Colloquium Towards Joint Free Bridges*, p. 33.

References

- Nickerson, R.L. (1999). "Application of High Performance Steel to Obtain More Cost-Effective Highway Bridges," *Proc., Materials and Construction – Exploring the Connection: Fifth ASCE Materials Engineering Congress*, ASCE, Reston, VA, pp. 551-557.
- Nickerson, R.L. (1997). "Tennessee Department of Transportation Martin Creek Bridge, HPS 70W Steel Fabrication and Erection Report and Weld Parameter Study Number 4," *Presented at the HPS Steering Committee Meeting*.
- Nickerson, R.L., Wright, W. (1996). "Weld Parameter Investigation for HPS 70W Steel," *Presented at the HPS Steering Committee Meeting*.
- Norton, E.K., Linzell, D.G., Laman, J.A. (2003). "Examination of Response of a Skewed Steel Bridge Superstructure During Deck Placement," *Transportation Research Record: Journal of the Transportation Research Board*, 1845, pp. 66–75.
- ODOT. (2002). *Construction and Material Specifications*, State of Ohio Department of Transportation (ODOT).
- Oesterle, R.G., Refai, T.M., Volz, J.S., Scanlon, A, and Weiss, W.J. (1998), *Jointless and Integral Abutment Bridges Analytical Research and Proposed Design Procedures*, Construction Technology Laboratories, Inc.; 1998.
- Ostwald, P. and Munoz, J. (1997), *Manufacturing Processes and Systems, 9th Ed.* John Wiley and Sons, New York, NY.
- Ramirez, R. W. (1985). *The FFT, Fundamentals and Concepts*, Englewood Cliffs, N.J. Prentice-Hall
- Sanders, W. W. (1984). "Distribution of wheel loads on highway bridges." *Proc., NCHRP Synthesis of Highway Practice III*, Transportation Research Board, National Research Council, Washington, D.C.
- Sause, R. and Fahnestock, L. A. (2001). "Strength and Ductility of HPS-100W I-Girders in Negative Flexure" *Journal of Bridge Engineering*, Vol. 6, No. 5, pp. 316-323
- Surana, C.S., and Humar, J.L. (1984). "Beam-and-Slab Bridges with Small Skew," *Canadian Journal of Civil Engineering*, Vol. 11, No. 1, pp. 117–121.
- Tarhini, R.M., Frederick, G.R. (1995). "Lateral Load Distribution in I-Grider Bridges," *Computers and Structures*, Vol. 54, No. 12, pp. 351-354.
- Thippeswamy, H.K., and Ganga Rao, H.V.S. (1995). "Analysis of In-Service Jointless Bridges," *Transportation Research Record: Journal of the Transportation Research Board*, Vol. 1476, pp. 162–170.
- Topkaya, C. (2002). *Behavior of Steel Trapezoidal Box Girders During Construction*, Ph.D. Dissertation, Department of Civil Engineering, University of Texas at Austin.

References

- Turer, A. (2000). *Condition Evaluation and Load Rating of Steel Stringer Highway Bridges Using Field Calibrated 2D-Grid and 3D-FE Models*,” Doctoral Dissertation, University of Cincinnati, Cincinnati, Ohio.
- Van Ooyen, K. (2002). “HPS Success,” *Modern Steel Construction*, Vol. 42, No. 9, pp. 36–38.
- Varney, R. F. and Galambos, C. F. (1965). “Field Dynamic Loading Studies of Highway Bridges in the U.S., 1948-1965.” *Highway Research Record 76: Design—Bridges and Structures*. Highway Research Board, National Research Council, Washington, D. C. pp.285-305.
- Verma, K. (2000). “Narrow-Gap Improved Electroslag Welding For Bridges,” *Proc., Steel Bridge Design and Construction for the New Millennium with Emphasis on High Performance Steel*, FHWA and NABRO, Baltimore, MD.
- Wassef, W., Kulicki, J., and Ritchie, P. (1996). “Bridges of the 21st Century with High Performance Steel,” *Proc., Building an International Community of Structural Engineers: Structures Congress XIV*, ASCE, New York, NY, pp. 117-124.
- Wasserman, E., Azizinamini, A., Pate, H., Greer, W. (1998). “Making the Grade,” *Civil Engineering*, Vol. 68, No. 4, pp. 69–71.
- Wasserman, E. (2002). “Optimization of HPS 70W Applications,” *Journal of Bridge Engineering*, Vol. 7, No. 1, pp. 1–5.
- Wilson, A.D. (1999). “Properties of recent production of A709 bridge steels.” *Proc., International Symposium on Steel for Fabricated Structures*, ASM International, Materials Park, OH, 41-43.
- Wolde-Tinsae, A.M., Greimann, L.F. (1988) “General Design Details for Integral Abutment Bridges,” *Civil Engineering Practice*, Vol. 3, No. 2, pp. 7–20.
- Wood, W. and Devletian J. (1987). *Improved Fracture Toughness and Fatigue Characteristics of Electroslag Welds*, Report FHWA/RD-87/026, U.S. Department of Transportation, Washington, D.C.
- Wright, W. J. (1997). “High Performance Steel: Research to Practice,” *Public Roads*, Spring 1997, pp. 64-38.
- Wright, W. (2002). “Fracture Toughness Requirements For Highway Bridges: Past And Future Trends,” *Progressive Structural Engineering Materials*, No. 4, pp. 96-104.
- Yakel, A., Mans, P., and Azizinamini, A. (1999). “Negative Bending Tests Of HPS-485W Bridge Girders,” *Proc., Materials and Construction: Exploring the Connection: 5th ASCE Materials Engineering Congress*, ASCE, Reston, VA, pp. 558-565
- Yost, L. (2002), “Welding High Performance Steel Bridges,” *Advanced Materials and Processes*, Nov 2002.

References

Zokaie, T., Osterkamp, T. A., and Imbsen, R. A. (1992). *Distribution of Wheel Loads on Highway Bridges*, National Cooperative Highway Research Program 12-26 Final Report, National Cooperative Highway Research Program, Washington, D.C.